

Schwinger Boson Study of the XXZ-Heisenberg Model on the Pyrochlore Lattice

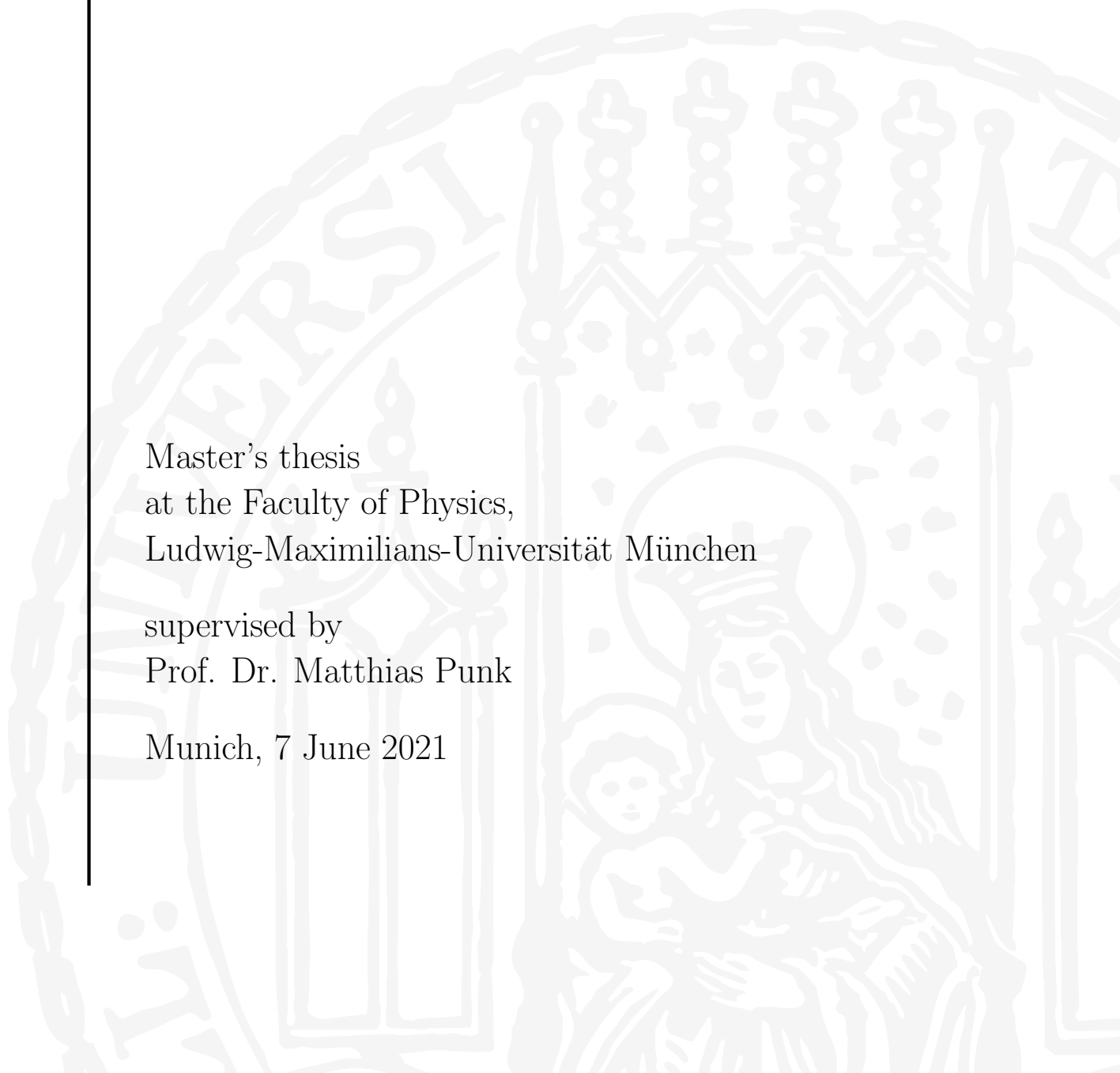
Benedikt Schneider

The published results can be found here: [\[1\]](#)

Master's thesis
at the Faculty of Physics,
Ludwig-Maximilians-Universität München

supervised by
Prof. Dr. Matthias Punk

Munich, 7 June 2021



Schwinger Bosonen Studie des XXZ-Heisenberg Modells auf dem Pyrochlor Gitter

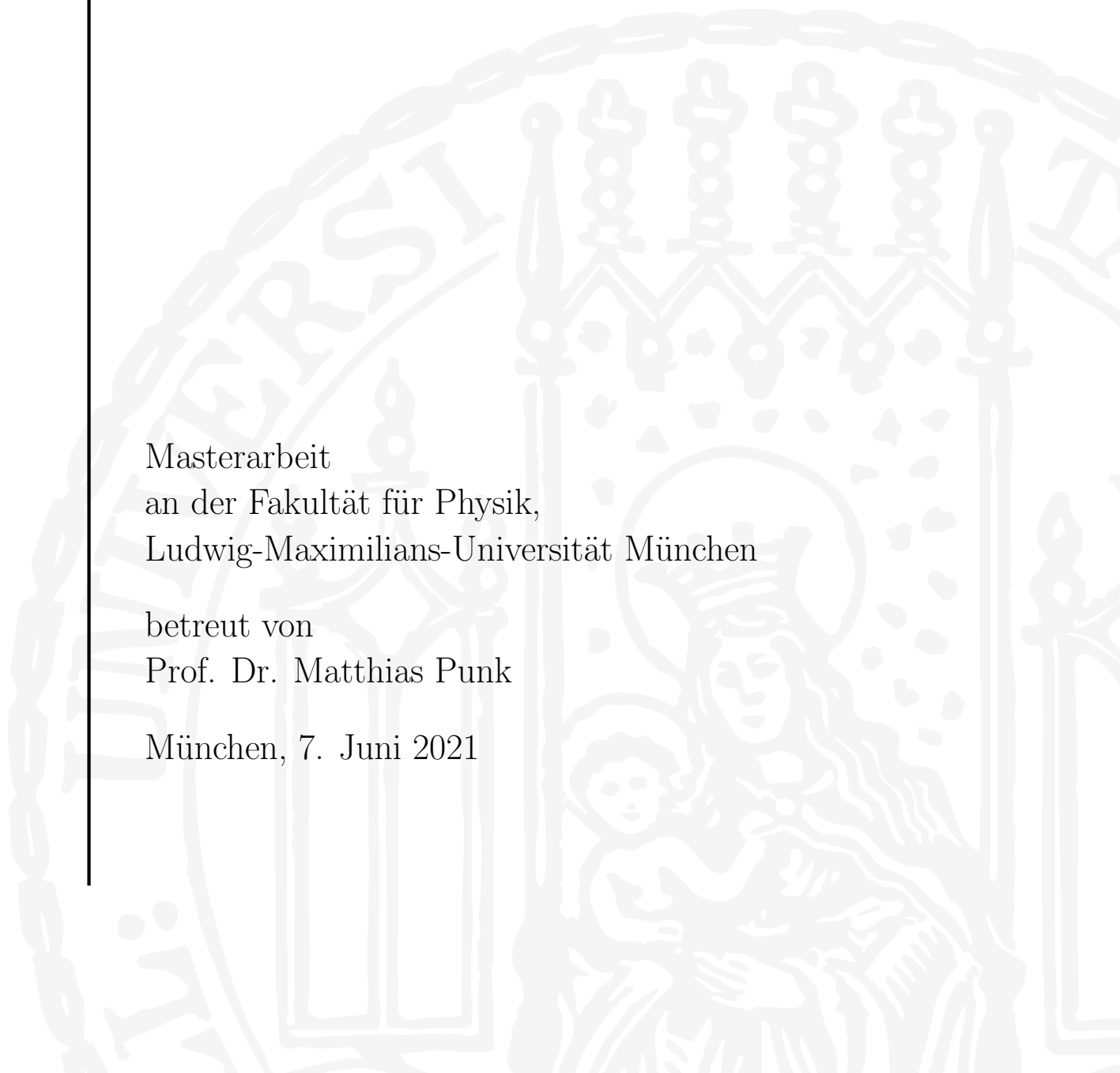
Benedikt Schneider

The published results can be found here: [\[1\]](#)

Masterarbeit
an der Fakultät für Physik,
Ludwig-Maximilians-Universität München

betreut von
Prof. Dr. Matthias Punk

München, 7. Juni 2021



Abstract

Rare earth pyrochlores are promising candidate materials to host quantum spin liquid ground states. The XXZ-Heisenberg model has been proposed as a minimal model to describe these states. Previous studies have found two magnetic and multiple spin liquid phases in the phase diagram. We study the XXZ-Heisenberg model on the pyrochlore lattice using the projective symmetry group and Schwinger boson mean field theory. We solve the mean field equations for 12 symmetric ansätze and characterize some of them by calculating their local spin structure factors and neutron scattering amplitudes. Close to the Heisenberg point we find excellent agreement with prior work for observables of one ansatz.

Additionally, we classify all possible weakly symmetric ansätze on the pyrochlore lattice setting the basis for future studies of chiral spin liquids.

We complement the spin liquid study by Holstein-Primakoff linear spin wave calculations for the magnetic phases of the model.

Acknowledgments

First and foremost, I want to thank Matthias Punk for suggesting this topic to me and supervising the project. I am extremely grateful for his constant support and the freedom to stir the project into directions that I found fascinating. I am grateful to Marc Ritter for our fruitful discussions about pyrochlore. Working with him made working from home in a pandemic feel less isolated.

I want to extend my gratitude to Jan von Delft and all members of the chair for providing a friendly and positive work environment. Special thanks go to Elias Walter for helping me with the cluster and to Marc for helping me with L^AT_EX and letting me use one of his figures.

Furthermore, I would like to thank Jad C. Halimeh for giving me insights on solving the mean field equations from a numerical point of view. Finally, I want to thank Adrian Fleidl, Anna Schmidt, Marc and Felix Palm for proofreading my thesis.

Contents

Contents	v
1 Introduction	1
2 The XXZ-Heisenberg Model and its Phases	3
2.1 Phases of the XXZ-Heisenberg Model	4
3 The Pyrochlore Lattice and its Symmetries	9
3.1 Pyrochlore Lattice	9
3.2 Brillouin Zone	10
3.3 Space Group Symmetries	11
4 Schwinger Boson Mean Field Theory and Projective Symmetry Group	13
4.1 From Spin Hamiltonian to Mean Field Ansatz	13
4.2 Projective Symmetry Group: Symmetric Ansatz	15
4.3 Weakly Symmetric Ansätze	18
5 Schwinger Boson Treatment of the XXZ-Heisenberg Hamiltonian	25
5.1 Mean Field Decoupling	25
5.2 Diagonalization of the Hamiltonian	28
5.3 Satisfying the Self-Consistency Equations	29
5.4 Spin Structure Factor	30
6 Magnetic Phases	33
6.1 All-In-All-Out (AIAO)	34
6.2 Easy-Plane Antiferromagnet (AF_{\perp})	35
7 Results	39
7.1 Mean Field Values	39
7.2 Structure Factors and Neutron Scattering Amplitudes	43
7.3 Discussion	51
8 Conclusion	53

A From Global to Local Spin Basis	55
B Solution of the Chiral Algebraic PSG	57
C Classification of Chiral Ansätze	63
D Fourier Transformation of the Hamiltonian	71
E Explicit Hamiltonians	73
F Analytic Results for Energy Bands	77
G Sublattice Boson Density in the AF_{\perp} Phase	79
H Supplementary Observables	81
Bibliography	85
Selbständigkeitserklärung	89

Introduction

Spin liquids are phases of spin systems that do not exhibit any long range order down to zero temperature. Therefore, they can not be classified by Landau's theory of spontaneous symmetry breaking. Instead, they exhibit topological order [2] with long range entanglement and non local excitations. These excitations carry fractional quantum numbers and can have anyonic exchange statistics. Kitaev proposed that such states could be used for stable quantum computing [3]. Anderson suggested that the behavior of cuprate superconductors is closely related to a parent spin liquid state [4]. Even if a spin system is only proximate to a spin liquid phase, its behaviour can be greatly influenced by the properties of the spin liquid [5]. There are a number of theoretical models that are known to host spin liquids including the Kitaev toric code [3] or honeycomb [6] models. Realization of these models is challenging since they have been constructed artificially with a focus on analytic solvability. Rare earth pyrochlores are spin liquid candidates that are found in nature. There have been multiple experiments finding no long range order down to low temperatures in the mK range which is a strong indication of spin liquids [5]. These pyrochlores have the structure $R_2M_2O_7$, with trivalent rare-earth ion R and non-magnetic tetravalent transition metal ion M sitting on intertwined lattices of corner sharing tetrahedra (see Fig. 2.1). For a subclass of those the crystal field splitting of the rare earth angular momentum manifold leads to an effective low energy behavior of Kramer doublets, that can be described by an effective spin 1/2 model [5]. The small effective spin value of $S = 1/2$ and high geometric frustration enhance correlations and might prevent long range order.

In this work we consider a simplified version of the general effective spin 1/2 model: The nearest neighbor local XXZ-Heisenberg model which has been regarded as a minimal quantum spin liquid model [7, 8]. The classical phase diagram harbors a rich variety of ground states including the all-in-all-out order, easy-plane antiferromagnetic order and spin ice [5]. However, the quantum phase diagram has not been solved yet. The most heavily studied phase of the model is probably the quantum spin ice which is expected for antiferromagnetic Ising interactions with small transverse interaction. It is a U(1) quantum spin liquid which is related to quantum electromagnetism [9]. That is, it can host emergent electric and magnetic monopole excitations that can interact via a gapless U(1) gauge boson. Recent studies also found a nematic spin liquid for strong antiferromagnetic transverse coupling that breaks the U(1) spin rotation symmetry of the Hamiltonian as well as C_3 symmetry

of the pyrochlore lattice [7, 8]. The fate of the ground state at the Heisenberg point, however, is still unclear. A lot of possible ground states have been suggested including dimer-ordered [10–14] and spin liquid states [15–17]. We are especially curious about the suggested monopole flux state, a chiral spin liquid that breaks time reversal as well as inversion symmetry [15]. Using Schwinger Boson Mean Field Theory we construct different gapped symmetric as well as weakly symmetric \mathbb{Z}_2 spin liquids as possible ground state candidates. To achieve this we use a previous classification of all possible symmetric spin liquids [18] and classify all possible weakly symmetric spin liquids using projective symmetry group as described by Messio et al. [19]. We calculate and compare the zero temperature ground state energies and calculate equal time spin-structure factors. Even though the gapped \mathbb{Z}_2 liquids cannot describe the gapless excitations of the U(1) quantum spin ice, we hope to be able to describe the spinon excitations correctly.

The outline of the thesis is as follows: In Chapt. 2 we present the origin of the general pseudospin $\mathcal{S} = \frac{1}{2}$ model and various phases that have previously been identified in the XXZ-Heisenberg model. In Chapt. 3 we describe the pyrochlore lattice and its symmetries. In Chapt. 4 we introduce Schwinger boson mean field theory and establish how the projective symmetry group can be used to systematically classify symmetric and weakly symmetric mean field ansätze. In Chapt. 5 we describe diagonalization of the resulting spin liquid Hamiltonians and describe how to calculate their corresponding spin structure factors. Magnetic phases are treated in Chapt. 6 via Holstein-Primakoff spin wave theory. The results for ground state energies and spin structure factors are presented in Chapt. 7. Finally, we summarize our results in Chapt. 8 and give an outlook for future work.

The XXZ-Heisenberg Model and its Phases

Rare earth pyrochlores of the type $R_2M_2O_7$ have their non-magnetic atoms M and rare earth atoms R sitting on two intertwined pyrochlore lattices each consisting of corner sharing tetrahedra where one tetrahedron of the type M lattice sits in the gap of the type R lattice (see Fig. 2.1).

In the materials of interest the single-ion physics dominates over the two-ion interactions. The ground state can thus be found by first finding the free-ion ground state according to Hund's rules which gives a degenerate manifold with fixed angular momentum J . The electric field imposed by the crystal ions lifts most of this $2J + 1$ fold degeneracy. For the materials that we are interested in the resulting low energy states are well separated from the higher energy states and form a doublet $|\pm\rangle$:

$$\hat{S}^z = \frac{|+\rangle\langle+| - |-\rangle\langle-|}{2}, \quad \hat{S}^\pm = |\pm\rangle\langle\mp|. \quad (2.1)$$

For a more detailed description see [5]. The degeneracy of the doublet is either ensured by the Kramers theorem or by the crystal symmetry. In general, there

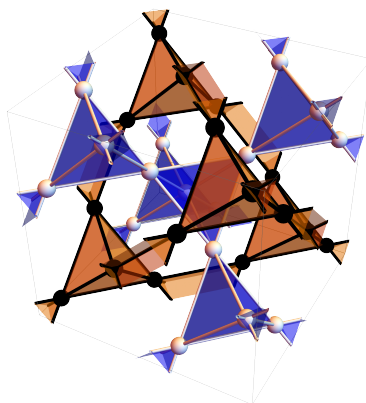


Figure 2.1: Crystal structure of $R_2M_2O_7$ pyrochlores. Rare earth atoms R are depicted in white and the non magnetic ions M are shown in black. The oxygen atoms are not shown. Adapted with permission from Ritter [20].

are three cases: The effective $\mathcal{S} = \frac{1}{2}$ Kramers doublet, dipolar-octopolar Kramers doublet or non-Kramers doublet. They differ in the transformation properties of the components S^z, S^\pm . In this work we will focus on the effective $\mathcal{S} = \frac{1}{2}$ Kramers doublet. When the crystal field energy scale is well separated from the interaction energy scale one can approximate the interactions in first order perturbation theory by constructing an effective nearest neighbor spin Hamiltonian H :

$$H = \sum_{\langle i,j \rangle} \sum_{\mu,\nu} \hat{S}_i^\mu J_{ij}^{\mu\nu} \hat{S}_j^\nu + \text{const.} \quad (2.2)$$

Going beyond first order perturbation theory introduces next and further nearest neighbor couplings. The tensor $J_{ij}^{\mu\nu}$ is heavily constrained by symmetry and in the most general case leads to the following spin Hamiltonian:

$$H = \sum_{\langle i,j \rangle} [J_{zz} \hat{S}_i^z \hat{S}_j^z - J_\pm (\hat{S}_i^+ \hat{S}_j^- + \hat{S}_i^- \hat{S}_j^+) + J_{\pm\pm} (\gamma_{ij} \hat{S}_i^+ \hat{S}_j^+ + \gamma_{ij}^* \hat{S}_i^- \hat{S}_j^-) + J_{z\pm} (\zeta_{ij} [\hat{S}_i^z \hat{S}_j^+ + \hat{S}_i^+ \hat{S}_j^z] + \zeta_{ij}^* [\hat{S}_i^z \hat{S}_j^- + \hat{S}_i^- \hat{S}_j^z])]. \quad (2.3)$$

The pseudospin operators are defined in a local basis that we introduce in Chapt. 3 and γ and ζ are bond-dependent phase factors. (For more details see [21, 22].) It is interesting to note that the sign of $J_{z\pm}$ is arbitrary which leads to a duality in the global spin basis. This relates the Heisenberg points in global and local spin bases for example [23].

2.1 Phases of the XXZ-Heisenberg Model

In this thesis we will consider the simplified model of Eq. (2.3) where $J_{z\pm} = J_{\pm\pm} = 0$: The so called XXZ-Heisenberg model. It can be written as

$$H = \sum_{\langle i,j \rangle} J_{zz} \hat{S}_i^z \hat{S}_j^z + J_\perp (\hat{S}_i^x \hat{S}_j^x + \hat{S}_i^y \hat{S}_j^y) \quad (2.4)$$

with $J_\perp = -\frac{1}{2}J_\pm$. To later compare our analytical results to the numerical results of Benton et al. [7] we choose the parametrization:

$$J_{zz} = J \cos(\theta) \quad J_\perp = J \sin(\theta) \quad (2.5)$$

with $\theta = \arctan(\frac{J_\perp}{J_{zz}})$ and set the energy scale to $J = 1$. The classical phase diagram has three phases:

All-In-All-Out Order (AIAO)

AIAO is a magnetically ordered state that has all spins point into one half and out of the other half of the tetrahedra in the lattice (see Fig. 2.2(a)).

Easy-Plane Antiferromagnet (AF $_\perp$)

AF $_\perp$ is a magnetically ordered state that has all spins point along the same axis in the local $S^x - S^y$ plane. In the global basis the spins have antiparallel components on neighboring sites (hence the name). It is sometimes referred to as XY antiferromagnet (see Fig. 2.2(b)).

Classical Spin Ice (SI)

The total spin pointing in or out of every tetrahedron vanishes for SI. This is achieved by two spins pointing in and two spins pointing out of every tetrahedron (see Fig. 2.2(c)). This is known as ice rule due to its similarity to the hydrogen configuration in water ice [9]. The classical ground state manifold is exponentially degenerate which leads to a residual entropy at zero temperature. For low temperature the prime experimental signature is a 6-spoke wheel structure in the neutron scattering structure factor with sharp pinch point singularities which are caused by the ice rules [24]. Excitations that break these ice rules act as emergent magnetic monopoles [25].

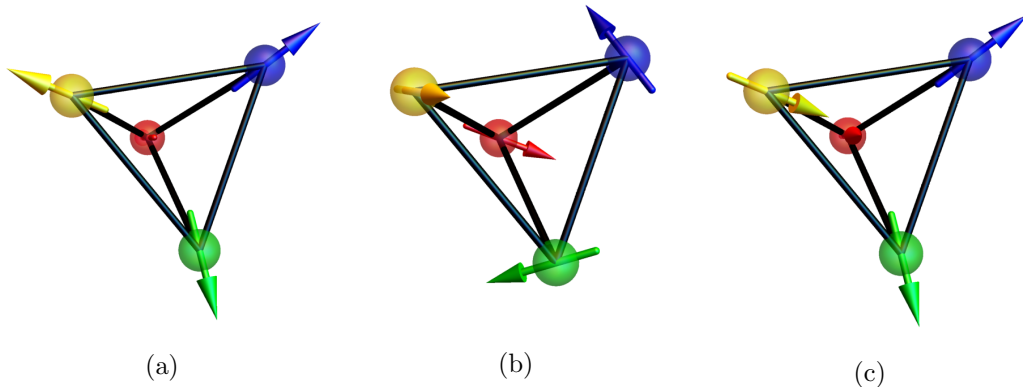


Figure 2.2: Spin configuration on one tetrahedron for the classical phases: (a) AIAO, (b) AF, (c) SI.

While the classical phase diagram is available even for the general model in Eq. (2.3) the quantum phase diagram of the XXZ-Heisenberg model is not. Quantum Monte-Carlo simulations can only access cases with $\theta \in [-\frac{\pi}{2}, 0]$ due to the sign problem [7]. Therefore, few attempts at mapping out the phase diagram of the quantum XXZ-Heisenberg model have been made. Methods employed in prior work include gauge mean field theory [26], augmented fermionic parton mean field theory [27] and a recent effort with multiloop pseudofermion functional renormalization group [20]. A study by Benton et al. [7] combined variational calculations, exact diagonalization as well as numerical linked-cluster and series expansions and found the phase diagram shown in Fig. 2.3. Apart from the AIAO and AF_{\perp} phase they found three distinct spin liquid phases:

Quantum Spin Ice (QSI₀)

QSI₀ is a gappless U(1) quantum spin liquid closely related to the classical spin ice. Due to its quantum nature, fulfilling the ice rule is not the only way of letting the total spin pointing in or out of every tetrahedron vanish. This can also be achieved by vanishing expectation value of every spin $\langle \hat{\mathbf{S}} \rangle = \mathbf{0}$. This effect causes the six spoke wheel structure as well as the pinch points to disappear. However, with rising temperature the structure is restored by thermal excitations of magnetic photons [24]. QSI₀ can be described by an effective U(1) gauge theory on the dual lattice that is created by replacing each tetrahedron by a vertex and each vertex by a bond. The

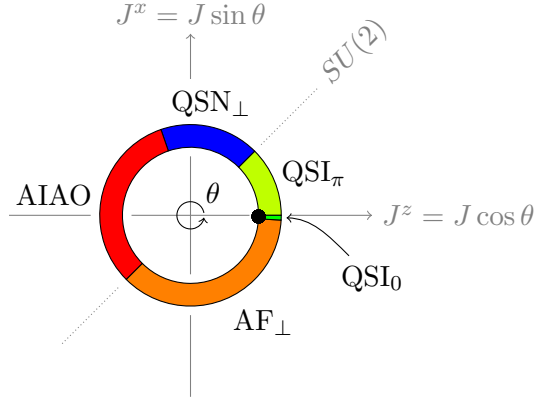


Figure 2.3: Schematic phase diagram of the XXZ-Heisenberg model. Adapted from Benton et al. [7].

resulting field theory is a lattice equivalent to compact quantum electrodynamics [9, 28].

π -Flux Quantum Spin Ice (QSI $_{\pi}$)

QSI $_{\pi}$ is similar to the QSI $_0$ phase but with flux of value π attached to the hexagonal plaquettes. It can experimentally be distinguished from QSI $_0$ by the higher spectral periodicity of its excitations [29]. Perturbation theory predicts a transition from QSI $_0$ to QSI $_{\pi}$ at $\theta = 0$ [28–30].

Nematic Spin Liquid (QSN $_{\perp}$)

QSN $_{\perp}$ is similar to QSI $_{\pi}$ but with antiferromagnetic correlations along a local axis in the $S^x - S^y$ plane instead of along the S^z axis. It breaks the C_3 symmetry of the pyrochlore lattice as well as the $U(1)$ spin rotation symmetry of the Hamiltonian and therefore, by Goldstone’s theorem, has to support a gappless Goldstone mode [8]. An appropriate trial wavefunction is $|\text{QSN}_{\perp}\rangle = R_z(\phi)R_y(\frac{\pi}{2})|\text{QSI}_{\pi}\rangle$ where R_z and R_y rotate all spins about their local z and y axes, respectively [7].

Benton et al. [7] showed that the QSI $_{\pi}$ phase is unstable to nematicity at the Heisenberg point. However, it is not clear if QSI $_{\pi}$ has a phase transition to another ground state for $J_{\perp} < J_z$. Such alternative ground states include chiral spin liquids and dimer ordered states.

Monopole Flux State

The monopole flux state is a chiral quantum spin liquid state that breaks inversion and time reversal symmetry. Spins on the corner of elementary triangle plaquettes have non-vanishing spin triple product $\langle \hat{\mathbf{S}}_i \cdot (\hat{\mathbf{S}}_j \times \hat{\mathbf{S}}_k) \rangle \neq 0$. The flux going in (or out) of every tetrahedron is 2π which is equivalent to putting a monopole of strength 2π at the center of every tetrahedron [15]. An alternative chiral spin liquid that has monopoles at the center of every tetrahedron but breaks time reversal and screw symmetry has been proposed by Kim and Han [17].

Dimer Ordered

Dimer ordered states consist of resonating nearest neighbor singlets. They are usually obtained from so called quantum dimer models that emerge as effective models for the spin model [10, 12–14, 31].

The Pyrochlore Lattice and its Symmetries

3.1 Pyrochlore Lattice

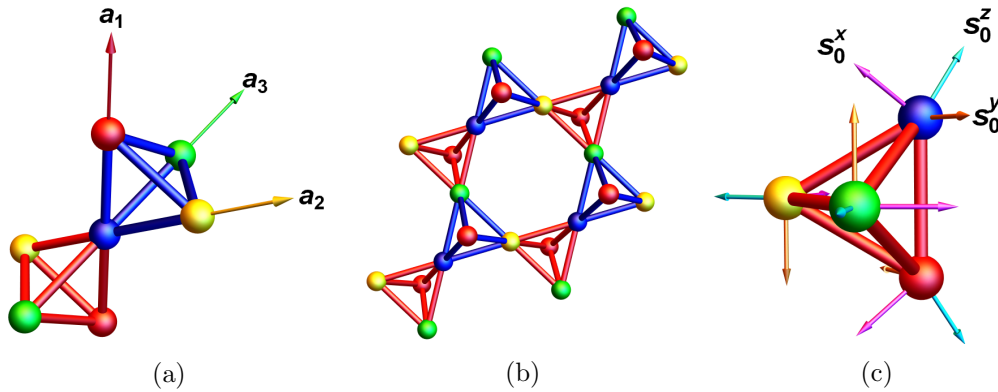


Figure 3.1: (a): A unit cell of the Pyrochlore lattice. Nearest neighbour sites are connected by bonds. Blue bonds are within a unit cell and red bonds are between neighbouring unit cells. The vectors a_1, a_2, a_3 are the fcc lattice vectors. (b): The enlarged pyrochlore unit cell is the unit cell for π -flux states. (c): The vectors on top of the sites are the basis vectors for the local spin basis defined in Eq. (3.4).

The Pyrochlore lattice is given by 4 face-centered cubic (fcc) sublattices: $\mu = 0, 1, 2, 3$. When connecting the nearest neighbour bonds the lattice consists of corner sharing tetrahedra (see Fig. 3.1). Following Liu et al. [18], we work with the standard fcc lattice vectors:

$$\begin{aligned} \mathbf{a}_0 &= (0, 0, 0), & \mathbf{a}_1 &= \frac{1}{2}(0, 1, 1), \\ \mathbf{a}_2 &= \frac{1}{2}(1, 0, 1), & \mathbf{a}_3 &= \frac{1}{2}(1, 1, 0), \end{aligned} \quad (3.1)$$

where we have added a zeroth basis vector to aid later notation. For easier use of symmetries we introduce the sublattice coordinates:

$$\begin{aligned}\mathbf{r}_\mu &= (r_1, r_2, r_3)_\mu = r_1 \mathbf{a}_1 + r_2 \mathbf{a}_2 + r_3 \mathbf{a}_3 + \frac{1}{2} \mathbf{a}_\mu \\ &= \frac{1}{2} (r_2 + r_3, r_1 + r_2, r_1 + r_3) + \frac{1}{2} \mathbf{a}_\mu.\end{aligned}\quad (3.2)$$

In this notation each set of four sites $\{\mathbf{r}_\mu : \mu = 0, 1, 2, 3\}$ spans a tetrahedron (Blue tetrahedra in Fig. 3.1). We will use the coordinates of sublattice 0 to label the unit cells. Nearest neighbor bonds between unit cells $(0, 0, 0)$, $(0, 0, -1)$, $(0, -1, 0)$, $(-1, 0, 0)$ form a tetrahedron as well (red tetrahedra in Fig. 3.1). We will refer to the blue tetrahedra as main and the red as inverse tetrahedra.

Following [22] we define local spin coordinates:

$$\mathbf{S}_\mu = (S^x, S^y, S^z)_\mu = S^x \mathbf{s}_\mu^x + S^y \mathbf{s}_\mu^y + S^z \mathbf{s}_\mu^z. \quad (3.3)$$

with sublattice dependent unit vectors

$$\begin{aligned}\mathbf{s}_\mu^z &= \frac{1}{\sqrt{3}}(1, 1, 1) - \frac{4}{\sqrt{3}} \mathbf{a}_\mu, & \mathbf{s}_\mu^y &= \mathbf{s}_\mu^z \times \mathbf{s}_\mu^x, \\ \mathbf{s}_0^x &= \frac{1}{\sqrt{6}}(-2, 1, 1), & \mathbf{s}_1^x &= \frac{1}{\sqrt{6}}(-2, -1, -1), \\ \mathbf{s}_2^x &= \frac{1}{\sqrt{6}}(2, 1, -1), & \mathbf{s}_3^x &= \frac{1}{\sqrt{6}}(2, -1, 1).\end{aligned}\quad (3.4)$$

Note, that this basis has the property that a $\frac{2\pi}{3}$ rotation around any local S^z axis of a tetrahedron in global coordinates corresponds to switching sublattices accordingly and rotating the local spins $\frac{2\pi}{3}$ around the new local z spin axis. This is equivalent to rotating the local spin basis $(-\frac{2\pi}{3})$ around the new local z spin axis.

3.2 Brillouin Zone

For the standard unit cell (Fig. 3.1a) the lattice vectors are given by Eq. (3.2), the reciprocal lattice basis vectors are defined by

$$b_1 = 2\pi(-1, 1, 1), \quad b_2 = 2\pi(1, -1, 1), \quad b_3 = 2\pi(1, 1, -1) \quad (3.5)$$

and the Brillouin zone is the standard fcc Brillouin zone with volume $\text{Vol}_{\text{B.Z.}} = 32\pi^3$. For the enlarged unit cell the lattice vectors are given by $a_1, 2a_2, 2a_3$ and the reciprocal lattice vectors are given by $b_1, \frac{b_2}{2}, \frac{b_3}{2}$. Therefore, the Brillouin zone is a non standard base-centered orthorhombic (orcc) Brillouin zone with volume $\text{Vol}_{\text{B.Z.}} = 8\pi^3$. It can be defined by the following system of inequalities:

$$|k_x| \leq \pi, \quad |k_y + k_z| \leq 2\pi, \quad |k_x + k_z - k_y| \leq \frac{3}{2}\pi, \quad |k_x - k_z + k_y| \leq \frac{3}{2}\pi. \quad (3.6)$$

A plot of the Brillouin zones including their high symmetry path can be seen in Fig. 3.2. Tab. 3.1 list the high symmetry points of the orcc Brillouin zone.

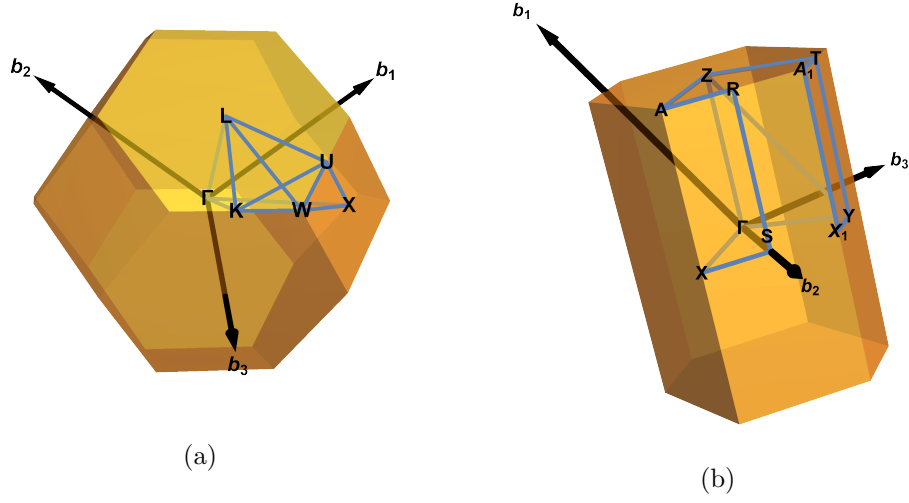


Figure 3.2: (a): Brillouin zone of the single unit cell including the high symmetry path. (b): Brillouin zone of the enlarged pyrochlore unit cell including the high symmetry path. The orcc Brillouin zone fits four times into the fcc Brillouin zone

Table 3.1: Table of high symmetry points of the Brillouin zone of pyrochlore lattice with enlarged unit cell.

	(k_x, k_y, k_z)		(k_x, k_y, k_z)
Γ	$\pi(0, 0, 0)$	T	$\pi(1, 1, 1)$
A	$\pi(0, \frac{1}{4}, \frac{7}{4})$	X	$\pi(0, \frac{-3}{4}, \frac{3}{4})$
A_1	$\pi(0, \frac{3}{4}, \frac{5}{4})$	X_1	$\pi(1, \frac{-1}{4}, \frac{1}{4})$
R	$\pi(\frac{1}{2}, \frac{1}{2}, \frac{3}{2})$	Y	$\pi(1, 0, 0)$
S	$\pi(\frac{1}{2}, \frac{-1}{2}, \frac{1}{2})$	Z	$\pi(0, 1, 1)$

3.3 Space Group Symmetries

The space group of the pyrochlore lattice is $Fd\bar{3}m$ (No.227). It is generated by the translations T_1, T_2, T_3 along the lattice vectors, a sixfold roto-reflection \bar{C}_6 around the S_0^z axis and a screw operation S [18]. In addition to these lattice symmetries we want to consider time-reversal symmetry \mathcal{T} which commutes with all space like symmetries and satisfies $\mathcal{T}^2 = -1$. The space group generators transform the different coordinates as follows:

$$T_i \mathbf{r}_\mu = (r_1 + \delta_{i,1}, r_2 + \delta_{i,2}, r_3 + \delta_{i,3})_\mu, \quad (3.7a)$$

$$\bar{C}_6 \mathbf{r}_\mu = (-r_3 - \delta_{\mu,3}, -r_1 - \delta_{\mu,1}, -r_2 - \delta_{\mu,2})_{\pi_{123}(\mu)}, \quad (3.7b)$$

$$S \mathbf{r}_\mu = (-r_1 - \delta_{\mu,1}, -r_2 - \delta_{\mu,2}, r_1 + r_2 + r_3 + 1 - \delta_{\mu,0})_{\mu + \delta_{\mu,3} - \delta_{\mu,0}}, \quad (3.7c)$$

$$I \mathbf{r}_\mu = (-r_1, -r_2, -r_3)_\mu, \quad (3.7d)$$

$$\mathcal{T} \mathbf{r}_\mu = \mathbf{r}_\mu, \quad (3.7e)$$

3. The Pyrochlore Lattice and its Symmetries

where $\pi_{123}(\mu)$ is the cyclic permutation of 1, 2, 3 and leaves $\mu = 0$ invariant. μ is always seen modulo 4. Due to the local spin basis the spin transforms like:

$$T_i \mathbf{S}_\mu = (S^x, S^y, S^z)_\mu, \quad (3.8a)$$

$$\bar{C}_6 \mathbf{S}_\mu = \left(-\frac{S^x}{2} - \frac{\sqrt{3}S^y}{2}, \frac{\sqrt{3}S^x}{2} - \frac{S^y}{2}, S^z \right)_{\pi_{123}(\mu)}, \quad (3.8b)$$

$$S \mathbf{S}_\mu = \left(\frac{S^x}{2} - \frac{\sqrt{3}S^y}{2}, -\frac{\sqrt{3}S^x}{2} - \frac{S^y}{2}, -S^z \right)_{\mu+\delta_{\mu,3}-\delta_{\mu,0}}, \quad (3.8c)$$

$$I \mathbf{S}_\mu = \mathbf{S}_\mu, \quad (3.8d)$$

$$\mathcal{T} \mathbf{S}_\mu = (-S^x, -S^y, -S^z)_\mu. \quad (3.8e)$$

When using the Schwinger boson spin representation $\hat{S}_i^m = \frac{1}{2} \hat{b}_i^\dagger \sigma^m \hat{b}_i$, the bosonic operators transform like $\mathcal{O}(\hat{S}_i^m) = \frac{1}{2} \hat{b}_{\mathcal{O}(i)}^\dagger U_{\mathcal{O}} \sigma^m U_{\mathcal{O}}^\dagger \hat{b}_{\mathcal{O}(i)}$ under action of a space group element \mathcal{O} and like $\mathcal{T}(\hat{S}_i^m) = \frac{1}{2} \hat{b}_i^\dagger \mathcal{K} U_{\mathcal{T}} \sigma^m U_{\mathcal{T}}^\dagger \mathcal{K} \hat{b}_i$ under time reversal symmetry. $\mathcal{K} = \mathcal{K}^{-1}$ denotes complex conjugation to everything standing right to it. The $SU(2)$ matrices $U_{\mathcal{O}}$ associated with the symmetry operations are:

$$U_{\mathcal{T}} = i\sigma_2, \quad U_{\bar{C}_6} = U_{C_3} = e^{-\frac{i}{2} \frac{2\pi}{3} (0,0,1)\vec{\sigma}}, \quad U_{T_i} = \sigma_0, \quad (3.9)$$

$$U_{S,\mu} = (-1)^{1-\delta_{\mu,1}} e^{-\frac{i}{2} \frac{2\pi}{2} \left(\frac{-\sqrt{3}}{2}, \frac{1}{2}, 0 \right) \vec{\sigma}}.$$

$\vec{\sigma} = (\sigma_1, \sigma_2, \sigma_3)$ is the Pauli vector. The matrix for the screw operation depends on which sublattice it acts on. Spins on sublattice 1 are rotated the other way around than spins on sublattice 2. Spins on sublattices 0 and 3 are rotated and then projected onto the local spin basis of the other sublattice. This results in an effective π rotation about the $(\frac{-\sqrt{3}}{2}, \frac{1}{2}, 0)$ axis. The sign of the effective rotation can be chosen freely and different signs correspond to different gauges. Here we choose the signs of rotation to be equal on sublattice 0, 2, 3.

The symmetry group generators fulfill the following algebraic relations

$$T_i T_{i+1} T_i^{-1} T_{i+1}^{-1} = 1, \quad (3.10a)$$

$$\bar{C}_6^6 = 1, \quad (3.10b)$$

$$S^2 T_3^{-1} = 1, \quad (3.10c)$$

$$\bar{C}_6 T_i \bar{C}_6^{-1} T_{i+1} = 1, \quad (3.10d)$$

$$S T_i S^{-1} T_3^{-1} T_i = 1, \quad i \in \{1, 2\}, \quad (3.10e)$$

$$S T_3 S^{-1} T_3^{-1} = 1, \quad (3.10f)$$

$$(\bar{C}_6 S)^4 = 1, \quad (3.10g)$$

$$(\bar{C}_6^3 S)^2 = 1, \quad (3.10h)$$

$$\mathcal{T}^2 = -1, \quad (3.10i)$$

$$\mathcal{T} \mathcal{O} \mathcal{T}^{-1} \mathcal{O}^{-1} = 1. \quad (3.10j)$$

where $i \in \{1, 2, 3\}$ and $i + 3 = i$. Eq. (3.10e) is valid for $i \in \{1, 2\}$ only. \mathcal{O} is a placeholder for an arbitrary space group generator: $\mathcal{O} \in \{T_1, T_2, T_3, \bar{C}_6, S\}$.

Schwinger Boson Mean Field Theory and Projective Symmetry Group

In this Chapter we introduce the formalism of how to construct and classify possible spin liquid states starting from a nearest neighbor spin Hamiltonian.

4.1 From Spin Hamiltonian to Mean Field Ansatz

We want to treat some general nearest neighbor spin Hamiltonian like

$$H = \sum_{\langle i,j \rangle} \hat{\mathbf{S}}_i J_{ij} \hat{\mathbf{S}}_j \quad (4.1)$$

in Schwinger boson mean field theory (SBMFT) where J_{ij} is a coupling tensor and the sum runs over nearest neighbour bonds on a lattice. We will use the Schwinger boson representation of the spin operators:

$$\hat{S}_i^\gamma = \frac{1}{2} \hat{b}_i^\dagger \sigma^\gamma \hat{b}_i \quad (4.2)$$

where $\hat{b} = \begin{pmatrix} \hat{b}_{i,\uparrow} \\ \hat{b}_{i,\downarrow} \end{pmatrix}$ are bosonic annihilation operators satisfying $[\hat{b}_{i,\alpha}, \hat{b}_{j,\beta}^\dagger] = \delta_{ij} \delta_{\alpha,\beta}$ and σ^m are the Pauli matrices. This representation is only faithful if we constrain the boson density per site to $2\mathcal{S}$:

$$\hat{n}_i = \hat{b}_i^\dagger \hat{b}_i = 2\mathcal{S}. \quad (4.3)$$

This limits the new Hilbert space to two states per site and ensures that the well known spin relation $\hat{\mathbf{S}}_i \hat{\mathbf{S}}_i = \frac{\hat{n}_i}{2} (\frac{\hat{n}_i}{2} + 1) = \mathcal{S}(\mathcal{S} + 1)$ is fulfilled. This can be done by adding a site dependent Lagrange multiplier $\sum_i \lambda_i (\hat{n}_i - 2\mathcal{S})$ [32] to the Hamiltonian. At this point it is possible to parametrize the Hamiltonian in terms of the hopping singlet \hat{B}_{ij} and hopping triplet \hat{t}_{ij}^h as well as pairing singlet \hat{A}_{ij} and pairing triplet

$\hat{t}_{ij}^{p,x}$ operators ($\gamma \in \{x, y, z\}$)

$$\begin{aligned}\hat{B}_{ij} &= \frac{1}{2} \hat{b}_i^\dagger \hat{b}_j, & \hat{A}_{ij} &= \frac{1}{2} \hat{b}_i (i\sigma^2) \hat{b}_j, \\ \hat{t}_{ij}^{h,\gamma} &= \frac{i}{2} \hat{b}_i^\dagger \sigma^\gamma \hat{b}_j, & \hat{t}_{ij}^{p,\gamma} &= -\frac{i}{2} \hat{b}_i (\sigma^\gamma \cdot i\sigma^2) \hat{b}_j.\end{aligned}\quad (4.4)$$

This results in

$$H = \sum_{\langle i,j \rangle} : \hat{\mathbf{h}}_{ij}^\dagger J_{ij}^h \hat{\mathbf{h}}_{ij} : + \hat{\mathbf{p}}_{ij}^\dagger J_{ij}^p \hat{\mathbf{p}}_{ij} + C_{ij} + \sum_i \lambda_i (\hat{n}_i - 2\mathcal{S}) \quad (4.5)$$

where $\hat{\mathbf{h}}_{ij}^\dagger = (\hat{B}_{ij}^\dagger, \hat{t}_{ij}^{h,x^\dagger}, \hat{t}_{ij}^{h,y^\dagger}, \hat{t}_{ij}^{h,z^\dagger})$ and $\hat{\mathbf{p}}_{ij}^\dagger = (\hat{A}_{ij}^\dagger, \hat{t}_{ij}^{p,x^\dagger}, \hat{t}_{ij}^{p,y^\dagger}, \hat{t}_{ij}^{p,z^\dagger})$. J_{ij}^h and J_{ij}^p are the hopping and pairing coupling matrices that depend on J_{ij} . $:$ denotes normal ordering. Note, that the parametrization in Eq. (4.5) is not unique since for $i \neq j$:

$$: \hat{B}_{ij}^\dagger \hat{B}_{ij} : + \hat{A}_{ij}^\dagger \hat{A}_{ij} =: \hat{t}_{ij}^{h,\gamma^\dagger} \hat{t}_{ij}^{h,\gamma} : + \hat{t}_{ij}^{p,\gamma^\dagger} \hat{t}_{ij}^{p,\gamma} = \frac{1}{4} \hat{n}_i \hat{n}_j = \mathcal{S}^2. \quad (4.6)$$

In the last equality we explicitly use the boson density constraint (Eq. (4.3)). At least in the case where J_{ij}^h and J_{ij}^p are diagonal it is therefore possible to parametrize the Hamiltonian only using either hopping or pairing operators. The resulting Hamiltonian in Eq. (4.5) is quartic in bosonic operators. To treat it we make two standard approximations: Firstly, we only consider a site independent Lagrange multiplier $\lambda_i = \lambda$. This results in the boson density constraint (Eq. (4.3)) being fulfilled only on average. Secondly, we employ the standard mean field approximation and ignore quadratic fluctuations around the mean value of the operators which means neglecting the last term in Eqs. (4.7).

$$\begin{aligned}: \hat{\mathbf{h}}_{ij}^\dagger J_{ij}^h \hat{\mathbf{h}}_{ij} : &= \hat{\mathbf{h}}_{ij}^\dagger J_{ij}^h \mathbf{h}_{ij} + \mathbf{h}_{ij}^\dagger J_{ij}^h \hat{\mathbf{h}}_{ij} - \mathbf{h}_{ij}^\dagger J_{ij}^h \mathbf{h}_{ij} + (\hat{\mathbf{h}}_{ij} - \mathbf{h}_{ij})^\dagger J_{ij}^h (\hat{\mathbf{h}}_{ij} - \mathbf{h}_{ij}), \\ \hat{\mathbf{p}}_{ij}^\dagger J_{ij}^p \hat{\mathbf{p}}_{ij} &= \hat{\mathbf{p}}_{ij}^\dagger J_{ij}^p \mathbf{p}_{ij} + \mathbf{p}_{ij}^\dagger J_{ij}^p \hat{\mathbf{p}}_{ij} - \mathbf{p}_{ij}^\dagger J_{ij}^p \mathbf{p}_{ij} + (\hat{\mathbf{p}}_{ij} - \mathbf{p}_{ij})^\dagger J_{ij}^p (\hat{\mathbf{p}}_{ij} - \mathbf{p}_{ij})\end{aligned}\quad (4.7a)$$

where

$$\mathbf{h}_{ij}^\dagger = \langle \hat{\mathbf{h}}_{ij}^\dagger \rangle = (\mathcal{B}_{ij}^*, t_{ij}^{h,x^*}, t_{ij}^{h,y^*}, t_{ij}^{h,z^*}) \quad (4.8a)$$

$$\mathbf{p}_{ij}^\dagger = \langle \hat{\mathbf{p}}_{ij}^\dagger \rangle = (\mathcal{A}_{ij}^*, t_{ij}^{p,x^*}, t_{ij}^{p,y^*}, t_{ij}^{p,z^*}). \quad (4.8b)$$

Note, that there are cases in the literature where the hopping fields are not mean field decoupled in normal ordered form, as we have done here, but where a constant of $-\frac{\mathcal{S}}{2} \text{Tr}(J_{i,j}^h)$ is added to the Hamiltonian [33]. Following the original SBMFT paper by Arovas and Auerbach [34] we do not apply this here. Adding such a constant leads to a wrong result for the ferromagnetic zero temperature ground state energy. This leaves us with a Hamiltonian that is quadratic in ladder operators:

$$H = \sum_{\langle i,j \rangle} \hat{b}_i^\dagger u_{ij}^h \hat{b}_j + \hat{b}_i^\dagger u_{ij}^p \hat{b}_j^\dagger + \text{h.c.} + f(\mathbf{h}_{ij}, \mathbf{p}_{ij}) + \lambda \sum_i (\hat{b}_i^\dagger \hat{b}_i - 2\mathcal{S}). \quad (4.9)$$

Here, h.c. labels the hermitian conjugate terms and f is given by

$$f(\mathbf{h}_{ij}, \mathbf{p}_{ij}) = -\mathbf{h}_{ij}^\dagger J_{ij}^h \mathbf{h}_{ij} - \mathbf{p}_{ij}^\dagger J_{ij}^p \mathbf{p}_{ij} + C_{ij} \quad (4.10)$$

while u_{ij}^h and u_{ij}^p are complex 2×2 matrices defined by

$$\begin{aligned} u_{ij}^h &= \frac{1}{2} \sum_{m=0}^3 i^{1-\delta_{m,0}} (\mathbf{h}_{ij}^\dagger J_{ij}^h)^m \sigma^m := a_{ij}^h \sigma^0 + i(b_{ij}^h \sigma^1 + c_{ij}^h \sigma^2 + d_{ij}^h \sigma^3) \\ &:= (a_{ij}^h, b_{ij}^h, c_{ij}^h, d_{ij}^h)^h, \end{aligned} \quad (4.11a)$$

$$\begin{aligned} u_{ij}^p &= \frac{1}{2} \sum_{m=0}^3 i^{1-\delta_{m,0}} (J_{ij}^p \mathbf{p}_{ij})^m \sigma^m (i\sigma^2) := a_{ij}^p i\sigma^2 + i(b_{ij}^p \sigma^1 + c_{ij}^p \sigma^2 + d_{ij}^p \sigma^3)(i\sigma^2) \\ &:= (a_{ij}^p, b_{ij}^p, c_{ij}^p, d_{ij}^p)^p. \end{aligned} \quad (4.11b)$$

This notation, that we have adapted from Liu et al. [18], is particularly helpful since a_{ij}^h and a_{ij}^p transform as scalars while $(b_{ij}^h, c_{ij}^h, d_{ij}^h)$ and $(b_{ij}^p, c_{ij}^p, d_{ij}^p)$ transform as $SO(3)$ vectors. The parameters a_{ij}^h to d_{ij}^h are functions of the mean fields h_{ij} and the coupling matrix J^h , while the parameters a_{ij}^p to d_{ij}^p are functions of the mean fields p_{ij} and the coupling matrix J^p . When exchanging $i \leftrightarrow j$ the matrices transform like $u_{ji}^h = (u_{ij}^h)^\dagger$ and $u_{ji}^p = (u_{ij}^p)^\top$ and the parameters transform like $(a_{ji}^h, b_{ji}^h, c_{ji}^h, d_{ji}^h) = (a_{ij}^{h*}, -b_{ij}^{h*}, -c_{ij}^{h*}, -d_{ij}^{h*})$ and $(a_{ji}^p, b_{ji}^p, c_{ji}^p, d_{ji}^p) = (-a_{ij}^p, b_{ij}^p, c_{ij}^p, d_{ij}^p)$. The set of matrices u_{ij}^h and u_{ij}^p or rather the set of expectation values \mathbf{h}_{ij} and \mathbf{p}_{ij} are known as the mean field ansatz. Once an ansatz is chosen, the Hamiltonian from Eq. (4.9) can be diagonalized by a Bogoliubov transform and a ground state can be constructed. The values of \mathbf{h}_{ij} and \mathbf{p}_{ij} have to be solved self consistently:

$$\mathbf{h}_{ij} = \langle \hat{\mathbf{h}}_{ij} \rangle, \quad \mathbf{p}_{ij} = \langle \hat{\mathbf{p}}_{ij} \rangle, \quad 2\mathcal{S} = \frac{1}{N} \sum_i \langle \hat{n}_i \rangle. \quad (4.12)$$

This is equivalent to finding the saddle point of the ground state energy E_0 :

$$\frac{\partial E_0}{\partial \mathbf{h}_{ij}^m} = 0, \quad \frac{\partial E_0}{\partial \mathbf{p}_{ij}^m} = 0, \quad \frac{\partial E_0}{\partial \lambda} = 0. \quad (4.13)$$

This will be further discussed in Chapt. 5.3

First, we have to choose a meaningful mean field ansatz. We are interested in finding spin liquid states that break either neither lattice symmetries nor time reversal symmetry (symmetric spin liquids) or break time reversal symmetry as well as lattice symmetries modulo time reversal (weakly symmetric spin liquids). Our mean field ansatz should reflect these properties.

A formal way to classify all possible mean field ansätze that satisfy a given set of symmetries is the projective symmetry group (PSG) treatment. It was first introduced by Wen for Abrikosov's Fermions and is summarised in his book [2, Chapter 9]. It was later generalised for symmetric Schwinger Bosons spin liquids by Wang and Vishwanath [32]. A generalization to weakly symmetric Schwinger Boson spin liquids was given by Messio et al. [19].

4.2 Projective Symmetry Group: Symmetric Ansatz

We want to construct a mean field ansatz that respects all lattice symmetries χ of the pyrochlore lattice as well as time reversal symmetry \mathcal{T} . The naive way of

doing this would be to fix matrices u_{ij}^h and u_{ij}^p on one bond and construct all other matrices by action of symmetry operators \mathcal{O}

$$u_{\mathcal{O}(ij)}^h = U_{\mathcal{O}} u_{ij}^h U_{\mathcal{O}}^\dagger, \quad (4.14a)$$

$$u_{\mathcal{O}(ij)}^p = U_{\mathcal{O}} u_{ij}^p U_{\mathcal{O}}^\dagger. \quad (4.14b)$$

While this is in fact a valid ansatz, it is by far not the only one. The reason for this is that the spin representation (4.2) has a $U(1)$ gauge redundancy. It is symmetric under multiplication of the ladder operators with a phase:

$$G : \hat{b}_j \rightarrow \hat{b}_j e^{i\phi[j]}. \quad (4.15)$$

This means every symmetry operation (including time reversal) is in generally accompanied by a gauge transformation $G_{\mathcal{O}}$. Let us define the gauge enriched operators as

$$\tilde{\mathcal{O}} = G_{\mathcal{O}} \mathcal{O} : \hat{b}_j \rightarrow e^{i\phi_{\mathcal{O}}[\mathcal{O}(j)]} U_{\mathcal{O}}^\dagger \hat{b}_{\mathcal{O}(j)}. \quad (4.16)$$

The mean field ansatz in Eq. (4.9) transforms like

$$u_{\mathcal{O}(ij)}^h = U_{\mathcal{O}} u_{ij}^h U_{\mathcal{O}}^\dagger e^{-i(\phi_{\mathcal{O}}[\mathcal{O}(i)] - \phi_{\mathcal{O}}[\mathcal{O}(j)])}, \quad (4.17a)$$

$$u_{\mathcal{O}(ij)}^p = U_{\mathcal{O}} u_{ij}^p U_{\mathcal{O}}^\dagger e^{-i(\phi_{\mathcal{O}}[\mathcal{O}(j)] + \phi_{\mathcal{O}}[\mathcal{O}(i)])}. \quad (4.17b)$$

The PSG is defined as the set of operators $\tilde{\mathcal{O}}$ that leaves a mean field ansatz invariant. There is a subgroup of the PSG of pure gauge transformations called the invariant gauge group (IGG). These formally accompany the symmetry operator $\mathbb{1}$. For a general ansatz on a frustrated lattice, Eqs. (4.17) indicate that the IGG can only be \mathbb{Z}_2 when including both nonzero u_{ij}^h and u_{ij}^p . For only nonzero u_{ij}^h the IGG can be $U(1)$ [32]. We are interested in ansätze with hopping as well as pairing terms. Therefore, we only consider the case $\text{IGG} = \mathbb{Z}_2$. Note, that on a bipartite lattice it is possible to define phases with different signs on neighboring sublattices and the IGG can therefore be $U(1)$ for nonzero u_{ij}^p .

To find all gauge inequivalent mean field ansätze we first have to find all distinct PSGs that are compatible with the symmetry group. In other words, we have to find all gauge inequivalent sets of symmetry enriched operators $\tilde{\mathcal{O}}$. The algebraic relations between the symmetry operators (e.g. Eq. (3.10)) greatly constrain the possible PSGs. Therefore, the set of all PSG equivalent classes is called algebraic PSG [35]. We can find the algebraic PSG by promoting the symmetry operators (including the identity operators) to symmetry enriched operators. Algebraic relations like $\mathcal{O}_1 \mathcal{O}_2 \cdots \mathcal{O}_n = \mathbb{1}$ transform to:

$$\tilde{\mathcal{O}}_1 \tilde{\mathcal{O}}_2 \cdots \tilde{\mathcal{O}}_n = G_{\mathcal{O}_1} \mathcal{O}_1 G_{\mathcal{O}_2} \mathcal{O}_2 \cdots G_{\mathcal{O}_n} \mathcal{O}_n \in \mathbb{Z}_2 \quad (4.18)$$

These new symmetry enriched algebraic relations can then be solved for the gauge transformations $G_{\mathcal{O}}$. It is helpful to rewrite Eq. (4.18) as

$$G_{\mathcal{O}_1} (\mathcal{O}_1 G_{\mathcal{O}_2} \mathcal{O}_1^{-1}) (\mathcal{O}_1 \mathcal{O}_2 G_{\mathcal{O}_3} \mathcal{O}_2^{-1} \mathcal{O}_1^{-1}) \cdots \in \mathbb{Z}_2 \quad (4.19)$$

and use

$$\mathcal{O}_i G_{\mathcal{O}_j} \mathcal{O}_i^{-1} : \hat{b}_i \rightarrow e^{i\phi_{\mathcal{O}_j}[\mathcal{O}_i^{-1}(i)]} \hat{b}_i. \quad (4.20)$$

This way Eq. (4.18) can be written as a phase equation:

$$\phi_{\mathcal{O}_1}[i] + \phi_{\mathcal{O}_2}[\mathcal{O}_1^{-1}(i)] + \phi_{\mathcal{O}_3}[\mathcal{O}_2^{-1}(\mathcal{O}_1^{-1}(i))] + \dots = n\pi, \quad (4.21)$$

where $n \in \{0, 1\}$.

To find the algebraic PSG for a symmetry group χ we have to list all algebraic relations and solve all emerging phase equations for the phases $\phi_{\mathcal{O}}$. Under a general gauge transformation all phases transform like

$$\phi_{\mathcal{O}_i}[i] \rightarrow \phi_{\mathcal{O}_i}[i] + \phi[i] - \phi[\mathcal{O}_i^{-1}i]. \quad (4.22)$$

Therefore, two seemingly distinct PSGs might actually be gauge equivalent. It is thus helpful to fix the gauge when solving the phase equations to ensure finding only gauge inequivalent PSGs. The algebraic \mathbb{Z}_2 PSG for pyrochlores point symmetry group $Fd\bar{3}m$ was solved by Liu et al. [18]. They found 16 different PSG equivalent classes defined by the phases:

$$\phi_{T_1}[\mathbf{r}_\mu] = 0, \quad (4.23a)$$

$$\phi_{T_2}[\mathbf{r}_\mu] = n_3\pi r_1, \quad (4.23b)$$

$$\phi_{T_3}[\mathbf{r}_\mu] = n_3\pi(r_1 + r_2), \quad (4.23c)$$

$$\phi_{\mathcal{T}}[\mathbf{r}_\mu] = 0, \quad (4.23d)$$

$$\begin{aligned} \phi_{\bar{C}_6}[\mathbf{r}_\mu] &= \delta_{\mu,1,2,3}(n_{ST_1} - n_3)\pi - r_1\delta_{\mu,\{2,3\}}n_3\pi \\ &\quad - r_2n_{\bar{C}_6T_1}\pi - r_3\delta_{\mu,2}n_3\pi - n_3\pi(r_1r_2 + r_1r_3), \end{aligned} \quad (4.23e)$$

$$\begin{aligned} \phi_S[\mathbf{r}_\mu] &= ((-)^{\mu,1,2,3}\frac{(n_{ST_1} - n_3)}{2} + \delta_{\mu,2}n_{\bar{C}_6S})\pi \\ &\quad + r_1\pi(n_3\delta_{\mu,1,2} - n_{ST_1}) + r_2\pi(n_3\delta_{\mu,2} - n_{ST_1}) \\ &\quad + r_3\pi n_3\delta_{\mu,1,2} - \frac{n_3\pi}{2}(r_1 + r_2)(r_1 + r_2 + 1), \end{aligned} \quad (4.23f)$$

where $n_3, n_{ST_1}, n_{\bar{C}_6S}, n_{\bar{C}_6}$ are all \mathbb{Z}_2 parameters that are either 0 or 1. We label the ansätze with $n_3\pi - (n_{\bar{C}_6S}n_{ST_1}n_{\bar{C}_6})$. When $n_3 = 1$ translation is non trivial and the unit cell is enlarged (see Fig. 3.1b). This results in spinons picking up an Aharonov-Bohm phase of π when moving around a hexagonal plaquette and the corresponding spin liquid states are thus dubbed π -flux states. The parameters $n_{ST_1}, n_{\bar{C}_6S}, n_{\bar{C}_6}$ can also be identified with Aharonov-Bohm phase of $n_{ST_1}\pi, n_{\bar{C}_6S}\pi, n_{\bar{C}_6}\pi$ respectively around different paths. For a detailed description see [18].

The next step is to construct all possible mean field ansätze that are compatible with Eq. (4.23): After choosing one of the PSG equivalence classes from the algebraic PSG we fix the matrices $u_{ij}^h = (a^h, b^h, c^h, d^h)^h$ and $u_{ij}^p = (a^p, b^p, c^p, d^p)^p$ for the bond $i = \mathbf{0}_0, j = \mathbf{0}_1$. Since we want the mean field ansatz to respect time reversal symmetry and the ansatz transforms as $\mathcal{T}(a^h, b^h, c^h, d^h)^h \rightarrow (a^{h*}, b^{h*}, c^{h*}, d^{h*})^h$ and equivalently for pairing terms, all parameters a^h (a^p) to d^h (d^p) have to be real. We can then use Eqs. (4.17) to map the hopping and pairing matrices onto all other bonds. A list of space group elements \mathcal{O} to do this can be found in [18, Appendix A]. All space group elements, that map the bond onto itself, constrain which parameters of u_{ij}^h and u_{ij}^p can be non zero depending on the chosen ansatz. An analysis of this

has been done by Liu et al. [18] in the global spin basis. We are, however, interested in the local basis. We transform their solution to the local spin basis by

$$(a_l^h, b_l^h, c_l^h, d_l^h)^h = U_0(a_g^h, b_g^h, c_g^h, d_g^h)^h U_1^\dagger. \quad (4.24)$$

Where the subscripts l and g are for “local” and “global” respectively. The matrices U_μ are the $SU(2)$ matrices corresponding to the transformation from global to local spin basis on sublattice μ . They are specified in Appendix A.

Using Eq. (4.24) gives us

$$a_l = -b_g, \quad (4.25a)$$

$$b_l = \frac{1}{\sqrt{6}}(-2a_g + c_g - d_g), \quad (4.25b)$$

$$c_l = \frac{1}{\sqrt{2}}(c_g + d_g), \quad (4.25c)$$

$$d_l = \frac{1}{\sqrt{3}}(a_g + c_g - d_g). \quad (4.25d)$$

Based on Eq. (4.25) we can translate their solution into Tab. 4.1. It lists all independent non zero parameters for nearest neighbor as well as possible next nearest neighbor and on-site parameters. The fixed parameters are defined as follows:

On-site bond: $i = \mathbf{0}_0, j = \mathbf{0}_0$

$$u_{\mathbf{0}_0\mathbf{0}_0}^h = (\alpha^h, \beta^h, \gamma^h, \delta^h)^h, \quad (4.26)$$

$$u_{\mathbf{0}_0\mathbf{0}_0}^p = (\alpha^p, \beta^p, \gamma^p, \delta^p)^p. \quad (4.27)$$

Nearest neighbor (NN) bond: $i = \mathbf{0}_0, j = \mathbf{a}_1$

$$u_{\mathbf{0}_0\mathbf{0}_1}^h = (a^h, b^h, c^h, d^h)^h, \quad (4.28)$$

$$u_{\mathbf{0}_0\mathbf{0}_1}^p = (a^p, b^p, c^p, d^p)^p. \quad (4.29)$$

Next-nearest neighbour (NNN) bond: $i = \mathbf{0}_1, j = \mathbf{0}_0 - \mathbf{a}_2$

$$u_{\mathbf{0}_1\mathbf{0}_2-\mathbf{a}_2}^h = (A^h, B^h, C^h, D^h)^h, \quad (4.30)$$

$$u_{\mathbf{0}_1\mathbf{0}_2-\mathbf{a}_2}^p = (A^p, B^p, C^p, D^p)^p. \quad (4.31)$$

4.3 Weakly Symmetric Ansätze

Weakly symmetric spin liquids break time reversal symmetry and some lattice symmetries modulo a global spin flip (action of time reversal symmetry). In the classical limit $\mathcal{S} \rightarrow \infty$ they correspond to non-coplanar spin states (such that $\langle \hat{S}_i(\hat{S}_j \times \hat{S}_k) \rangle \neq 0$). To construct a weakly symmetric ansatz, we start by defining a parity $\epsilon_{\mathcal{O}}$ for each symmetry operator $\mathcal{O} \in \chi$. $\epsilon_{\mathcal{O}} = 1$ when an ansatz respects the symmetry and $\epsilon_{\mathcal{O}} = -1$ when \mathcal{O} maps the system to its time reversed state. Let us define the subset χ_e of all symmetry operators that necessarily have even parity $\epsilon_{\mathcal{O}} = 1$ and the set of operators with undetermined parity as $\chi_o = (\chi - \chi_e)$. χ_e contains at least all squares of symmetry operators $T_1^2, T_2^2, T_3^2, S^2, \overline{C}_6^2 = C_3^{-1}$ since

$n_3\pi - (n_{\bar{C}_6S} n_{ST_1} n_{\bar{C}_6})$	On-Site	NN	NNN	Constraints
0-(000)	α^h	b^h, d^h	A^h, B^h, D^h, B^p	$B^h = \frac{C^h}{\sqrt{3}}, B^p = -\sqrt{3}C^p$
0-(001)	α^h	b^h, d^h, a^p	A^h, B^h, D^h, B^p	$B^h = \frac{C^h}{\sqrt{3}}, B^p = -\sqrt{3}C^p$
0-(010)	α^h, δ^p	b^h, d^h, a^p	$A^h, B^h, D^h, A^p, B^p, D^p$	$B^h = \frac{C^h}{\sqrt{3}}, B^p = \frac{C^p}{\sqrt{3}}$
0-(011)	α^h	b^h, d^h	$A^h, B^h, D^h, A^p, B^p, D^p$	$B^h = \frac{C^h}{\sqrt{3}}, B^p = \frac{C^p}{\sqrt{3}}$
0-(100)	α^h	a^h, c^p	A^h, B^h, D^h, B^p	$B^h = \frac{C^h}{\sqrt{3}}, B^p = -\sqrt{3}C^p$
0-(101)	α^h	a^h, b^p, d^p	A^h, B^h, D^h, B^p	$B^h = \frac{C^h}{\sqrt{3}}, B^p = -\sqrt{3}C^p$
0-(110)	α^h, δ^p	a^h, b^p, d^p	$A^h, B^h, D^h, A^p, B^p, D^p$	$B^h = \frac{C^h}{\sqrt{3}}, B^p = \frac{C^p}{\sqrt{3}}$
0-(111)	α^h	a^h, c^p	$A^h, B^h, D^h, A^p, B^p, D^p$	$B^h = \frac{C^h}{\sqrt{3}}, B^p = \frac{C^p}{\sqrt{3}}$
π -(000)	α^h, δ^p	b^h, d^h, a^p	B^h, B^p	$B^h = -\sqrt{3}C^h, B^p = -\sqrt{3}C^p$
π -(001)	α^h	b^h, d^h	B^h, B^p	$B^h = -\sqrt{3}C^h, B^p = -\sqrt{3}C^p$
π -(010)	α^h	b^h, d^h	B^h, A^p, B^p, D^p	$B^h = -\sqrt{3}C^h, B^p = \frac{C^p}{\sqrt{3}}$
π -(011)	α^h	b^h, d^h, a^p	B^h, A^p, B^p, D^p	$B^h = -\sqrt{3}C^h, B^p = \frac{C^p}{\sqrt{3}}$
π -(100)	α^h, δ^p	a^h, b^p, d^p	B^h, B^p	$B^h = -\sqrt{3}C^h, B^p = -\sqrt{3}C^p$
π -(101)	α^h	a^h, c^p	B^h, B^p	$B^h = -\sqrt{3}C^h, B^p = -\sqrt{3}C^p$
π -(110)	α^h	a^h, c^p	B^h, A^p, B^p, D^p	$B^h = -\sqrt{3}C^h, B^p = \frac{C^p}{\sqrt{3}}$
π -(111)	α^h	a^h, b^p, d^p	B^h, A^p, B^p, D^p	$B^h = -\sqrt{3}C^h, B^p = \frac{C^p}{\sqrt{3}}$

Table 4.1: All independent non-zero on-site, nearest neighbor and next-nearest neighbor parameters for the different PSG equivalence classes in the local spin basis. Bonds are fixed on $\mathbf{0}_0 \rightarrow \mathbf{0}_0, \mathbf{0}_0 \rightarrow \mathbf{0}_1, \mathbf{0}_1 \rightarrow \mathbf{0}_2 - \mathbf{a}_2$. All other parameters are constrained to be zero. The table can be translated from [18, Tab. 2] by using Eq. (4.25).

their parities are $\epsilon_{\mathcal{O}} = (\pm 1)^2 = 1$. Since $S^2 = T_3$ modulo a 2π spin rotation, we will drop S^2 from the set of generators.

Now we can translate the algebraic relations (Eq. (3.10)) into equations for the parity to find more generators of χ_e . The nontrivial equations are:

$$\epsilon_{S^2} \epsilon_{T_3} = 1, \quad (4.32a)$$

$$\epsilon_{C_3} \epsilon_{T_i} = \epsilon_{T_{i+1}} \epsilon_{C_3}. \quad (4.32b)$$

Eq. (4.32a) shows that T_3 has even parity. Therefore, Eq. (4.32b) implies that this is also true for T_1 and T_2 . The parities of \bar{C}_6 and S stay undetermined. This concludes the treatment by Messio et al. [19]. We are, however, still missing one generator of χ_e . In general, once generators of even and undetermined parity are found by inspecting the algebraic group relations of the full symmetry group, we also have to consider operators of the form $\mathcal{O}_o^{-1} \mathcal{O}_e \mathcal{O}_o$ where $\mathcal{O}_o \in \chi_o$ and $\mathcal{O}_e \in \chi_e$. With this approach we can construct the symmetry operator $C'_3 := ISC_3IS = S^{-1}C_3S$ which has $\epsilon_{C'_3} = \epsilon_S^2 \epsilon_I^2 \epsilon_{C_3} = 1$. C'_3 is a $\frac{2\pi}{3}$ rotation about the local S^z axis of sublattice 3 on the inverse tetrahedron. Since C'_3 cannot be written with combinations of $\{T_1, T_2, T_3, C_3\}$ we have to add it to the set of generators. $IC_3I = C_3$ gives no new generator and therefore χ_e is generated by $\{T_1, T_2, T_3, C_3, C'_3\}$ while $\bar{C}_6, S \in \chi_o$. The

algebraic relations of χ_e are

$$T_i T_{i+1} T_i^{-1} T_{i+1}^{-1} = 1, \quad (4.33a)$$

$$C_3^3 = 1, \quad (4.33b)$$

$$C_3'^3 = 1, \quad (4.33c)$$

$$(C_3 C_3')^2 = 1, \quad (4.33d)$$

$$C_3 T_i C_3^{-1} T_{i+1}^{-1} = 1, \quad (4.33e)$$

$$C_3' T_1 (C_3')^{-1} T_1 T_2^{-1} = 1, \quad (4.33f)$$

$$C_3' T_2 (C_3')^{-1} T_1 = 1, \quad (4.33g)$$

$$C_3' T_3 (C_3')^{-1} T_1 T_3^{-1} = 1, \quad (4.33h)$$

where $i = i + 3$. The chiral algebraic PSG is then defined as the algebraic PSG of χ_e . We solve the chiral algebraic PSG in Appendix B.

$$\phi_{T_1}[\mathbf{r}_\mu] = 0, \quad (4.34a)$$

$$\phi_{T_2}[\mathbf{r}_\mu] = n_3 \pi r_1, \quad (4.34b)$$

$$\phi_{T_3}[\mathbf{r}_\mu] = n_3 \pi (r_1 + r_2), \quad (4.34c)$$

$$\phi_{C_3}[\mathbf{r}_\mu] = \frac{2\pi k}{3} \delta_{\mu 0} + n_3 \pi (r_1 r_2 + r_1 r_3), \quad (4.34d)$$

$$\begin{aligned} \phi_{C_3'}[\mathbf{r}_\mu] = & -\frac{2\pi k}{3} \delta_{\mu 3} + \left(\frac{2\pi k}{3} + n_{C_3 C_3'} + n_{C_3' T_2}\right) (-\delta_{\mu 0} + \delta_{\mu 2}) \pi \\ & + r_1 \pi n_{C_3' T_2} + r_3 \pi \frac{r_3 - 1}{2} n_3 + n_3 \pi r_1 r_2 \\ & + r_2 \pi \left(\frac{r_2 - 1}{2} n_3 + n_{C_3' T_2}\right), \end{aligned} \quad (4.34f)$$

where $k \in \{-1, 0, 1\}$, $n_3, n_{C_3 C_3'}, n_{C_3' T_2} \in \{0, 1\}$ and one gauge choice left to set one field to be real. n_3 once again determines the size of the unit cell.

The next step is to find all compatible ansätze. Since elements of χ_e cannot map between main and inverse tetrahedra but from one bond on a main tetrahedron to every other bond on any main tetrahedron we have two independent bonds: One on a main and one on an inverse tetrahedron. We choose the bonds 01 ($\mathbf{0}_0 \rightarrow \mathbf{0}_1$) and I01 ($\mathbf{0}_0 \rightarrow \mathbf{0}_1 - \mathbf{a}_1$). We label the mean field parameters $(a_1^t, b_1^t, c_1^t, d_1^t)$ on bond 01 and $(a_2^t, b_2^t, c_2^t, d_2^t)$ on bond I01. With Eqs. (4.17) the mean field parameters of all other bonds can be calculated. The weakly symmetric ansätze can break \mathcal{T} , I and S while satisfying \mathcal{TI} and \mathcal{TS} . Therefore, the mean field parameters are complex numbers in general: $a_i^h = |a_i^h| e^{i\phi_{a_i^h}}, \dots, a_i^p = |a_i^p| e^{-i\phi_{a_i^h}}$. The different sign convention of the phases comes from the fact that a^h depends on \mathcal{B}^* while a^p depends on \mathcal{A} . We fix the mean field moduli on both bonds ($|a_1^t| = |a_2^t|, |b_1^t| = |b_2^t| \dots$) and find all possible ansätze that respect the PSG of χ_e by mapping the bonds 01 and I01 onto themselves with $S^{-1} C_3 S C_3$ (note, that this also flips the bond). For the 01 bond this results in

$$(a_1^h, b_1^h, c_1^h, d_1^h) = (-a_1^{h*}, b_1^{h*}, c_1^{h*}, d_1^{h*}) e^{-i\pi(\frac{4k}{3} + n_{C_3 C_3'} + n_{C_3' T_2})}, \quad (4.35)$$

$$(a_1^p, b_1^p, c_1^p, d_1^p) = (a_1^p, -b_1^p, -c_1^p, -d_1^p) e^{i\pi(n_{C_3 C_3'} + n_{C_3' T_2})}. \quad (4.36)$$

For the $I01$ bond this results in

$$(a^h, b^h, c^h, d^h) = (-a^{h*}, b^{h*}, c^{h*}, d^{h*}) e^{-i\pi(\frac{4\pi k}{3} + n_{C_3 C'_3})}, \quad (4.37)$$

$$(a^p, b^p, c^p, d^p) = (a^p, -b^p, -c^p, -d^p) e^{i\pi n_{C_3 C'_3}}. \quad (4.38)$$

For $n_{C'_3 T_2} = 1$ the pairing fields can be non zero on one tetrahedron and have to be zero on the other tetrahedron. Such ansätze break I and S as well as \mathcal{TI} and \mathcal{TS} and thus correspond to ansätze that we do not want to consider. Therefore, we set $n_{C'_3 T_2} = 0$ for the rest of the present work. This also means that a^p cannot appear in an ansatz together with b^p, c^p, d^p . Apart from this restriction all other combinations of hopping and pairing fields are allowed depending on the phases of a^h, b^h, c^h, d^h which will be determined by flux transformations. To find out which phases $\phi_{a_i}, \phi_{b_i} \dots$ are allowed, we have to consider the transformation of expectation values of gauge invariant products of field variables [19]. For example: $\hat{B}_{ij} \hat{B}_{jk} \hat{B}_{ki}$ or $\hat{A}_{ij} \hat{B}_{jk} \hat{A}_{ki}^\dagger$. These are analogous to the Wilson loop operators in gauge theory. The loop operators are directly related to products of spins and therefore have a straight forward physical interpretation. For example the triple product of the spins at sites i, j, k can be written using two of these loops:

$$\hat{S}_i(\hat{S}_j \times \hat{S}_k) = -2i : (\hat{B}_{ij} \hat{B}_{jk} \hat{B}_{ki} - \hat{B}_{ij}^\dagger \hat{B}_{jk}^\dagger \hat{B}_{ki}^\dagger) : . \quad (4.39)$$

In SBMFT the expectation values of loop operators can be written as products of the mean fields : $\langle \hat{B}_{ij} \hat{B}_{jk} \hat{B}_{ki} \rangle \approx \mathcal{B}_{ij} \mathcal{B}_{jk} \mathcal{B}_{ki}$. Using Eq. (4.39) we can directly see that ansätze that respect time reversal symmetry (have real parameters) can not correspond to non-coplanar states.

The complex argument of the loops, called fluxes, boil down to a sum of complex arguments of the mean field parameters, e.g:

$$\text{Arg} \left(\langle \hat{B}_{ij} \hat{B}_{jk} \hat{B}_{ki} \rangle \right) = \text{Arg}(\mathcal{B}_{ij}) + \text{Arg}(\mathcal{B}_{jk}) + \text{Arg}(\mathcal{B}_{ki}). \quad (4.40)$$

Under the action of an operator $\mathcal{O}_o \in \chi_o$, Eq. (4.40) transforms like

$$\begin{aligned} \mathcal{O}_o \text{Arg} \left(\langle \hat{B}_{ij} \hat{B}_{jk} \hat{B}_{ki} \rangle \right) &= \epsilon_{\mathcal{O}_o} (\text{Arg}(\mathcal{B}_{\mathcal{O}_o(ij)}) + \text{Arg}(\mathcal{B}_{\mathcal{O}_o(jk)}) + \text{Arg}(\mathcal{B}_{\mathcal{O}_o(ki)})) \\ &= \text{Arg}(\mathcal{B}_{ij}) + \text{Arg}(\mathcal{B}_{jk}) + \text{Arg}(\mathcal{B}_{ki}). \end{aligned} \quad (4.41)$$

The flux is invariant under \mathcal{O}_o if $\epsilon_{\mathcal{O}_o} = 1$ and the flux changes its sign if $\epsilon_{\mathcal{O}_o} = -1$. We can write down equations like Eq. (4.41) for all independent fluxes on the lattice and then solve for the phases $\text{Arg}(\mathcal{B}_{ij}) = \phi_{\mathcal{B}_{ij}}$ depending on the parities of all elements in χ_0 . This is done in Appendix C. The solutions are presented in Tab. 4.2.

Table of Weakly Symmetry Ansätze

We list \mathbb{Z}_2 spin liquid ansätze with at least one pairing field and at least one singlet field in Tab. 4.2. Ansätze that only allow for hopping fields can also be derived by the phase equations. They are, however, behaving as $U(1)$ spin liquids at nearest neighbor level and are thus subject to the Higgs mechanism.

The following lists of solutions assume that all listed fields have non zero absolute

values. The absolute values as well as all phases labeled by $\phi_i = \text{Any}$ are determined by the mean field equations. One of the phases $\phi_i = \text{Any}$ can be fixed to $\phi_i = 0$ by the remaining gauge freedom. If one wants to construct an ansatz with less mean field parameters (i.e. setting the modulus of one field to zero), all phases of that field type have to be set to "Any" in the table. For example we have $\phi_{t_2^{p,x}} = \phi_{t_1^{p,z}} + \phi_{t_2^{p,z}} - \phi_{t_1^{p,x}}$ but want to construct an ansatz with $|t^{p,z}|_{ij} = 0$: The phase relation becomes $\phi_{t_2^{p,x}} = \text{Any}$ and $\phi_{t_2^{p,x}}$ has to be determined by the saddle point equations or can be set to zero by the remaining gauge freedom. The ansätze are related to the symmetric ones of Liu et al. [18] in multiple ways. Firstly, the ansätze with $\epsilon_I = \epsilon_S = 1$ include all symmetric ones by construction. Secondly, it can occur that a symmetry breaking field acquires an absolute value of zero through the saddle point equations. This can reduce a weakly symmetric ansatz to a symmetric one. For example, if for any ansatz $n_3\pi - (0, p_1, -1, \epsilon_I, 0)$ in Tab. 4.2 the saddle point equations give $|\mathcal{B}| = 0$, the ansätze are equivalent to the symmetric ones $n_3\pi - (0, p_1, 1, 1, 0)$.

Table 4.2: Table of all weakly symmetric mean field ansätze with at least one pairing field and at least one singlet field on the pyrochlore lattice. There is still one gauge freedom left to either fix ϕ_1 or ϕ_2 for one field. The allowed fields are fixed on bonds $\mathbf{0}_0 \rightarrow \mathbf{0}_1$ and $\mathbf{0}_0 \rightarrow \mathbf{0}_1 - \mathbf{a}_1$. All other fields are constrained to be 0. The remaining free parameters can be determined by the saddle point equations. The new \mathbb{Z}_2 parameter $p_1 \in \{0, 1\}$ attaches an extra $p_1\pi$ flux to bow tie loops. Note, that $\epsilon_I = \epsilon_{\bar{C}_6}$ (see Appendix C).

$n_3\pi - (n_{C_3C'_3}, p_1, \epsilon_I \epsilon_S, \epsilon_I, k)$ Supported Fields	Complex Phases of Mean Fields ϕ	
$n_3\pi - (0, p_1, 1, \epsilon_I, 0)$ \mathcal{A} $t^{h,\gamma}$ $\gamma \in \{x, z\}$	$\phi_{t_1^{h,\gamma}} = 0$ $\phi_{t_2^{h,\gamma}} = \phi_{t_1^{h,\gamma}} + n_3\pi$	For $(\epsilon_I, \epsilon_S) = (1, 1)$ $\phi_{A_1} = \text{Any}$ $\phi_{A_2} = \phi_{A_1} + p_1\pi$ For $(\epsilon_I, \epsilon_S) = (-1, -1)$ $\phi_{A_1} = \text{Any}$ $\phi_{A_2} = \text{Any}$
$n_3\pi - (0, p_1, -1, \epsilon_I, 0)$ \mathcal{A} \mathcal{B} $t^{h,\gamma}$ $\gamma \in \{x, z\}$	$\phi_{B_1} = \frac{\pi}{2}$ $\phi_{B_2} = \epsilon_I \phi_{B_1} + n_3\pi$ $\phi_{t_1^{h,\gamma}} = 0$ $\phi_{t_2^{h,\gamma}} = \phi_{t_1^{h,\gamma}} + n_3\pi$	$\phi_{A_1} = \text{Any}$ $\phi_{A_2} = \phi_{A_1} + p_1\pi$
$n_3\pi - (1, p_1, 1, \epsilon_I, 0)$ Nr.1 \mathcal{B} $t^{h,y}$ $t^{p,\gamma}$ $\gamma \in \{x, z\}$	$\phi_{B_1} = 0$ $\phi_{B_2} = \epsilon_I \phi_{B_1} + n_3\pi$ $\phi_{t_1^{h,y}} = \frac{\pi}{2}$ $\phi_{t_2^{h,y}} = \epsilon_I \phi_{t_1^{h,y}} + n_3\pi$	For $(\epsilon_I, \epsilon_S) = (1, 1)$ $\phi_{t_1^{p,\gamma}} = \text{Any}$ $\phi_{t_2^{p,\gamma}} = \phi_{t_1^{p,\gamma}} + p_1\pi$ For $(\epsilon_I, \epsilon_S) = (-1, -1)$ $\phi_{t_1^{p,\gamma}} = \text{Any}$ $\phi_{t_2^{p,z}} = \text{Any}$ $\phi_{t_2^{p,x}} = \phi_{t_1^{p,z}} + \phi_{t_2^{p,z}} - \phi_{t_1^{p,x}}$
$n_3\pi - (1, p_1, 1, \epsilon_I, 0)$ Nr.2 \mathcal{B} $t^{h,y}$ $t^{p,y}$	$\phi_{B_1} = 0$ $\phi_{B_4} = \phi_{B_1} + n_3\pi$ $\phi_{t_1^{h,y}} = \frac{\pi}{2}$ $\phi_{t_4^{h,y}} = \epsilon_I \phi_{t_1^{h,y}} + n_3\pi$	For $(\epsilon_I, \epsilon_S) = (1, 1)$ $\phi_{t_1^{p,y}} = \text{Any}$ $\phi_{t_2^{p,y}} = \phi_{t_1^{p,y}} + p_1\pi$ For $(\epsilon_I, \epsilon_S) = (-1, -1)$ $\phi_{t_1^{p,y}} = \text{Any}$ $\phi_{t_2^{p,y}} = \text{Any}$
$n_3\pi - (1, p_1, -1, \epsilon_I, 0)$ \mathcal{B} $t^{p,\gamma}$ $t^{h,\eta}$ $\gamma \in \{x, y, z\}$ $\eta \in \{x, z\}$	$\phi_{B_1} = 0$ $\phi_{B_2} = \phi_{B_1} + n_3\pi$ $\phi_{t_1^{h,\eta}} = \frac{\pi}{2}$ $\phi_{t_2^{h,\eta}} = \epsilon_I \phi_{t_1^{h,\eta}} + n_3\pi$	$\phi_{t_1^{p,z}} = \text{Any}$ $\phi_{t_1^{p,x}} = \phi_{t_1^{p,z}}$ $\phi_{t_1^{p,y}} = \phi_{t_1^{p,z}} + \frac{\pi}{2}$ $\phi_{t_2^{p,z}} = \phi_{t_1^{p,z}} + p_1\pi$ $\phi_{t_2^{p,x}} = \phi_{t_1^{p,x}} + p_1\pi$ $\phi_{t_2^{p,y}} = \epsilon_I \phi_{t_1^{p,y}} + p_1\pi$
$n_3\pi - (0, p_1, -1, 1, k)$ \mathcal{A}	$\phi_{A_1} = \text{Any}$ $\phi_{A_2} = \phi_{A_1} + p_1\pi$	

Schwinger Boson Treatment of the XXZ-Heisenberg Hamiltonian

5.1 Mean Field Decoupling

To treat the XXZ-Heisenberg Hamiltonian (2.4) in SBMFT we start by rewriting it in the following way:

$$\begin{aligned}
 H &= \sum_{\langle ij \rangle} J_{\perp} (\hat{S}_i^x \hat{S}_j^x + \hat{S}_i^y \hat{S}_j^y) + J_{zz} \hat{S}_i^z \hat{S}_j^z \\
 &= \sum_{\langle ij \rangle} J_{\perp} \hat{\mathbf{S}}_i \hat{\mathbf{S}}_j + \Delta J \hat{S}_i^z \hat{S}_j^z = \sum_{\langle ij \rangle} J_{zz} \hat{\mathbf{S}}_i \hat{\mathbf{S}}_j - \Delta J (\hat{S}_i^x \hat{S}_j^x + \hat{S}_i^y \hat{S}_j^y) \quad (5.1)
 \end{aligned}$$

with $\Delta J = J_{zz} - J_{\perp}$. We can bring the Hamiltonian into the form of Eq. (4.5) by using the identities

$$\hat{\mathbf{S}}_i \hat{\mathbf{S}}_j =: \hat{B}_{ij}^{\dagger} \hat{B}_{ij} : - \hat{A}_{ij}^{\dagger} \hat{A}_{ij} \quad (5.2a)$$

$$= 2 : \hat{B}_{ij}^{\dagger} \hat{B}_{ij} : - S^2 \quad (5.2b)$$

$$= S^2 - 2 \hat{A}_{ij}^{\dagger} \hat{A}_{ij}, \quad (5.2c)$$

$$\hat{S}_i^{\gamma} \hat{S}_j^{\gamma} =: \hat{B}_{ij}^{\dagger} \hat{B}_{ij} : - \hat{t}_{ij}^{p,\gamma \dagger} \hat{t}_{ij}^{p,\gamma} \quad (5.2d)$$

$$=: \hat{t}_{ij}^{h,\gamma \dagger} \hat{t}_{ij}^{h,\gamma} : - \hat{A}_{ij}^{\dagger} \hat{A}_{ij}. \quad (5.2e)$$

Since the different PSG classes only allow a limited amount of different mean field parameters, we will eliminate some parameters by using Eq. (4.6). This results in different J^h , J^p that, together with the choice of the PSG, completely define the mean field Hamiltonian. We choose meaningful ansätze as well as a suitable mean field decouplings in a way that preserves the $SU(2)$ spin rotation symmetry at the Heisenberg point.

We motivate our choice of ansätze by previous studies of the model. For $-0.05 < \theta < \frac{\pi}{4}$ Benton et al. [7] found QSI states and for $\frac{\pi}{4} < \theta < 1.927$ the QSN $_{\perp}$ state. The QSI breaks no lattice symmetries and has $U(1)$ spin rotation symmetry with dominating antiferromagnetic correlations in S^z direction. The only symmetric mean field ansätze that have these features are: 0-(101), 0-(110), π -(100), π -(111)

with mean field decoupling:

$$J^h = \text{diag}((J_\perp + J_{zz}), 0, 0, 0), \quad (5.3a)$$

$$J^p = \text{diag}(0, 0, 0, J_\perp - J_{zz}), \quad (5.3b)$$

$$C_{ij} = -J_\perp \mathcal{S}^2, \quad (5.3c)$$

resulting in

$$a^h = \frac{J_{zz} + J_\perp}{2} \mathcal{B}, \quad u_{\mathbf{0}_0, \mathbf{0}_1}^h = (a^h, 0, 0, 0)^h, \quad (5.4a)$$

$$d^p = \frac{J_\perp - J_{zz}}{2} t^{p,z}, \quad u_{\mathbf{0}_0, \mathbf{0}_1}^p = (0, 0, 0, d^p)^p. \quad (5.4b)$$

However, they do not allow for antiferromagnetic correlations in the $S^x - S^y$ plane which should play a vital role for $\theta > 0$. The nematic spin liquid found by Benton et al. [7] has antiferromagnetic correlations in the $S^x - S^y$ plane and breaks the $U(1)$ spin rotation symmetry as well as the C_3 lattice symmetry. We will focus on the breaking of the $U(1)$ spin rotation symmetry and consider the symmetric ansätze 0-(100), 0-(101), 0-(110), 0-(111), π -(100), π -(101), π -(110), π -(111) with nematic mean field decoupling:

$$J^h = \text{diag}(J_\perp, 0, 0, 0), \quad (5.5a)$$

$$J^p = \text{diag}(0, J_{zz} - J_\perp, J_{zz} - J_\perp, 0), \quad (5.5b)$$

$$C_{ij} = J_{zz} \mathcal{S}^2. \quad (5.5c)$$

These break the $U(1)$ spin rotation symmetry but leave the C_3 lattice symmetry intact. Note, that breaking of the $U(1)$ spin rotation symmetry has to be done manually by setting corresponding mean field parameters (b^p or c^p depending on the ansatz) to 0. To discriminate between ansätze 0-(101), 0-(110), π -(100), π -(111) with $U(1)$ symmetric and $U(1)$ breaking decoupling we refer to the latter as 0-(101)-Nem, 0-(110)-Nem, π -(100)-Nem, π -(111)-Nem. The mean field parameters are given by

$$a^h = \frac{J_\perp}{2} \mathcal{B}, \quad u_{\mathbf{0}_0, \mathbf{0}_1}^h = (a^h, 0, 0, 0)^h, \quad (5.6a)$$

$$b^p = \frac{J_{zz} - J_\perp}{2} t^{p,x}, \quad u_{\mathbf{0}_0, \mathbf{0}_1}^p = (0, b^p, 0, 0)^p, \quad (5.6b)$$

for 0-(101)-Nem, 0-(110)-Nem, π -(100)-Nem, π -(111)-Nem and by

$$a^h = \frac{J_\perp}{2} \mathcal{B}, \quad u_{\mathbf{0}_0, \mathbf{0}_1}^h = (a^h, 0, 0, 0)^h, \quad (5.7a)$$

$$c^p = \frac{J_{zz} - J_\perp}{2} t^{p,x}, \quad u_{\mathbf{0}_0, \mathbf{0}_1}^p = (0, 0, c^p, 0)^p, \quad (5.7b)$$

for 0-(100), 0-(111), π -(101), π -(110). Since the ansätze 0-(101)-Nem, 0-(110)-Nem, π -(100)-Nem, π -(111)-Nem, 0-(100), 0-(111), π -(101), π -(110) only allow for singlet hopping terms and no singlet pairing terms, they are unable to correctly describe the antiferromagnetic correlations at the Heisenberg point.

Therefore, we will also consider ansätze 0-(001) , 0-(010) , π -(000) , π -(011) with mean field decoupling:

$$J^h = \text{diag}(0, 0, 0, J_{zz} - J_{\perp}), \quad (5.8a)$$

$$J^p = \text{diag}(-(J_{\perp} + J_{zz}), 0, 0, 0), \quad (5.8b)$$

$$C_{ij} = J_{\perp} \mathcal{S}^2, \quad (5.8c)$$

resulting in

$$d^h = \frac{J_{\perp} - J_{zz}}{2} t^{h,z}, \quad u_{\mathbf{0}_0, \mathbf{0}_1}^h = (0, 0, 0, d^h)^h, \quad (5.9a)$$

$$a^p = -\frac{J_{zz} + J_{\perp}}{2} \mathcal{A}, \quad u_{\mathbf{0}_0, \mathbf{0}_1}^p = (a^p, 0, 0, 0)^p. \quad (5.9b)$$

These ansätze can capture the antiferromagnetic correlations near the Heisenberg point. It also includes ferromagnetic perturbations away from the Heisenberg point. Kim et al. [17] and Burnell et al. [15] proposed multiple chiral spin liquid states for the Heisenberg point. They proposed a state that breaks I and \mathcal{T} but preserve the \mathcal{TI} called monopole flux state, as well as a state that breaks S as well as \mathcal{T} but preserve \mathcal{TS} . Their characteristic feature is that each triangular flux has a value of $\pm \frac{\pi}{2}$. Both of these states can be described by the weakly symmetric ansätze of type $n_3\pi - (0, p_1, -1, \epsilon_I, 0)$ (see Tab. 4.2) with $\epsilon_I = -1$ corresponding to the monopole flux state and $\epsilon_I = 1$ corresponding to the screw symmetry breaking state. Each case has four distinct weakly symmetric ansätze. Two with standard and two with enlarged unit cell parametrized with (n_3, p_1) . The remaining gauge freedom can be used to fix $\phi_{A_1} = 0$. Due to the analysis in Appendix C all symmetry allowed triplet fields can be included that might get a non zero expectation value away from the Heisenberg point. While we do not treat these ansätze in this work, we propose to study them with decoupling

$$J^h = \text{diag}\left(\frac{J_{zz} + J_{\perp}}{2}, \frac{-J_{zz} + J_{\perp}}{2}, \frac{-J_{zz} + J_{\perp}}{2}, \frac{J_{zz} - J_{\perp}}{2}\right), \quad (5.10a)$$

$$J^p = \text{diag}(-J_{\perp}, 0, 0, 0), \quad (5.10b)$$

$$C_{ij} = 0, \quad (5.10c)$$

resulting in

$$a_i^h = \frac{J_{zz} + J_{\perp}}{4} \mathcal{B}_i^*, \quad b_i^h = \frac{-J_{zz} + J_{\perp}}{4} (t_i^{h,x})^*, \quad (5.11a)$$

$$d_i^h = \frac{J_{zz} - J_{\perp}}{4} (t_i^{h,z})^*, \quad a_i^p = -\frac{J_{\perp}}{2} \mathcal{A}_i, \quad (5.11b)$$

$$u_{\mathbf{0}_0, \mathbf{0}_1}^h = (a_1^h, b_1^h, 0, d_1^h)^h, \quad u_{I(\mathbf{0}_0), I(\mathbf{0}_1)}^h = (a_2^h, b_2^h, 0, d_2^h)^h, \quad (5.11c)$$

$$u_{\mathbf{0}_0, \mathbf{0}_1}^p = (0, 0, 0, d_1^p)^p, \quad u_{I(\mathbf{0}_0), I(\mathbf{0}_1)}^p = (a_2^p, 0, 0, 0)^p, \quad (5.11d)$$

where $t^{h,y}$ has to be manually set to 0. $\mathcal{B}_i = |\mathcal{B}|e^{-i\phi_{\mathcal{B}_i}}$, $\mathcal{B}_i = |\mathcal{B}|e^{-i\phi_{\mathcal{B}_i}}$, $\mathcal{B}_i = |\mathcal{B}|e^{-i\phi_{\mathcal{B}_i}}$, $\mathcal{B}_i = |\mathcal{B}|e^{-i\phi_{\mathcal{B}_i}}$. The complex phases of the mean fields are found in Tab. 4.2.

The problem of the symmetric ansätze and their mean field decouplings in the XXZ Model is that the PSG is very restrictive on the allowed mean field parameters. For example for $0 < \theta < \frac{\pi}{4}$ prior work expects a U(1) symmetric spin liquid with

antiferromagnetic correlations in $S^x - S^y$ plane as well as in the S^z direction [20]. One expects stronger antiferromagnetic correlation in S^z than in the $S^x - S^y$ direction. Such a state could either be constructed with mean field parameters \mathcal{A} as well as $t^{h,x}$ and $t^{h,y}$ on every bond or with as $t^{p,x}$, $t^{p,y}$ and $t^{p,z}$ allowed on every bond. There is no symmetric ansatz that fulfills these properties. However, the weakly symmetric ansätze $n_3\pi - (1, p_1, -1, \epsilon_I, 0)$ allow for $t^{p,x}$, $t^{p,y}$ and $t^{p,z}$. They do however break \mathcal{T} as well as either \mathcal{TI} or \mathcal{TS} . Nevertheless, they would be interesting ansätze to consider for $0 < \theta < \frac{\pi}{2}$ as they could correctly describe the antiferromagnetic correlations and they have the potential to be unstable to nematicity at $\theta = \frac{\pi}{4}$ with out breaking any spin symmetry a priori. We propose to use the decoupling

$$J^h = \text{diag}(J_{zz} + 2J_{\perp}, 0, 0, 0), \quad (5.12a)$$

$$J^p = \text{diag}\left(0, \frac{-J_{\perp}}{2}, \frac{-J_{\perp}}{2}, \frac{-J_{zz}}{2}\right), \quad (5.12b)$$

$$C_{ij} = 0, \quad (5.12c)$$

resulting in

$$a_i^h = \frac{J_{zz} + 2J_{\perp}}{2} \mathcal{B}_i^*, \quad b_i^p = -\frac{J_{\perp}}{2} t_i^{p,x}, \quad (5.13a)$$

$$c_i^p = -\frac{J_{\perp}}{2} t_i^{p,y}, \quad d_i^p = -\frac{J_{zz}}{2} t_i^{p,z}, \quad (5.13b)$$

$$u_{\mathbf{0}_0, \mathbf{0}_1}^h = (a_1^h, 0, 0, 0)^h, \quad u_{I(\mathbf{0}_0), I(\mathbf{0}_1)}^h = (a_2^h, 0, 0, 0)^h, \quad (5.13c)$$

$$u_{\mathbf{0}_0, \mathbf{0}_1}^p = (0, b_1^p, c_1^p, d_1^p)^p, \quad u_{I(\mathbf{0}_0), I(\mathbf{0}_1)}^p = (0, b_2^p, c_2^p, d_2^p)^p. \quad (5.13d)$$

5.2 Diagonalization of the Hamiltonian

By applying the Fourier transform

$$b_{\mathbf{r}\mu} = \sqrt{\frac{N_{SL}}{N}} \sum_{\mathbf{k}} b_{\mathbf{k},\mu} e^{-i\mathbf{k}\mathbf{r}\mu}, \quad (5.14)$$

the resulting Hamiltonian (Eq. (4.9)) can be brought into the form

$$H = \frac{1}{2} \sum_{\mathbf{k}} \hat{\psi}_{\mathbf{k}}^{\dagger} \mathcal{H}(\mathbf{k}) \hat{\psi}_{\mathbf{k}} + 3Nf(J_h, J_p) - N\lambda(2\mathcal{S} + 1). \quad (5.15)$$

N is the number of atoms on the lattice and $\mathcal{H}(\mathbf{k})$ has the form

$$\mathcal{H}(\mathbf{k}) = \begin{pmatrix} H^h(\mathbf{k}) + \lambda\mathbb{1}_d & H^p(\mathbf{k}) \\ H^p(\mathbf{k})^{\dagger} & H^h(-\mathbf{k})^{\top} + \lambda\mathbb{1}_d \end{pmatrix}. \quad (5.16)$$

For $n_3 = 0$ ($n_3 = 1$) $\hat{\psi}_{\mathbf{k}}$ is the 16 (64) component Nambu spinor and $d = 8$ ($d = 32$). A derivation of Eq. (5.16) is given in Appendix D. The explicit form of H^h and H^p is given in Appendix E.

The Hamiltonian (5.15) can be diagonalized by a Bogoliubov transformation [36]. We therefore introduce matrices $V(\mathbf{k})$ such that:

$$\hat{\psi}_{\mathbf{k}} = V(\mathbf{k}) \hat{\Gamma}_{\mathbf{k}}, \quad (5.17)$$

$$V(\mathbf{k})^{\dagger} \tau^3 V(\mathbf{k}) = \tau^3, \quad (5.18)$$

$$V(\mathbf{k})^{\dagger} \mathcal{H}(\mathbf{k}) V(\mathbf{k}) = \Omega(\mathbf{k}). \quad (5.19)$$

Here, $\hat{\Gamma}_{\mathbf{k}} = (\hat{\gamma}_{\mathbf{k},1}, \dots, \hat{\gamma}_{\mathbf{k},d}, \hat{\gamma}_{-\mathbf{k},1}^\dagger, \dots, \hat{\gamma}_{-\mathbf{k},d}^\dagger)$ is the Bogoliubov spinor, $\tau^3 = \sigma^3 \otimes \mathbb{1}_d$ and $\Omega(\mathbf{k})$ is a diagonal matrix where the first d entries are $\omega_i(\mathbf{k})$ ($i \in \{1, d\}$) and the last d entries are $\omega_i(-\mathbf{k})$. $\omega_i(\mathbf{k})$ are also the first d eigenvalues of the matrix $\tau^3 \mathcal{H}(k)$ [36]. Eq. (5.18) ensures that the new bosonic operators $\hat{\gamma}_{\mathbf{k},i}$ fulfill the commutation relations $[\hat{\gamma}_{\mathbf{k},i}, \hat{\gamma}_{\mathbf{k}',j}] = 0$ and $[\hat{\gamma}_{\mathbf{k},i}, \hat{\gamma}_{\mathbf{k}',j}^\dagger] = \delta_{i,j} \delta_{\mathbf{k},\mathbf{k}'}$. Thus, we can write Eq. (5.15) as

$$H(\mathbf{k}) = \sum_{\mathbf{k}} \sum_i^d \omega_i(\mathbf{k}) \hat{\gamma}_{\mathbf{k},i}^\dagger \hat{\gamma}_{\mathbf{k},i} + \frac{1}{2} \sum_{\mathbf{k}} \sum_i^d \omega_i(\mathbf{k}) + 3Nf(J^h, J^p) - N\lambda(2S + 1). \quad (5.20)$$

By substituting the sum $\sum_{\mathbf{k}} \rightarrow \frac{2N}{\text{Vol}_{\text{B.Z.}} d} \int_{\text{B.Z.}} dk^3$ in the thermodynamic limit, the ground state energy per site is given by

$$\frac{E_0}{N} = \frac{1}{\text{Vol}_{\text{B.Z.}} d} \int_{\text{B.Z.}} dk^3 \sum_i^d \omega_i(\mathbf{k}) + 3f(J^h, J^p) - \lambda(2S + 1). \quad (5.21)$$

The excitations that are created by $\hat{\gamma}_{\mathbf{k},i}^\dagger$ are called spinons and carry fractional spin of $\frac{1}{2}$. As a final step, we find the correct values of the mean field by solving the self consistency (4.12) or equivalently the saddle point equations (4.13). Once the mean field values are determined self consistently the mean field energy reduces to

$$\frac{E_0}{N} = 3\mathbf{h}_{ij}^\dagger J_{ij}^h \mathbf{h}_{ij} + 3\mathbf{p}_{ij}^\dagger J_{ij}^p \mathbf{p}_{ij} + 3C_{ij} \quad (5.22)$$

We compare ground state energies and mean field moduli in Chapt. 7. Some analytic results for $\omega_i(\mathbf{k})$ can be found in Appendix F.

5.3 Satisfying the Self-Consistency Equations

To satisfy the self-consistency equations (4.12) we apply three different approaches. For the symmetric ansätze we find the saddle point of the free energy. For ansätze 0-(101) and π -(111) one can show that $\mathcal{B} = -\frac{2S}{6}$ by inspecting the analytic form of the spinon dispersion (see Appendix F). For ansätze 0-(001) and π -(011) the same inspection results in $t^{p,z} = 0$. The rest of the parameters are found by numerical methods. Finding the saddle point of the free energy numerically is challenging for the physical spin value of $S = \frac{1}{2}$. The parameters of the saddle point are close to the critical parameters where the spinon gap closes and the Bogoliubov transformation fails. Gradient descent algorithms are prone to overshoot and jump into this numerically badly behaved regime where eigenvalues of $\tau^3 H(k)$ are often complex. We therefore calculate the critical values λ_{crit} for which the excitation gap closes as function of the mean field parameters. We can then constrain our search for saddle point solutions to the parameter space with $\lambda > \lambda_{\text{crit}}$. λ_{crit} is formally defined as

$$\min_{l,\mathbf{k}} \omega_l(\mathbf{k}, \lambda_{\text{crit}}, u^h, u^p) = 0. \quad (5.23)$$

For the symmetric 0-flux ansätze Liu et al. [18] give values for λ_{crit} . For the π -flux ansätze we use the fact that $\omega_l(\mathbf{k}, \lambda, u^h, u^p) = \lambda \omega_l(\mathbf{k}, 1, \frac{u^h}{\lambda}, \frac{u^p}{\lambda})$. This reduces the dimension of the parameter space by 1. We also notice that the minimum of the

eigenvalues of $H(k)$ and $\tau^3 H(k)$ are 0 for the same mean field parameters. Working with eigenvalues of the Hermitian matrix $H(k)$ is numerically better behaved since they stay real when crossing 0. It is therefore straightforward to find the contour in mean field parameter space, where the minimum eigenvalue of $H(k)$ equals to 0. We then finally calculate λ_{crit} as a function of u^h and u^p . Alternatively, one can try to analytically solve $\det(H(k)) = 0$ for λ .

5.4 Spin Structure Factor

To compare the mean field states to experiment and other numerical studies of the XXZ-Heisenberg model we will calculate the local and global static spin structure factors. The local static spin structure factors give information about spin-spin correlations of the state while the global static spin structure factor can be measured in neutron scattering experiments. The local spin structure factor is given by the tensor

$$\mathcal{S}^{\alpha,\beta}(\mathbf{q}) = \frac{1}{3N} \sum_{l,j} e^{i\mathbf{q}(\mathbf{r}_l - \mathbf{r}_j)} \langle \hat{\mathbf{S}}_l^\alpha \cdot \hat{\mathbf{S}}_j^\beta \rangle, \quad (5.24)$$

with \mathbf{S}_l^α in the local spin basis. The global spin structure factor is given by

$$\tilde{\mathcal{S}}^{\alpha,\beta}(\mathbf{q}) = \frac{1}{3N} \sum_{l,j} e^{i\mathbf{q}(\mathbf{r}_l - \mathbf{r}_j)} \langle (R_l^\top \hat{\mathbf{S}}_l)^\alpha \cdot (R_j^\top \hat{\mathbf{S}}_j)^\beta \rangle, \quad (5.25)$$

where R_l^\top is the rotation matrix that rotates the spin at site l into the global basis (see Appendix A). Neutron scattering experiments do not directly measure the global spin structure factor but instead measure the scattering amplitude [8]:

$$\mathcal{S}_{\text{tot}}(\mathbf{q}) = (\delta_{\alpha,\beta} - \frac{\mathbf{q}^\alpha \mathbf{q}^\beta}{\mathbf{q}^2}) \tilde{\mathcal{S}}^{\alpha,\beta}(\mathbf{q}). \quad (5.26)$$

Following Fennell et al. [37] we calculate the neutron scattering amplitude along the $[h, h, l]$ plane and split the total global structure factor $\mathcal{S}_{\text{tot}}(\mathbf{q})$ into a spin flip (SF) channel

$$\mathcal{S}_{\text{SF}}(\mathbf{q}) = \frac{(\mathbf{P} \times \mathbf{q})^\alpha (\mathbf{P} \times \mathbf{q})^\beta}{\mathbf{q}^2} \tilde{\mathcal{S}}^{\alpha,\beta}(\mathbf{q}) \quad (5.27)$$

and a no spin flip (NSF) channel

$$\mathcal{S}_{\text{NSF}}(\mathbf{q}) = \mathbf{P}^\alpha \mathbf{P}^\beta \tilde{\mathcal{S}}^{\alpha,\beta}(\mathbf{q}), \quad (5.28)$$

where $\mathbf{P} = \frac{1}{\sqrt{2}}(1, -1, 0)$ is the polarization vector of the neutrons. In the $[h, h, l]$ plane they fulfill $\mathcal{S}_{\text{tot}}(\mathbf{q}) = \mathcal{S}_{\text{SF}}(\mathbf{q}) + \mathcal{S}_{\text{NSF}}(\mathbf{q})$. Experimentally splitting up measurements into the polarization channels is advantageous since the pinch points that are characteristic for the spin ice phase are only visible in the SF channel. When measuring $\mathcal{S}_{\text{tot}}(\mathbf{q})$ the contributions from the NSF channel smear out the features [37].

We can obtain both local and global structure factors with the Bogoliubov transformation matrices $V(\mathbf{k})$:

$$V(\mathbf{k}) = \begin{pmatrix} V_{11}(\mathbf{k}) & V_{12}(\mathbf{k}) \\ V_{21}(\mathbf{k}) & V_{22}(\mathbf{k}) \end{pmatrix}, \quad \Sigma^\alpha = \mathbb{1}_{NSL} \otimes \sigma^\alpha, \quad (5.29)$$

$$\mathcal{S}^{\alpha,\beta}(\mathbf{q}) = \frac{1}{3N} \sum_{\mathbf{k}} \text{Tr} \left(V_{12}^\dagger(\mathbf{k}) \Sigma^\alpha V_{11}(\mathbf{k} - \mathbf{q}) [V_{21}^\dagger(\mathbf{k} - \mathbf{q}) (\Sigma^\beta)^\top V_{22}(\mathbf{k}) + V_{11}^\dagger(\mathbf{k} - \mathbf{q}) \Sigma^\beta V_{12}(\mathbf{k})] \right). \quad (5.30)$$

The global structure factor $\tilde{\mathcal{S}}^{\alpha,\beta}(\mathbf{q})$ can be calculated by using Eq. (5.30) and replacing $\Sigma^\gamma \rightarrow U \Sigma^\gamma U^\dagger$ with

$$U = \mathbb{1}_{N_{SL/4}} \otimes \begin{pmatrix} U_1 & & & \\ & U_2 & & \\ & & U_3 & \\ & & & U_4 \end{pmatrix}. \quad (5.31)$$

U_i are the $SU(2)$ matrices that rotate from the global to the local basis (see Appendix A).

Magnetic Phases

As described in Chapt. 2, Benton et al. found AIAO as well as AF_{\perp} magnetic order in the phase diagram of the XXZ-Heisenberg model [7]. We want to incorporate these phases into our study by calculating the first order quantum correction to their ground state in Holstein-Primakoff spin wave theory [38]. We make the common ansatz

$$\hat{S}_i^z = (\mathcal{S} - \hat{a}_i^{\dagger} \hat{a}_i), \quad (6.1a)$$

$$\hat{S}_i^+ = \sqrt{2\mathcal{S}} \sqrt{1 - \frac{\hat{a}_i^{\dagger} \hat{a}_i}{2\mathcal{S}}} \hat{a}_i, \quad (6.1b)$$

$$\hat{S}_i^- = \sqrt{2\mathcal{S}} \hat{a}_i^{\dagger} \sqrt{1 - \frac{\hat{a}_i^{\dagger} \hat{a}_i}{2\mathcal{S}}}, \quad (6.1c)$$

where we choose the z -direction to be parallel to the magnetization axis. For AIAO this is the local z -axis while for the easy-plane antiferromagnet it is somewhere in the local x - y -plane. To ensure that $|\langle S^z \rangle| \leq \mathcal{S}$ we have to restrict the basis of the Hilbert space to $\{|0\rangle, \dots, |2\mathcal{S}\rangle\}$ for every site. For $\mathcal{S} = \frac{1}{2}$ this can be done by adding the term $U \sum_i \hat{a}_i^{\dagger} \hat{a}_i^{\dagger} \hat{a}_i \hat{a}_i$ together with the limit $\lim_{U \rightarrow \infty}$. This is also known as the hardcore boson constraint. Since the square roots of the bosonic operators are hard to deal with, one usually Taylor expands Eqs. (6.1b) and (6.1c) for small $\frac{\hat{n}_i}{2\mathcal{S}}$. Vogl et al. [39] recently showed that, assuming the hardcore constraint is fulfilled, the approximation for $\mathcal{S} = \frac{1}{2}$

$$\hat{S}_i^z = (\mathcal{S} - \hat{a}_i^{\dagger} \hat{a}_i), \quad (6.2a)$$

$$\hat{S}_i^+ = \sqrt{2\mathcal{S}} \left(1 + \left(\sqrt{1 - \frac{1}{2\mathcal{S}}} - 1\right) \hat{a}_i^{\dagger} \hat{a}_i\right) \hat{a}_i, \quad (6.2b)$$

$$\hat{S}_i^- = \sqrt{2\mathcal{S}} \hat{a}_i^{\dagger} \left(1 + \left(\sqrt{1 - \frac{1}{2\mathcal{S}}} - 1\right) \hat{a}_i^{\dagger} \hat{a}_i\right), \quad (6.2c)$$

is actually exact.

6.1 All-In-All-Out (AIAO)

After expressing the Hamiltonian (5.1) with Eqs. (6.2) and choosing the magnetization axis to be parallel to the local z -axis we get

$$H_{AIAO} = \sum_{\langle i,j \rangle} J_{zz} \mathcal{S}^2 - 2\mathcal{S} J_{zz} (\hat{a}_i^\dagger \hat{a}_i + \hat{a}_i \hat{a}_i^\dagger) + J_\perp \mathcal{S} (\hat{a}_j^\dagger \hat{a}_i + \hat{a}_i \hat{a}_j^\dagger) \quad (6.3)$$

$$+ J_{zz} \hat{n}_i \hat{n}_j + U \sum_i \hat{a}_i^\dagger \hat{a}_i^\dagger \hat{a}_i \hat{a}_i + \text{u.p.t.},$$

where we have labelled all unphysical terms that evaluate to 0 on the physical Hilbert space as u.p.t. . To calculate the first quantum correction we will neglect the interaction term and the hardcore boson constraint. This is a valid approximation if $\langle \hat{n}_i \rangle \ll 1$. We apply the Fourier transform

$$\hat{a}_{\mathbf{r}\mu} = \sqrt{\frac{4}{N}} \sum_{\mathbf{k}} \hat{a}_{\mathbf{k},\mu} e^{-i\mathbf{k}\mathbf{r}\mu}, \quad \hat{a}_{\mathbf{r}\mu}^\dagger = \sqrt{\frac{4}{N}} \sum_{\mathbf{k}} \hat{a}_{\mathbf{k},\mu}^\dagger e^{i\mathbf{k}\mathbf{r}\mu} \quad (6.4)$$

and bring the Hamiltonian into the form

$$H_{AIAO}(\mathbf{k}) = 3N J_{zz} \mathcal{S}(\mathcal{S} + 1) + \frac{1}{2} \sum_{\mathbf{k}} \hat{A}_{\mathbf{k}}^\dagger \begin{pmatrix} H_{AIAO}^h(\mathbf{k}) & 0 \\ 0 & H_{AIAO}^h(\mathbf{k}) \end{pmatrix} \hat{A}_{\mathbf{k}}, \quad (6.5)$$

where $\hat{A}_{\mathbf{k}}^\dagger = (\hat{a}_{\mathbf{k},1}^\dagger, \dots, \hat{a}_{\mathbf{k},4}^\dagger, \hat{a}_{-\mathbf{k},1}, \dots, \hat{a}_{-\mathbf{k},4})$ is an eight component Nambu spinor and

$$(H_{AIAO}^h(\mathbf{k}))_{\mu,\nu} = 2\mathcal{S} J_\perp \cos\left(\frac{1}{2}(\mathbf{a}_\mu - \mathbf{a}_\nu)\mathbf{k}\right) (1 - \delta_{\mu,\nu}) - 6\mathcal{S} J_{zz} \delta_{\mu\nu}. \quad (6.6)$$

By applying a Bogoliubov transform $\hat{A}_{\mathbf{k}} = V(\mathbf{k}) \hat{\Gamma}_{\mathbf{k}}$, the Hamiltonian can be diagonalized and we get

$$H_{AIAO}(\mathbf{k}) = 3N J_{zz} \mathcal{S}(\mathcal{S} + 1) + \sum_{\mathbf{k}} \sum_i \omega_i(\mathbf{k}) \hat{\gamma}_i^\dagger \hat{\gamma}_i + \frac{1}{2} \sum_{\mathbf{k}} \sum_i \omega_i(\mathbf{k}), \quad (6.7)$$

where

$$\omega_{1,2} = -6J_{zz}\mathcal{S} - 2J_\perp\mathcal{S}, \quad (6.8a)$$

$$\omega_{\pm} = -6J_{zz}\mathcal{S} + 2J_\perp\mathcal{S} \left(1 \pm \sqrt{1 + \cos\left(\frac{k_1}{2}\right) \cos\left(\frac{k_2}{2}\right) + \cos\left(\frac{k_2}{2}\right) \cos\left(\frac{k_3}{2}\right) + \cos\left(\frac{k_1}{2}\right) \cos\left(\frac{k_3}{2}\right)} \right). \quad (6.8b)$$

Therefore, the quantum corrected ground state energy is

$$\frac{E_0}{N} = 3N J_{zz} \mathcal{S}(\mathcal{S} + 1) + \frac{1}{8\text{Vol}_{B.Z.}} \int_{B.Z.} d^3k \sum_i \omega_i(\mathbf{k}) = 3J_{zz} \mathcal{S}^2, \quad (6.9)$$

which is the classical ground state energy. The ground state satisfies $\langle \hat{n}_i \rangle = 0 \forall i$. It is therefore valid to neglect the interaction term and hardcore constraint.

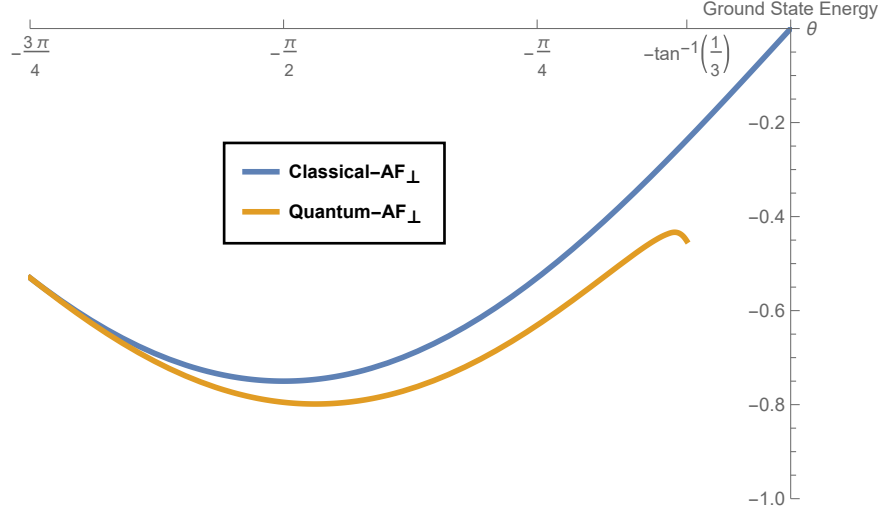


Figure 6.1: Ground state energy of the classical and quantum-AF_⊥ phase. The behaviour of the quantum-AF_⊥ phase is not reliable for $\theta \gtrsim -0.35$ due to the divergence of the boson density which we have assumed to be small.

6.2 Easy-Plane Antiferromagnet (AF_⊥)

For the AF_⊥ phase we choose our magnetization axis to be parallel to the local x -axis. Using Eqs. (6.2) we get:

$$H_{\text{AF}\perp} = \sum_{\langle i,j \rangle} J_{\perp} \mathcal{S}(\mathcal{S} + 1) - J_{\perp} \mathcal{S}(\hat{a}_i^{\dagger} \hat{a}_i + \hat{a}_i \hat{a}_i^{\dagger}) + \frac{J_{\perp} + J_{zz}}{2} \mathcal{S}(\hat{a}_j^{\dagger} \hat{a}_i + \hat{a}_i \hat{a}_j^{\dagger}) + \frac{J_{zz} - J_{\perp}}{2} \mathcal{S}(a_i^{\dagger} \hat{a}_j^{\dagger} + \hat{a}_i \hat{a}_j) + J_{\perp} n_i n_j + U \sum_i \hat{a}_i^{\dagger} \hat{a}_i^{\dagger} \hat{a}_i \hat{a}_i + \text{u.p.t.}, \quad (6.10)$$

where once again u.p.t labels terms that do not contribute in the physical Hilbert space. To calculate the quantum correction we will once again neglect the interaction term and hardcore constraint. Using the Fourier transform (6.4) we get:

$$H_{\text{AF}\perp} = 3N J_{\perp} \mathcal{S}(\mathcal{S} + 1) + \frac{1}{2} \sum_{\mathbf{k}} \hat{A}_{\mathbf{k}}^{\dagger} \begin{pmatrix} H_{\text{AF}\perp}^h(\mathbf{k}) & H_{\text{AF}\perp}^p(\mathbf{k}) \\ H_{\text{AF}\perp}^p(\mathbf{k}) & H_{\text{AF}\perp}^h(\mathbf{k}) \end{pmatrix} \hat{A}_{\mathbf{k}}, \quad (6.11)$$

with the 8 component spinor $\hat{A}_{\mathbf{k}}$ and

$$(H_{\text{AF}\perp}^h(\mathbf{k}))_{\mu,\nu} = (J_{zz} + J_{\perp}) \mathcal{S} \cos\left(\frac{1}{2}(\mathbf{a}_{\mu} - \mathbf{a}_{\nu}) \cdot \mathbf{k}\right) (1 - \delta_{\mu,\nu}) - 6J_{zz} \mathcal{S} \delta_{\mu\nu}, \quad (6.12)$$

$$(H_{\text{AF}\perp}^p(\mathbf{k}))_{\mu,\nu} = (J_{zz} - J_{\perp}) \mathcal{S} \cos\left(\frac{1}{2}(\mathbf{a}_{\mu} - \mathbf{a}_{\nu}) \cdot \mathbf{k}\right) (1 - \delta_{\mu,\nu}). \quad (6.13)$$

After Bogoliubov transformation of the Hamiltonian we have

$$H_{\text{AF}\perp}(\mathbf{k}) = 3N J_{\perp} \mathcal{S}(\mathcal{S} + 1) + \sum_{\mathbf{k}} \sum_i^4 \omega(\mathbf{k}) \hat{\gamma}_i^{\dagger} \hat{\gamma}_i + \frac{1}{2} \sum_{\mathbf{k}} \sum_i^4 \omega(\mathbf{k}). \quad (6.14)$$

Since $H_{\text{AF}\perp}^h$ and $H_{\text{AF}\perp}^p$ commute, the magnon dispersion has the form $\omega_i(\mathbf{k}) = \sqrt{\lambda_{h,i}^2 - \lambda_{p,i}^2}$, where $\lambda_{h,i}$ and $\lambda_{p,i}$ are the i^{th} eigenvalues of $H_{\text{AF}\perp}^h$ and $H_{\text{AF}\perp}^p$, respectively:

$$\omega_{1,2}(\mathbf{k}) = \mathcal{S} \sqrt{(6J_{\perp} + (J_{\perp} + J_{zz}))^2 - (J_{\perp} - J_{zz})^2}, \quad (6.15a)$$

$$\omega_{\pm}(\mathbf{k}) = \mathcal{S} \sqrt{(6J_{\perp} - (J_{\perp} + J_{zz})f_{\pm}(\mathbf{k}))^2 - ((J_{\perp} - J_{zz})f_{\pm}(\mathbf{k}))^2}, \quad (6.15b)$$

$$f_{\pm}(\mathbf{k}) = 1 \pm \sqrt{1 + \cos\left(\frac{k_1}{2}\right) \cos\left(\frac{k_2}{2}\right) + \cos\left(\frac{k_2}{2}\right) \cos\left(\frac{k_3}{2}\right) + \cos\left(\frac{k_1}{2}\right) \cos\left(\frac{k_3}{2}\right)}. \quad (6.15c)$$

The ground state energy is therefore

$$\frac{E_0}{N} = 3J_{\perp} \mathcal{S}(\mathcal{S} + 1) + \frac{1}{8\text{Vol}_{BZ}} \int_{BZ} dk^3 \sum_i \omega_i(\mathbf{k}). \quad (6.16)$$

To verify our assumptions we calculate the boson density averaged over all sublattices \bar{n} :

$$\begin{aligned} \bar{n} &= \frac{1}{N} \left\langle \sum_i \hat{a}_i^{\dagger} \hat{a}_i \right\rangle = -\frac{1}{2} + \frac{1}{2N} \left\langle \sum_{\mathbf{k}} A_{\mathbf{k}}^{\dagger} A_{\mathbf{k}} \right\rangle \\ &= -\frac{1}{2} + \frac{1}{2N} \left\langle \sum_{\mathbf{k}} \Gamma_{\mathbf{k}}^{\dagger} V(\mathbf{k})^{\dagger} V(\mathbf{k}) \Gamma_{\mathbf{k}} \right\rangle. \end{aligned} \quad (6.17)$$

Since $H_{\text{AF}\perp}^h$ and $H_{\text{AF}\perp}^p$ commute, the Bogoliubov transformation matrix can be written as

$$V(\mathbf{k}) = \begin{pmatrix} U \cosh(D) & U \sinh(D) \\ U \sinh(D) & U \cosh(D) \end{pmatrix}, \quad (6.18)$$

where U is a unitary matrix that diagonalizes both $H_{\text{AF}\perp}^h$ and $H_{\text{AF}\perp}^p$ (U is given in Appendix G) and D is a diagonal matrix satisfying:

$$\sinh(2D_{ii}) \lambda_{h,i} + \cosh(2D_{ii}) \lambda_{p,i} = 0, \quad (6.19a)$$

$$\cosh(2D_{ii}) \lambda_{h,i} + \sinh(2D_{ii}) \lambda_{p,i} = \omega_i, \quad (6.19b)$$

which is equivalent to

$$\cosh(2D_{ii}) = \frac{\omega_i \lambda_{h,i}}{\lambda_{h,i}^2 - \lambda_{p,i}^2} = \frac{\lambda_{h,i}}{\omega_i}, \quad (6.20a)$$

$$\sinh(2D_{ii}) = -\frac{\lambda_{p,i}}{\omega_i}. \quad (6.20b)$$

Plugging $V(\mathbf{k})$ into Eq. (6.17) finally results in:

$$\begin{aligned} \bar{n} &= -\frac{1}{2} + \frac{1}{2N} \sum_{\mathbf{k}} \sum_i \left\langle 2\hat{\gamma}_{i,\mathbf{k}}^{\dagger} \hat{\gamma}_{i,\mathbf{k}} \cosh(2D_{ii}) \right\rangle + \cosh(2D_{ii}) \\ &\quad + \left\langle \sinh(2D_{ii}) (\hat{\gamma}_{i,\mathbf{k}}^{\dagger} \hat{\gamma}_{i,-\mathbf{k}}^{\dagger} + \hat{\gamma}_{i,\mathbf{k}} \hat{\gamma}_{i,-\mathbf{k}}) \right\rangle \\ &= \frac{1}{8\text{Vol}_{BZ}} \sum_i \int_{BZ} \left(\frac{\lambda_{h,i}}{\omega_i} - 1 \right). \end{aligned} \quad (6.21)$$

Comparing with the exact expression for $\omega_i(\mathbf{k})$, we see that the mean boson density is 0 for $J_{zz} - J_\perp = 0$ and grows monotonically with $|J_{zz} - J_\perp|$. It diverges at $J_{zz} = -3J_\perp$. This is exactly the coupling at which the gap closes ($\omega_{1,2}(\mathbf{k}) = 0$) and the mode gets completely populated. Here, our assumption $\hat{n}_i \ll 1$ breaks down. To get meaningful results for $J_{zz} > -3J_\perp$ one would need to incorporate interactions and the hardcore boson constraint. Qualitatively, this divergence is an indication for a phase transition. A plot of the ground state energy and mean boson densities can be found in Fig. 6.1 and Fig. 6.2, respectively. The sublattice specific mean boson density is calculated in Appendix G.

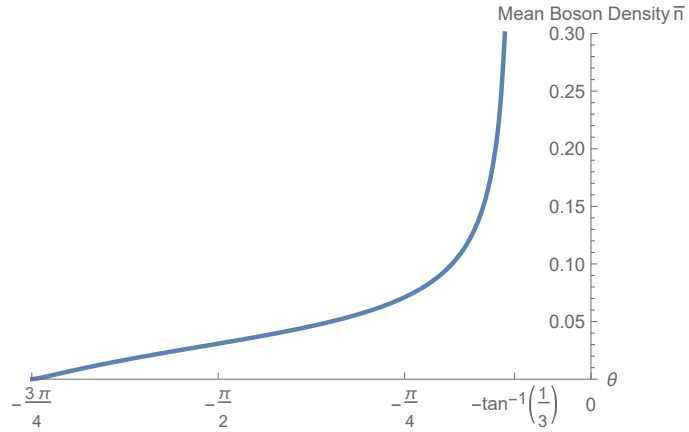


Figure 6.2: The boson density averaged over all lattice sites. For $J_{zz} = -3J_\perp$ the boson density diverges and our assumptions fail.

Results

In this chapter we present the numerical results for the symmetric ansätze with mean field decouplings specified in Chapt. 5. First, we give solutions for the mean field values and plot the resulting mean field energies of the underlying ansätze. To better characterize some of them we choose 5 ansätze and plot their local spin structure factor and neutron scattering amplitude.

7.1 Mean Field Values

Table 7.1: Mean field values for the ansätze 0-(001), 0-(010), π -(000), π -(011) for $\theta \in \{-45^\circ, 135^\circ\}$.

Ansatz	\mathcal{A}	$t^{h,z}$	$2\lambda/(J_\perp + J_{zz})$
0-(001)	-0.393125	0	1.38799
0-(010)	-0.390149	0	1.35930
π -(000)	-0.393365	0	1.39103
π -(011)	-0.389534	0	1.34659

Values for the mean field parameters are obtained by finding the saddle point of the mean field ground state energy as explained in Chapt. 5.3 for $\mathcal{S} = \frac{1}{2}$ and for $\theta \in \{-45^\circ, 135^\circ\}$

The resulting values for ansätze 0-(001), 0-(010), π -(000), π -(011) can be found in Tab. 7.1. For all four ansätze the only field that obtains a non-zero value are is \mathcal{A} which remains constant for all θ . This results in an effective $SU(2)$ symmetry of the mean field states. This feature is found to be independent of the decoupling. While the values for the fields \mathcal{A} and $t^{h,z}$ stay the same regardless of the decoupling, the mean field energy does differ between decoupling (5.2a) and (5.2c). Evidently, it is not reliable to compare mean field energies between different decouplings.

The resulting values for ansätze 0-(101) and π -(111) can be found in Tab. 7.2. The value for \mathcal{B} is found analytically to be $\mathcal{B} = -\frac{1}{6}$. We use this as a benchmark for our numerical methods. At $\theta \approx 23^\circ$, the spinon gap closes for 0-(101) and at $\theta \approx -16^\circ$ the spinon gap closes for π -(111). The values for ansatz π -(100) can be found in Fig. 7.1a. Its spinon gap closes at $\theta \approx -37^\circ$. 0-(110) has no self-consistent solution to the mean field equations for $\mathcal{S} = \frac{1}{2}$.

Table 7.2: Mean field values for the ansätze 0-(101) and π -(111).

Ansatz	\mathcal{B}	$t^{p,z}$	$\frac{(\lambda-2\mathcal{B}(J_{\perp}+J_{zz}))}{J_{\perp}-J_{zz}}$
0-(101)	$-\frac{1}{6}$	-0.424972	-0.851955
π -(111)	$-\frac{1}{6}$	-0.428073	-0.866502

The parameters for ansätze 0-(100), π -(101), π -(110), 0-(110)-Nem, π -(100)-Nem, π -(111)-Nem can be found in Fig. 7.1. For the nematic decoupling the ansätze with equal $n_3, n_{\overline{C}_6, \mathcal{S}}, n_{\overline{C}_6}$ and different n_{ST_1} are connected. Their mean values of $t^{h,x}$ and $t^{h,y}$ are the same, while the values of \mathcal{B} have a different sign. This also results in degenerate mean field energies between these ansätze. All of these ansätze only have self consistent solutions for $\theta > 45^\circ$. At $\theta = 45^\circ$, the spinon gap closes. 0-(111) and 0-(101)-Nem do not have solutions for $\mathcal{S} = \frac{1}{2}$.

The ground state energies of all ansätze as well as the magnetic phases can be seen in Fig. 7.2. Since the mean field energies are sensitive to the choice of decoupling, we compare energies only between states of the same decoupling. For the U(1) symmetric decoupling with \mathcal{A} fields (Eq. (5.8)), π -(000) has the lowest energy for all $\theta \in \{-45^\circ, 135^\circ\}$. For the U(1) symmetric decoupling with \mathcal{B} fields (Eq. (5.3)), π -(111) has the lowest energy for $\theta \in \{-45^\circ, 23^\circ\}$. From $\theta \lesssim -15^\circ$ π -(100) has the lowest energy until it crosses π -(111) again at $\theta \approx -18^\circ$. π -(111) then gaps out at $\theta \approx -15^\circ$. For $\theta \in \{-15^\circ, 9^\circ\}$ the ansatz 0-(101) has the lowest energy and from $\theta \in \{9^\circ, 45^\circ\}$ the ansatz π -(100) has the lowest energy.

For the nematic decoupling (Eq. (5.5)) 0-(100) and 0-(110)-Nem both have the lowest energy from $45^\circ \lesssim \theta < 135^\circ$.

For $\theta \gtrsim -20^\circ$ the ground state energy results for AF_{\perp} are not reliable due to the divergence of the boson density which is assumed to be small.

Table 7.3: The mean field values at four different coupling strengths. Note that all pairing fields have magnitudes around 0.4.

Ansatz	θ	Mean Field Values
0-(100)	90°	$\mathcal{B} = 0.081$ $t^{p,y} = -0.400$ $\lambda = 0.648$
0-(110)	90°	$\mathcal{B} = -0.081$ $t^{p,x} = -0.400$ $\lambda = 0.648$
π -(100)	20°	$\mathcal{B} = 0.070$ $t^{p,z} = -0.383$ $\lambda = 0.349$
0-(101)	5°	$\mathcal{B} = -\frac{1}{6}$ $t^{p,z} = -0.425$ $\lambda = 0.594$
π -(000)	45°	$\mathcal{A} = -0.393$ $t^{h,z} = 0$ $\lambda = 0.983$

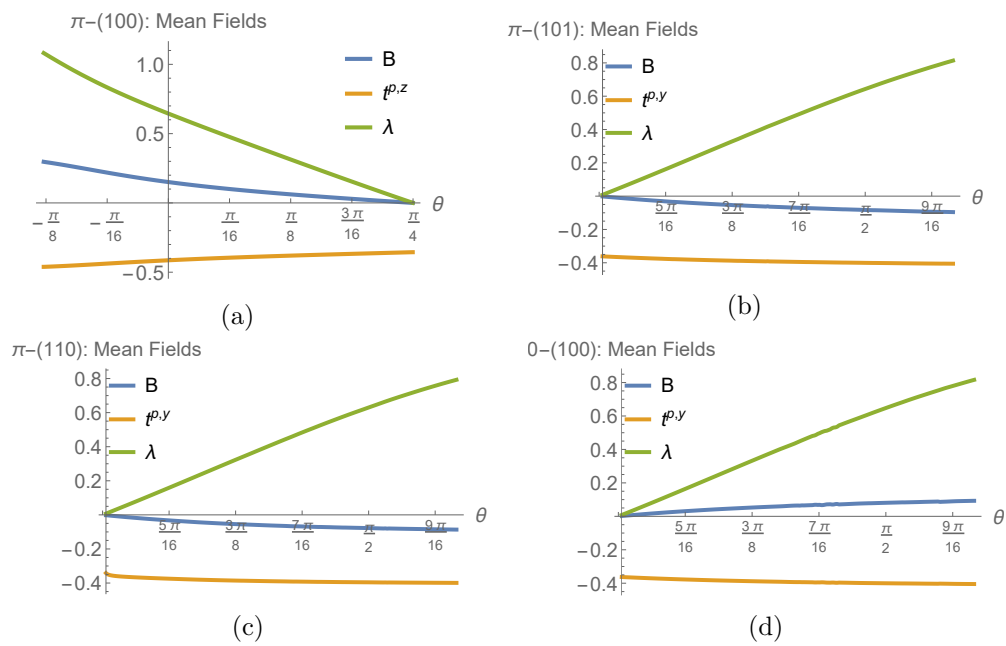


Figure 7.1: Mean field values for ansätze: (a) π -(100) (b) π -(101); π -(111)-Nem has the same values for $t^{p,x}$ as π -(101) has for $t^{p,y}$ and a different sign for \mathcal{B} , (c) π -(110); π -(100)-Nem has the same values for $t^{p,x}$ as π -(110) has for $t^{p,y}$ and a different sign for \mathcal{B} , (d) 0-(100); 0-(110)-Nem has the same values for $t^{p,x}$ as 0-(100) has for $t^{p,y}$ and a different sign for \mathcal{B} .

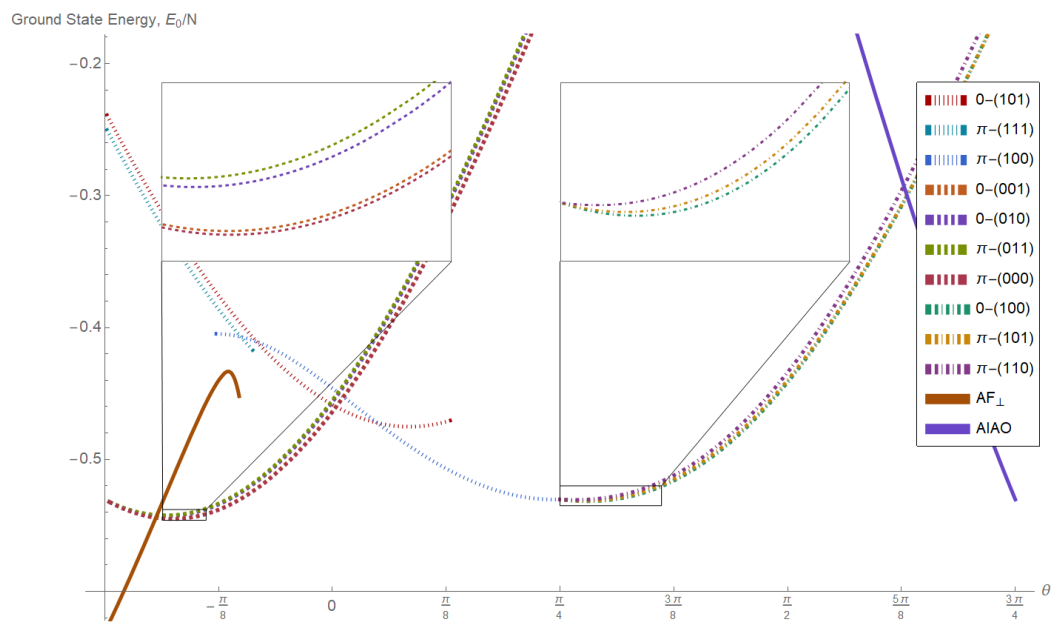


Figure 7.2: Ground state energies of the symmetric ansätze and the magnetic phases. 0-(110)-Nem, π -(100)-Nem, π -(111)-Nem have the same energy as 0-(100), π -(110), π -(101), respectively. SBMFT Energies are given by Eq. (5.22). Different line styles indicate different mean field decouplings.

7.2 Structure Factors and Neutron Scattering Amplitudes

To better characterize the mean field states, we calculate the local spin structure factor (Eq. (5.24)) as well as the neutron scattering amplitude (Eq. (5.26)). We choose 5 states at 4 different coupling angles. The specified points can be found in Tab. 7.3. Further structure factors and neutron scattering amplitudes can be found in Appendix H. To make results comparable with Ritter [20], we marked the extended Brillouin zone in every plot of the local spin structure factor. It is eight times as large as the Brillouin zone defined in Chapt. 3.

π -(000)

For π -(000), the saddle point equations set the $t^{h,z} = 0$ and therefore increase the symmetry of the state to $SU(2)$. Its local spin structure factor is shown in Fig. 7.3. It only has one independent component $\mathcal{S}^{xx} = \mathcal{S}^{yy} = \mathcal{S}^{zz}$. All off-diagonal components vanish. The structure factor shows broad pinch points at $q = (2\pi, 2\pi, 2\pi)$ and $q = (0, 0, 4\pi)$. The broad nature of the pinch points is due to quantum fluctuations violating the so called ice rules [40]. The local structure factor is similar to results of prior work for the Heisenberg point ($\theta = 45^\circ$) [11, 16, 40–43].

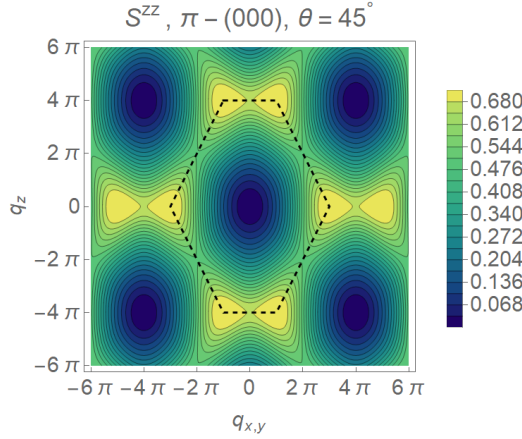


Figure 7.3: Local spin structure factor of the π -(000) plotted in the $[q_{x,y}, q_{x,y}, q_z]$ plane for $\theta = -5^\circ$. The qualitative features do not depend on θ . The saddle point equations increased the symmetry to $SU(2)$ by setting $t^{h,z} = 0$. Therefore, all diagonal elements of the structure factor are equal and all off-diagonal elements vanish. The black dashed line shows the boundary of the extended Brillouin zone.

The neutron scattering amplitude can be found in Fig. 7.4. The NSF channel is dominated by broad vertical features which are 4π -periodic. The SF channel has a characteristic bow tie structure where the general features are separated by the lines $q_z = \pm q_{x,z}$. It has broad features in $[0, 0, q_z]$ direction and features similar to the local spin structure factor in the $[q_{x,z}, q_{x,z}, 0]$ direction. In the sum of both channels the features of the SF channel can still be seen but are smeared out. The neutron scattering amplitude is very similar to those of the pseudo Heisenberg anti-ferromagnet which has been found to be a candidate ground state for the Heisenberg point [8] as well as the result of a recent pseudofermion functional renormalization group study for $\theta = 20^\circ$ [20].

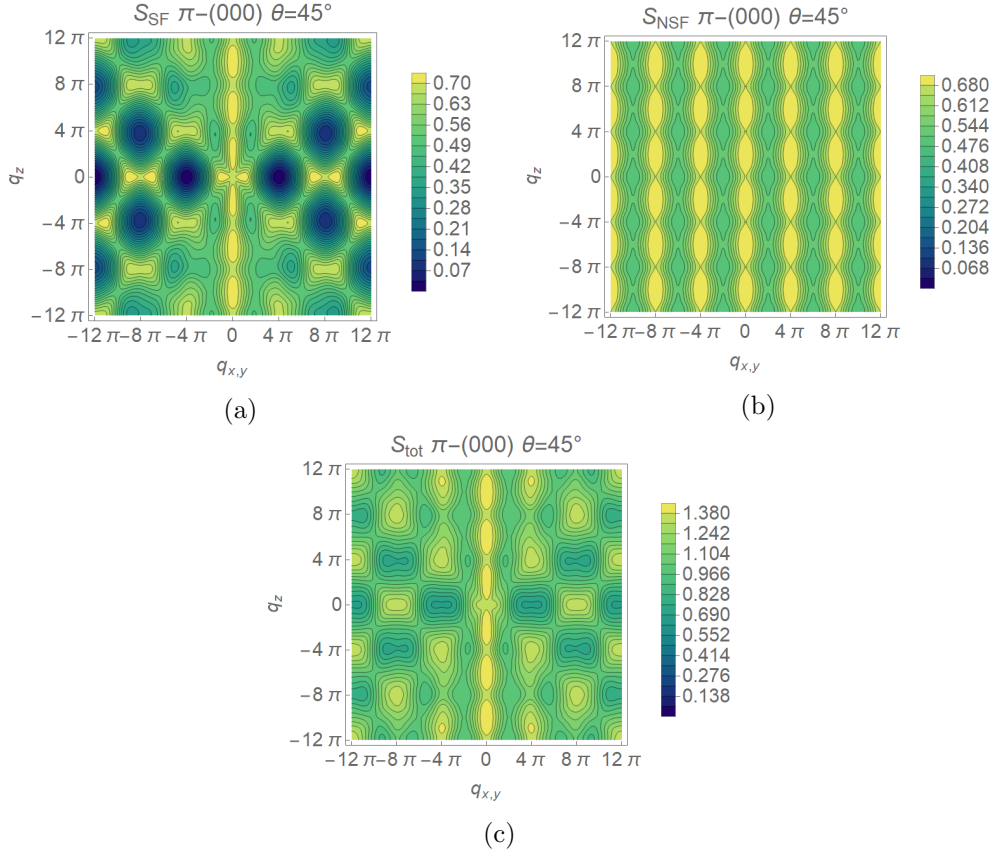


Figure 7.4: Neutron scattering amplitude of the π -(000) ansatz plotted in the $[q_{x,y}, q_{x,y}, q_z]$ plane: (a) SF channel, (b) NSF channel (c) Sum of both channels.

0-(101)

The structure factor of 0-(101) is shown in Fig. 7.5. The only two independent components are $S^{xx} = S^{yy}$ and S^{zz} all off-diagonal components vanish. There are ferromagnetic correlations in the $S^x - S^y$ direction and antiferromagnetic correlations in the S^z direction. The magnetic correlations in $S^x - S^y$ direction have the same structure as the correlations of AF_\perp but the features are not as sharp [20]. Its neutron scattering amplitude can be seen in Fig. 7.6. It is also dominated by the sharp features. The SF channel has the same peak structure as the total spin flip channel of AF_\perp and the NSF channel of both are similar as well [20]. This is an indication that 0-(101) might be a quantum disordered version of AF_\perp . This agrees with the results of Liu et al. [18] that find AF_\perp order to be generically present when the spinon gap of 0-(101) closes and the spinons condense.

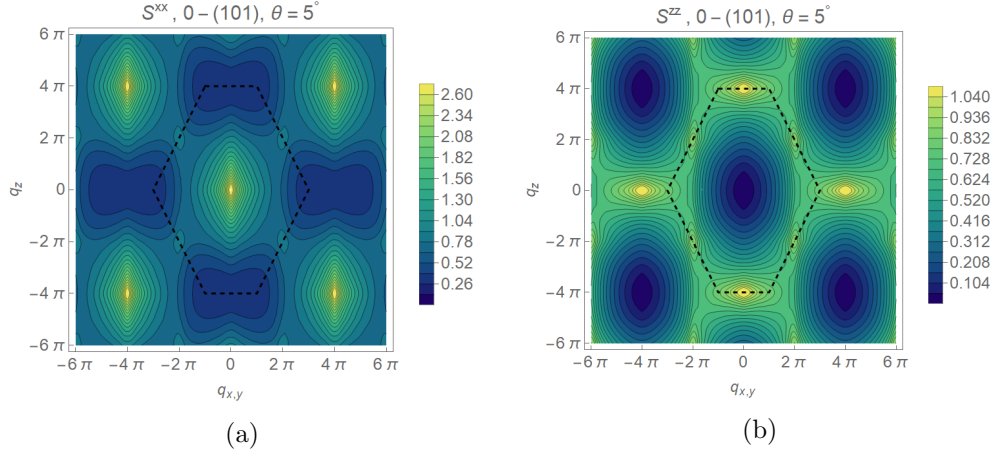


Figure 7.5: Local spin structure factor of the 0-(101) with $U(1)$ symmetric decoupling plotted in the $[q_{x,y}, q_{x,y}, q_z]$ plane for $\theta = 5^\circ$: (a) $\mathcal{S}^{xx} = \mathcal{S}^{yy}$, (b) \mathcal{S}^{zz} . All off-diagonal components vanish. The black dashed line shows the boundary of the extended Brillouin zone.

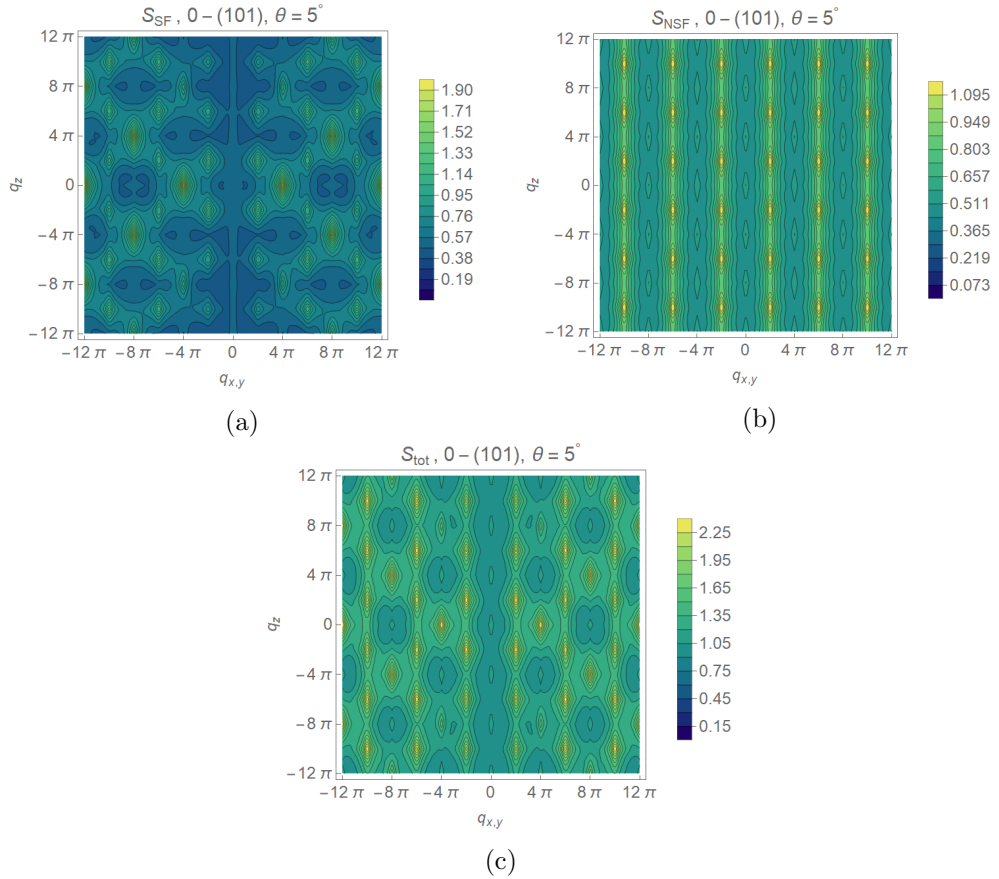


Figure 7.6: Neutron scattering amplitude of the 0-(101) ansatz plotted in the $[q_{x,y}, q_{x,y}, q_z]$ plane: (a) SF channel, (b) NSF channel (c) Sum of both channels.

π -(100)

The local spin structure factor of π -(100) is shown in Fig. 7.7. The only two independent components are $\mathcal{S}^{xx} = \mathcal{S}^{yy}$ and \mathcal{S}^{zz} all off-diagonal components vanish. There are ferromagnetic correlations in the $S^x - S^y$ direction and antiferromagnetic correlation in the S^z direction. The structure factor has broad pinch points at $q = (2\pi, 2\pi, 2\pi)$ but is missing them at $q = (0, 0, 4\pi)$. The features are much broader than those of the local spin structure factor of ansatz 0-(101). This might be due to the smaller value of \mathcal{B} .

Its neutron scattering amplitude can be seen in Fig. 7.8. It is similar to that of ansatz 0-(101) but with much broader features. This makes the double bow tie structure in the SF and total channel more apparent. It is interesting to note, that the local structure factor does look similar to the one of QSI₀ [20]. The only apparent difference being the absence of the $q = (0, 0, 4\pi)$ pinch points. However, the neutron scattering amplitude of π -(100) and QSI₀ have no similar features [20].

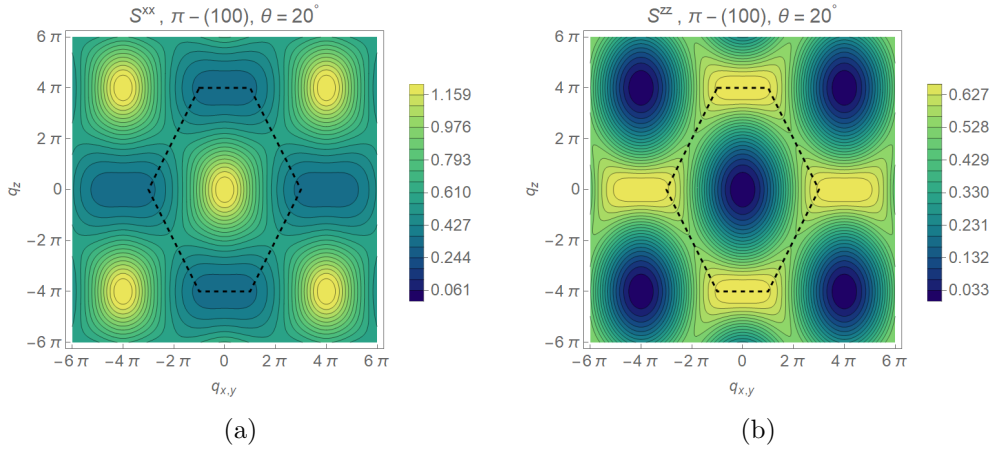


Figure 7.7: Local spin structure factor of the 0-(101) with $U(1)$ symmetric decoupling plotted in the $[q_x, y, q_x, y, q_z]$ plane for $\theta = 20^\circ$. (a) $\mathcal{S}^{xx} = \mathcal{S}^{yy}$, (b) \mathcal{S}^{zz} . All off-diagonal components vanish. The black dashed line shows the boundary of the extended Brillouin zone.

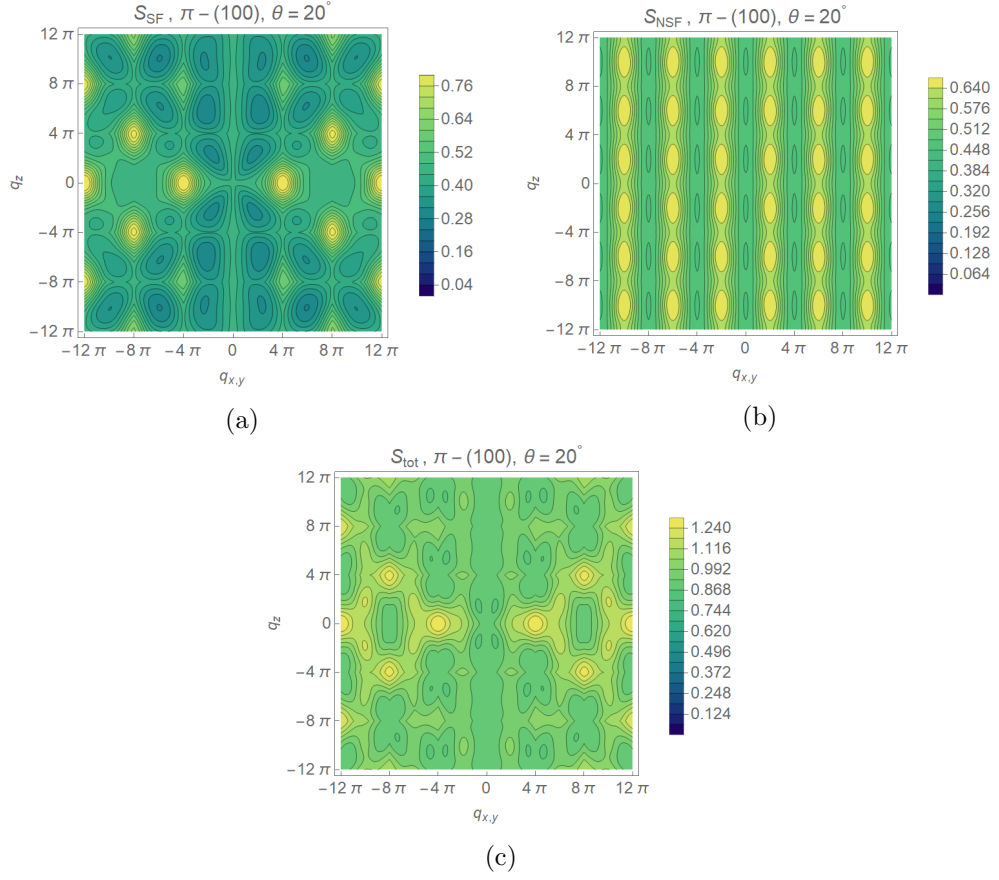


Figure 7.8: Neutron scattering amplitude of the π -(100) ansatz plotted in the $[q_x, y, q_x, y, q_z]$ plane: (a) SF channel, (b) NSF channel (c) Sum of both channels.

0-(100)

The local spin structure factor of 0-(100) is shown in Fig. 7.9. All three diagonal components are different and the off-diagonal element \mathcal{S}^{xy} does not vanish. This is because the state, while breaking the $U(1)$ spin rotation symmetry, still satisfies the C_3 lattice symmetry. This can be understood in the classical limit: $S_i^x S_j^y = (S^2 - S_i^z S_j^z) \frac{\sqrt{3}}{2} \neq 0$. The structure factor has pinch points in the \mathcal{S}^{xy} component at $q = (0, 0, 0)$ and $q = (2\pi, 2\pi, 2\pi)$. This is also the only component with negative correlations. The features are very broad in the \mathcal{S}^{xx} and \mathcal{S}^{yy} component.

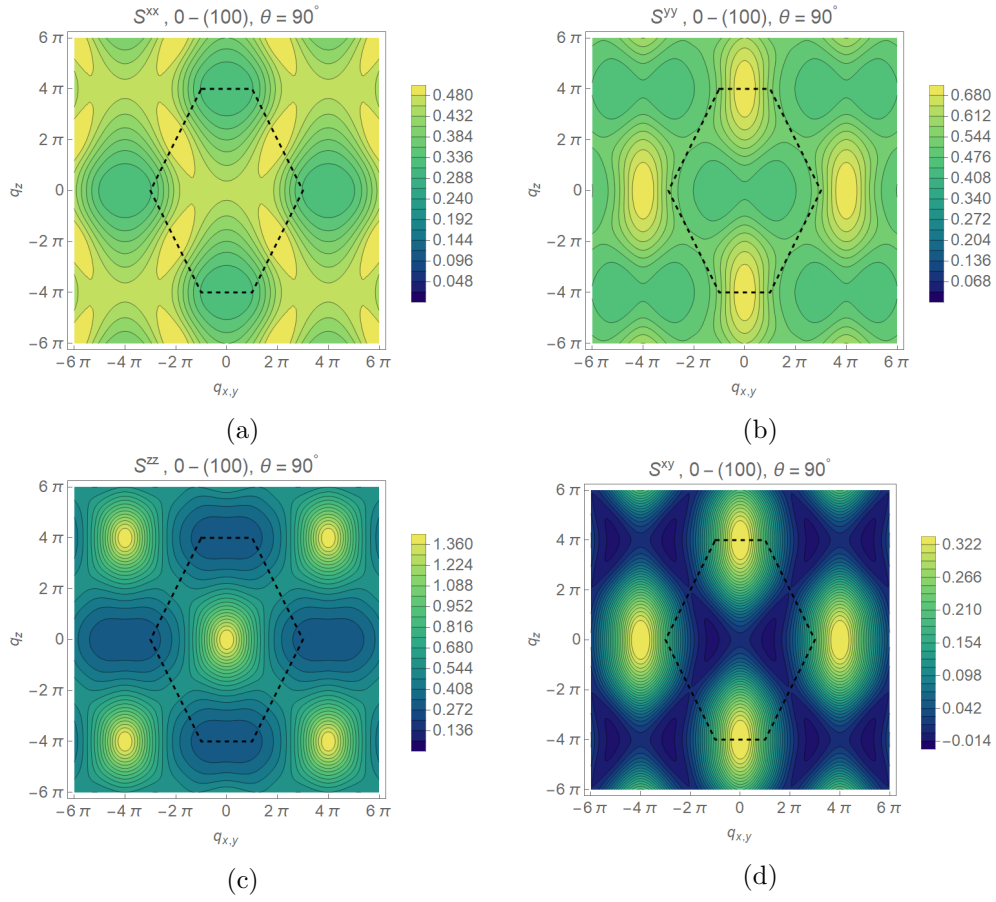


Figure 7.9: Local spin structure factor of the 0-(100) with $U(1)$ symmetry breaking decoupling plotted in the $[q_x, y, q_x, y, q_z]$ plane for $\theta = 90^\circ$. (a) \mathcal{S}^{xx} , (b) \mathcal{S}^{yy} , (c) \mathcal{S}^{zz} , (d) \mathcal{S}^{xy} . The black dashed line shows the boundary of the extended Brillouin zone.

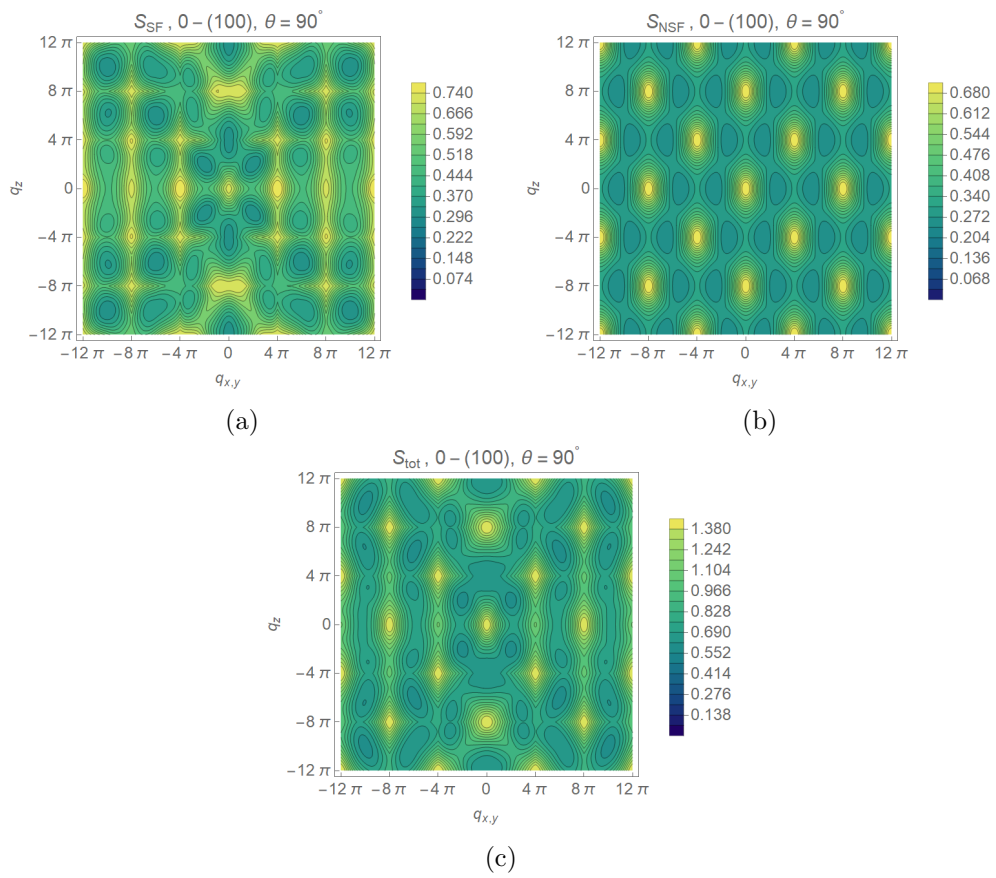


Figure 7.10: Neutron scattering amplitude of the 0-(100) ansatz plotted in the $[q_x, y, q_x, y, q_z]$ plane: (a) SF channel, (b) NSF channel (c) Sum of both channels.

0-(110)-Nem

The local spin structure factor of 0-(110)-Nem is shown in Fig. 7.11. In the same way as for 0-(100), all three diagonal components are different and the off-diagonal element \mathcal{S}^{xy} does not vanish. This is because the state, while breaking the $U(1)$ spin rotation symmetry, still satisfies the C_3 lattice symmetry. The local structure factor has broad pinch points in the \mathcal{S}^{xy} component, where it also has negative correlations. The features are very broad in the \mathcal{S}^{xx} and \mathcal{S}^{yy} component. Its local spin structure factor is related to the one of 0-(100) by a 90° spin rotation around the S^z axis. \mathcal{S}^{xx} and \mathcal{S}^{yy} are exchanged while \mathcal{S}^{zz} remains the same. The \mathcal{S}^{xy} component has a different sign because the spin rotation maps $S^x \rightarrow S^y$ and $S^y \rightarrow -S^x$.

All channels of the neutron scattering amplitude in Fig. 7.12 are dominated by a hexagonal structure. The NSF channel has peaks where the NSF channel of 0-(100) has troughs. This is not true for the SF channel.

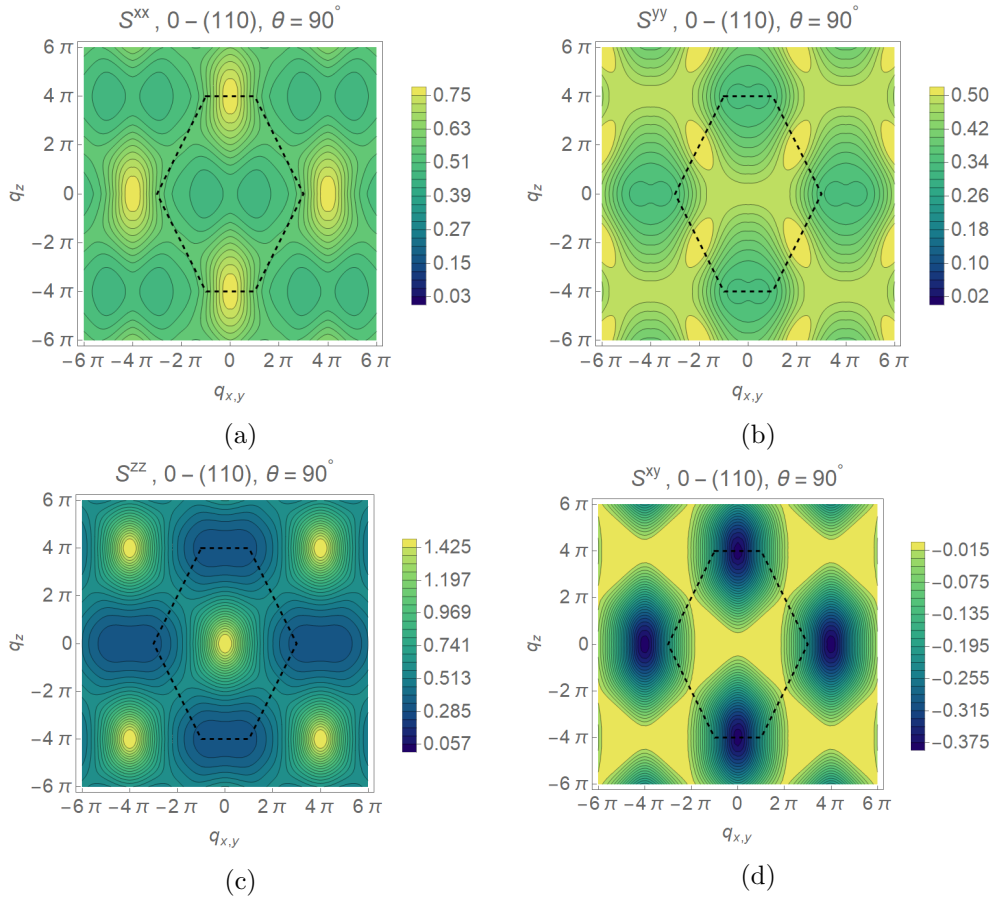


Figure 7.11: Local spin structure factor of the 0-(110)-Nem with $U(1)$ symmetry breaking decoupling plotted in the $[q_{x,y}, q_{x,y}, q_z]$ plane for $\theta = 90^\circ$. (a) \mathcal{S}^{xx} , (b) \mathcal{S}^{yy} , (c) \mathcal{S}^{zz} , (d) \mathcal{S}^{xy} . The black dashed line shows the boundary of the extended Brillouin zone.

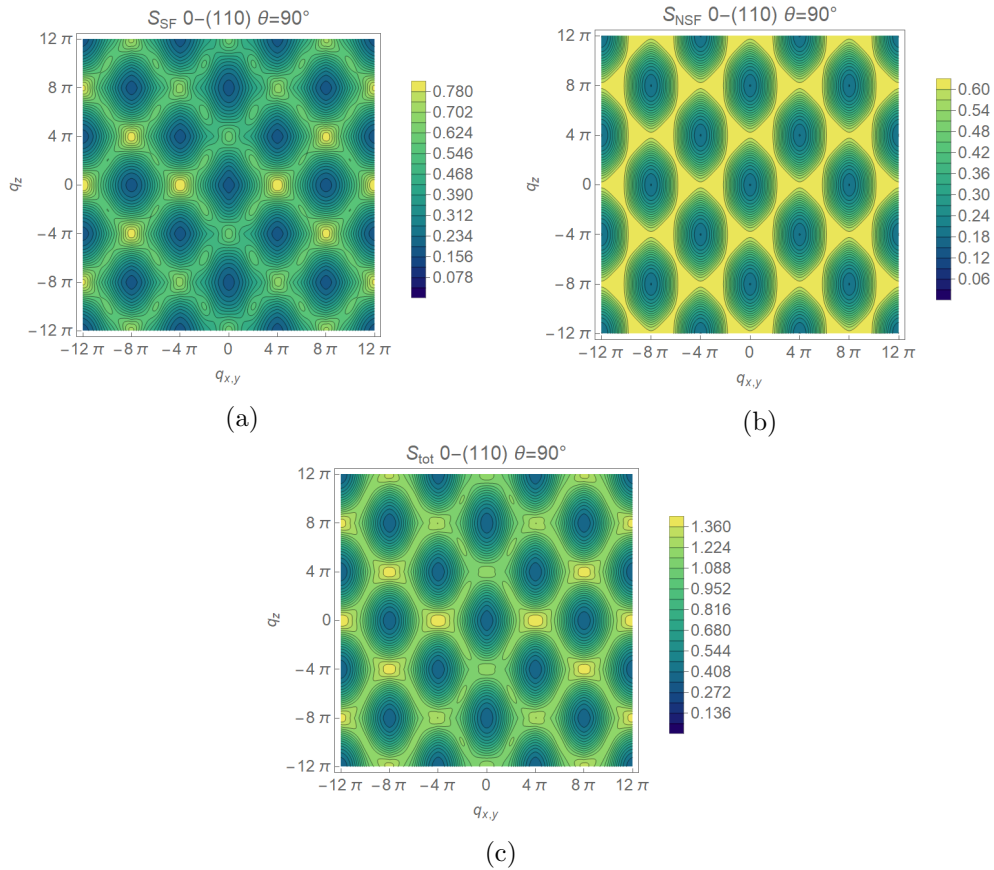


Figure 7.12: Neutron scattering amplitude of the 0-(100) ansatz plotted in the $[q_x, q_y, q_z]$ plane: (a) SF channel, (b) NSF channel (c) Sum of both channels.

7.3 Discussion

When comparing the solutions to the mean field equations, it is crucial to emphasize that the results are heavily dependent on the mean field decoupling. We especially want to highlight the difference of the solutions for 0-(101) and 0-(101)-Nem. Here, the coupling angles θ for which the mean field equations have solutions are completely different. They depend solely on the mean field decoupling and not on the chosen mean field ansatz. This strong dependence on the mean field decoupling makes a rigorous analysis challenging. Especially, since there is a priori no best mean field decoupling to choose. It is even possible to continuously interpolate between different mean field decouplings. In special cases this leads to a continuous change of the mean field ground state energy depending on the decoupling. This issue rules out the mean field energy as a ground state indicator. Therefore, a meaningful ground state indicator has to be found. In our analysis we resort to the comparison of observables with ground states determined by other methods.

As a rule of thumb, close to the antiferromagnetic Heisenberg point a mean field decoupling with \mathcal{A} fields describes the antiferromagnetic correlations well. Close to the ferromagnetic Heisenberg point a mean field decoupling with \mathcal{B} fields should be chosen. For general XXZ coupling angles, triplet fields can capture the $SU(2)$

symmetry breaking. This is reflected in our results for 0-(101) and π -(000). From a ferromagnetic perspective the mean field decoupling for 0-(101) is able to capture the ferromagnetic correlations in \mathcal{B} . The antiferromagnetic correlations in S^z direction that break $SU(2)$ symmetry are described by $t^{p,z}$ for $\theta \in \{-90^\circ, 0^\circ\}$. This is expected to break down for $\theta > 0^\circ$. The comparison of global observables shows similarity to AF_\perp but no similarity to QSI_0 .

On the other hand, the mean field decoupling for π -(000) is able to describe the antiferromagnetic correlations at the Heisenberg point in the \mathcal{A} field. This is seen in the excellent agreement of the structure factor and neutron scattering amplitude to published results at the Heisenberg point. In the present decoupling, the $t^{h,z}$ field is capable of capturing $SU(2)$ breaking correlations. However, the mean field equations set $t^{h,z} = 0$. Therefore, the resulting state is $SU(2)$ symmetric. A priori, we do not expect an $SU(2)$ symmetric state to describe the ground state far away from the Heisenberg point well. However, a study for $\theta = 20^\circ$ shows only minor $SU(2)$ breaking. This indicates stability for the $SU(2)$ symmetric π -(000) ansatz well into the XXZ coupling regime. We expect this similarity to break down no later than at $\theta = 0^\circ$, as ferromagnetic correlations should be present in the $S^x - S^y$ plane for negative coupling angles. These cannot be described with \mathcal{A} and $t^{h,z}$.

A symmetric ansatz that is able to describe all correlations correctly from $\theta \in \{-90^\circ, 90^\circ\}$ is not available due to the heavy restriction on allowed mean fields by the PSG (see Tab. 4.1). However, the weakly symmetric ansätze $n_3\pi - (1, p_1, -1, \epsilon_I, 0)$ can have \mathcal{B} as well as $t^{p,x}$, $t^{p,y}$, $t^{p,z}$ fields on every bond (see Tab. 4.2). Investigating its behavior in a future study could be insightful.

For the $U(1)$ symmetry breaking ansätze 0-(100) and 0-(110)-Nem we find degenerate mean field energies. Their local spin structure factors are related by a 90° spin rotation around the S^z axis. However, the difference of their neutron scattering amplitudes is non-trivial. Due to the mean field decoupling with \mathcal{B} and $t^{p,x}$ or $t^{p,y}$ fields we expect the ansätze do be able to correctly describe correlations for $\theta \in \{90^\circ, 135^\circ\}$. To the best of our knowledge states with these symmetries have not yet been reported in the XXZ-Model. Contrary to the $U(1)$ symmetry breaking nematic spin liquid described by Benton et al. [7], they do not break C_3 symmetry. However, to decide which of the $U(1)$ symmetry breaking states better describe the ground more further investigations are needed.

Conclusion

We studied the XXZ-Heisenberg Model on the pyrochlore lattice using SBMFT with 12 symmetric ansätze and 4 different mean field decouplings. We solved the mean field equations self consistently. We calculated mean field energies, the local structure factors and neutron scattering amplitudes for five selected states. For 0-(101) we found partial agreement with neutron scattering of the AF_{\perp} phase. Structure factor and neutron scattering amplitudes of the π -(000) ansatz show excellent agreement with previous work for the Heisenberg point as well as with one study for $\theta = 20^{\circ}$. A closer analysis of this ansatz and other π -flux ansätze like presented by Liu et al. for the 0-flux states [7] appears to be promising. However, we propose to compare the neutron scattering amplitudes of different π -flux states instead of the trace of the static spin susceptibility. We found the off-diagonal terms of the global spin susceptibility to strongly influence the neutron scattering amplitude. Including them avoids misleadingly similar results for different ansätze. Furthermore, the investigation of spinon condensation patterns that appear when the spinon gap closes can show connections of spin liquid ansätze to magnetic orders. This connection between quantum spin liquid and classical ground state can serve as a criterion to select or rule out an ansatz as a quantum ground state candidate.

Additionally, we supplemented the results of SBMFT by calculating the first order corrections to the ground states in Holstein-Primakoff spin wave theory. Our results show that the quantum AIAO ground state energy is the classical AIAO energy. The quantum AF_{\perp} ground state energy is lower than its classical counterpart. However, linear spin wave theory breaks down for $\theta \gtrsim 20^{\circ}$ due to divergence of the magnon density.

Using PSG we classified all weakly symmetric mean field ansätze on the lattice. To the best of our knowledge this is the first time this has been done for a 3D lattice. We went beyond the formalism of Messio et al. [19] by including triplet fields into our weakly symmetric PSG analysis. We identified the 8 weakly symmetric ansätze $n_3\pi - (0, p_1, -1, \epsilon_I, 0)$ as corresponding to chiral spin liquids that have been proposed as ground state candidates in fermionic mean field theory by Kim et al. [17] and Burnell et al. [15]. In future studies it would be highly interesting to solve the mean field equations and calculate spin structure factors as well as neutron scattering amplitudes for those ansätze. Since we included triplet terms in our PSG analysis for the weakly symmetric ansätze, the stability of such states to perturbations by $SU(2)$ breaking interactions can be investigated. Furthermore, the weakly

8. Conclusion

symmetric ansätze $n_3\pi - (1, p_1, -1, \epsilon_I, 0)$ allow a mean field decoupling that has potential to correctly capture the antiferromagnetic correlations for $\theta \in \{0^\circ, 90^\circ\}$ and could capture instability to nematicity at $\theta = 45^\circ$. Due to the higher amount of independent mean field parameters a more computational approach to solving the mean field equations is needed.

From Global to Local Spin Basis

The sublattice $SO(3)$ rotation matrices to change from global to local spin basis on sublattice μ are given by [8]

$$\begin{aligned}
 R_0 &= \frac{1}{\sqrt{6}} \begin{pmatrix} -2 & 0 & \sqrt{2} \\ 1 & -\sqrt{3} & \sqrt{2} \\ 1 & \sqrt{3} & \sqrt{2} \end{pmatrix}, & R_1 &= \frac{1}{\sqrt{6}} \begin{pmatrix} -2 & 0 & \sqrt{2} \\ -1 & \sqrt{3} & -\sqrt{2} \\ -1 & -\sqrt{3} & -\sqrt{2} \end{pmatrix}, \\
 R_2 &= \frac{1}{\sqrt{6}} \begin{pmatrix} 2 & 0 & -\sqrt{2} \\ 1 & -\sqrt{3} & \sqrt{2} \\ -1 & -\sqrt{3} & -\sqrt{2} \end{pmatrix}, & R_3 &= \frac{1}{\sqrt{6}} \begin{pmatrix} 2 & 0 & -\sqrt{2} \\ -1 & \sqrt{3} & -\sqrt{2} \\ 1 & \sqrt{3} & \sqrt{2} \end{pmatrix}.
 \end{aligned} \tag{A.1}$$

The corresponding $SU(2)$ matrices U_μ are

$$\begin{aligned}
 U_0 &= \begin{pmatrix} \frac{1}{\sqrt{3-\sqrt{3}}} e^{i\frac{2\pi 11}{48}} & \frac{1}{\sqrt{3+\sqrt{3}}} e^{i\frac{2\pi 5}{48}} \\ \frac{1}{\sqrt{3+\sqrt{3}}} e^{i\frac{2\pi 19}{48}} & \frac{1}{\sqrt{3-\sqrt{3}}} e^{-i\frac{2\pi 11}{48}} \end{pmatrix}, & U_1 &= \begin{pmatrix} \frac{1}{\sqrt{3+\sqrt{3}}} e^{-i\frac{2\pi 7}{48}} & \frac{1}{\sqrt{3-\sqrt{3}}} e^{-i\frac{2\pi}{48}} \\ \frac{1}{\sqrt{3-\sqrt{3}}} e^{-i\frac{2\pi 23}{48}} & \frac{1}{\sqrt{3+\sqrt{3}}} e^{i\frac{2\pi 7}{48}} \end{pmatrix}, \\
 U_2 &= \begin{pmatrix} \frac{1}{\sqrt{3+\sqrt{3}}} e^{i\frac{2\pi 5}{48}} & \frac{1}{\sqrt{3-\sqrt{3}}} e^{-i\frac{2\pi 13}{48}} \\ \frac{1}{\sqrt{3-\sqrt{3}}} e^{-i\frac{2\pi 11}{48}} & \frac{1}{\sqrt{3+\sqrt{3}}} e^{-i\frac{2\pi 5}{48}} \end{pmatrix}, & U_3 &= \begin{pmatrix} \frac{1}{\sqrt{3-\sqrt{3}}} e^{-i\frac{2\pi}{48}} & \frac{1}{\sqrt{3+\sqrt{3}}} e^{i\frac{2\pi 17}{48}} \\ \frac{1}{\sqrt{3+\sqrt{3}}} e^{i\frac{2\pi 7}{48}} & \frac{1}{\sqrt{3-\sqrt{3}}} e^{i\frac{2\pi}{48}} \end{pmatrix}.
 \end{aligned} \tag{A.2}$$

The u matrices introduced in Chpt. 4 transform like

$$(u_{\mu\nu}^h)_l = U_\mu (u_{\mu\nu}^h)_g U_\mu^\dagger, \tag{A.3}$$

$$(u_{\mu\nu}^p)_l = U_\mu (u_{\mu\nu}^p)_g U_\mu. \tag{A.4}$$

Solution of the Chiral Algebraic PSG

The symmetry enriched algebraic relations of χ_e are

$$(G_{T_i} T_i)(G_{T_{i+1}} T_{i+1})(G_{T_i} T_i)^{-1}(G_{T_{i+1}} T_{i+1})^{-1} \in \mathbb{Z}_2, \quad (\text{B.1a})$$

$$(G_{C_3} C_3)^3 \in \mathbb{Z}_2, \quad (\text{B.1b})$$

$$(G_{C'_3} C'_3)^3 \in \mathbb{Z}_2, \quad (\text{B.1c})$$

$$(G_{C_3} C_3)(G_{C'_3} C'_3)(G_{C_3} C_3)(G_{C'_3} C'_3) \in \mathbb{Z}_2 \quad (\text{B.1d})$$

$$(G_{C_3} C_3)(G_{T_i} T_i)(G_{C_3} C_3)^{-1}(G_{T_{i+1}} T_{i+1})^{-1} \in \mathbb{Z}_2, \quad (\text{B.1e})$$

$$(G_{C'_3} C'_3)(G_{T_1} T_1)(G_{C'_3} C'_3)^{-1}(G_{T_2} T_2)^{-1}(G_{T_1} T_1) \in \mathbb{Z}_2, \quad (\text{B.1f})$$

$$(G_{C'_3} C'_3)(G_{T_2} T_2)(G_{C'_3} C'_3)^{-1}(G_{T_1} T_1) \in \mathbb{Z}_2, \quad (\text{B.1g})$$

$$(G_{C'_3} C'_3)(G_{T_3} T_3)(G_{C'_3} C'_3)^{-1}(G_{T_3} T_3)^{-1}(G_{T_1} T_1) \in \mathbb{Z}_2. \quad (\text{B.1h})$$

These can be rewritten into the following phase equations

$$\phi_{T_i}[\mathbf{r}_\mu] + \phi_{T_{i+1}}[T_i^{-1}(\mathbf{r}_\mu)] - \phi_{T_i}[T_{i+1}^{-1}(\mathbf{r}_\mu)] - \phi_{T_{i+1}}[\mathbf{r}_\mu] = \pi n_i, \quad (\text{B.2a})$$

$$\begin{aligned} \phi_{C_3}[\mathbf{r}_\mu] + \phi_{C'_3}[(C_3)^{-1}(\mathbf{r}_\mu)] + \phi_{C_3}[(C_3 C'_3)^{-1}(\mathbf{r}_\mu)] \\ + \phi_{C'_3}[C'_3(\mathbf{r}_\mu)] = \pi n_{C_3, C'_3}, \end{aligned} \quad (\text{B.2b})$$

$$\phi_{C_3}[\mathbf{r}_\mu] + \phi_{C_3}[C_3^{-1}(\mathbf{r}_\mu)] + \phi_{C_3}[C_3^{-2}(\mathbf{r}_\mu)] = \pi n_{C_3}, \quad (\text{B.2c})$$

$$\phi_{C'_3}[\mathbf{r}_\mu] + \phi_{C'_3}[(C'_3)^{-1}(\mathbf{r}_\mu)] + \phi_{C'_3}[(C'_3)^{-2}(\mathbf{r}_\mu)] = \pi n_{C'_3}, \quad (\text{B.2d})$$

$$\phi_{C_3}[\mathbf{r}_\mu] + \phi_{T_i}[C_3^{-1}(\mathbf{r}_\mu)] - \phi_{C_3}[T_{i+1}^{-1}(\mathbf{r}_\mu)] - \phi_{T_{i+1}}[\mathbf{r}_\mu] = \pi n_{C_3 T_i}, \quad (\text{B.2e})$$

$$\begin{aligned} \phi_{C'_3}[\mathbf{r}_\mu] + \phi_{T_1}[(C'_3)^{-1}(\mathbf{r}_\mu)] - \phi_{C'_3}[T_1^{-1} T_2(\mathbf{r}_\mu)] \\ - \phi_{T_2}[T_1^{-1}(\mathbf{r}_\mu)] + \phi_{T_1}[T_1(\mathbf{r}_\mu)] = \pi n_{C'_3 T_1}, \end{aligned} \quad (\text{B.2f})$$

$$\begin{aligned} \phi_{C'_3}[\mathbf{r}_\mu] + \phi_{T_2}[(C'_3)^{-1}(\mathbf{r}_\mu)] - \phi_{C'_3}[T_1^{-1}(\mathbf{r}_\mu)] \\ + \phi_{T_1}[T_1(\mathbf{r}_\mu)] = \pi n_{C'_3 T_2}, \end{aligned} \quad (\text{B.2g})$$

$$\begin{aligned} \phi_{C'_3}[\mathbf{r}_\mu] + \phi_{T_3}[(C'_3)^{-1}(\mathbf{r}_\mu)] - \phi_{C'_3}[T_1^{-1} T_3(\mathbf{r}_\mu)] \\ - \phi_{T_3}[T_1^{-1}(\mathbf{r}_\mu)] + \phi_{T_1}[T_1(\mathbf{r}_\mu)] = \pi n_{C'_3 T_3}. \end{aligned} \quad (\text{B.2h})$$

where $n_X \in \{0, 1\}$

Gauge Freedom

In the process of solving the phase equations we will fix the gauge. Since we have 4 fcc sublattices we have freedom to choose 16 independent gauges. Four for every direction r_1, r_2, r_3 and a constant one for every sublattice $\mu = 0, 1, 2, 3$:

$$G_1 : \phi_1[\mathbf{r}_\mu] = n_{G1,\mu}\pi r_1, \quad (\text{B.3a})$$

$$G_2 : \phi_2[\mathbf{r}_\mu] = n_{G2,\mu}\pi r_2, \quad (\text{B.3b})$$

$$G_3 : \phi_3[\mathbf{r}_\mu] = n_{G3,\mu}\pi r_3, \quad (\text{B.3c})$$

$$G_4 : \phi_4[\mathbf{r}_\mu] = \phi_\mu. \quad (\text{B.3d})$$

A general gauge transformations changes the phases given by the PSG phase equations like:

$$\phi_X[\mathbf{r}_\mu] \rightarrow \phi_G[\mathbf{r}_\mu] + \phi_X[\mathbf{r}_\mu] - \phi_G[X^{-1}(\mathbf{r}_\mu)]. \quad (\text{B.4})$$

Due to the IGG = \mathbb{Z}_2 , we are also free to add a site independent \mathbb{Z}_2 phase to any of the five phases $\phi_{\mathcal{O}}[\mathbf{r}_\mu]$ [32] corresponding to the five generators of χ_e . That makes 16 gauge and 5 IGG choices in total. With the first 12 gauge choices (Eq. (B.3a)-(B.3c)) we can fix the phases associated with the translation operators to $\phi_{T_1}[(r_1, r_2, r_3)_\mu] = \phi_{T_2}[(0, r_2, r_3)_\mu] = \phi_{T_3}[(0, 0, r_3)_\mu] = 0$. Note, that this can only be satisfied for open boundary conditions [32, Appendix A]

Phase for Translation

Using our choice $\phi_{T_1}[(r_1, r_2, r_3)_\mu] = \phi_{T_2}[(0, r_2, r_3)_\mu] = \phi_{T_3}[(0, 0, r_3)_\mu] = 0$ Eq. (B.2a) becomes:

$$\phi_{T_2}[(r_1 - 1, r_2, r_3)_\mu] - \phi_{T_2}[\mathbf{r}_\mu] = n_1\pi, \quad (\text{B.5})$$

$$\phi_{T_2}[\mathbf{r}_\mu] - \phi_{T_2}[(r_1, r_2, r_3 - 1)_\mu] + \phi_{T_3}[(r_1, r_2 - 1, r_3)_\mu] - \phi_{T_3}[\mathbf{r}_\mu] = n_2\pi, \quad (\text{B.6})$$

$$\phi_{T_3}[\mathbf{r}_\mu] - \phi_{T_3}[(r_1 - 1, r_2, r_3)_\mu] = n_3\pi. \quad (\text{B.7})$$

Therefore:

$$\phi_{T_2}[\mathbf{r}_\mu] = -n_1\pi r_1 + f_{T_2}(r_2, r_3), \quad (\text{B.8})$$

$$\phi_{T_3}[\mathbf{r}_\mu] = n_3\pi r_1 + f_{T_3}(r_2, r_3). \quad (\text{B.9})$$

with unknown functions $f_{T_2}(r_2, r_3)$ and $f_{T_3}(r_2, r_3)$. We can find a constraint by plugging in equations (B.8) and (B.9) into (B.6):

$$f_{T_2}(r_2, r_3) - f_{T_2}(r_2 - 1, r_3) + f_{T_3}(r_2 - 1, r_3) - f_{T_3}(r_2, r_3) = n_2\pi. \quad (\text{B.10})$$

To solve this, we can choose $f_{T_2}(r_2, r_3) = 0$ and $f_{T_3}(r_2, r_3) = -n_2\pi r_2$ and arrive at

$$\phi_{T_1}[\mathbf{r}_\mu] = 0, \quad (\text{B.11})$$

$$\phi_{T_2}[\mathbf{r}_\mu] = -n_1\pi r_1, \quad (\text{B.12})$$

$$\phi_{T_3}[\mathbf{r}_\mu] = n_3\pi r_1 - n_2\pi r_2. \quad (\text{B.13})$$

Phase for C_3 Rotation

Writing out Eq. (B.2e) we get:

$$\begin{aligned}
& \phi_{C_3}[\mathbf{r}_\mu] - \phi_{C_3}[(r_1, r_2 - 1, r_3)_\mu] + \phi_{T_1}[(r_2, r_3, r_1)_{\pi_{321}(\mu)}] - \phi_{T_2}[(r_1, r_2, r_3)_\mu] \\
&= \phi_{C_3}[\mathbf{r}_\mu] - \phi_{C_3}[(r_1, r_2 - 1, r_3)_\mu] - n_1\pi r_1 \\
&= n_{C_3 T_1} \pi,
\end{aligned} \tag{B.14a}$$

$$\begin{aligned}
& \phi_{C_3}[\mathbf{r}_\mu] - \phi_{C_3}[(r_1, r_2, r_3 - 1)_\mu] + \phi_{T_2}[(r_2, r_3, r_1)_{\pi_{321}(\mu)}] + \phi_{T_3}[(r_1, r_2, r_3)_\mu] \\
&= \phi_{C_3}[\mathbf{r}_\mu] - \phi_{C_3}[(r_1, r_2, r_3 - 1)_\mu] + n_3\pi r_1 - n_2\pi r_2 - n_1\pi r_2 \\
&= n_{C_3 T_2} \pi,
\end{aligned} \tag{B.14b}$$

$$\begin{aligned}
& \phi_{C_3}[\mathbf{r}_\mu] - \phi_{C_3}[(r_1 - 1, r_2, r_3)_\mu] + \phi_{T_3}[(r_2, r_3, r_1)_{\pi_{321}(\mu)}] + \phi_{T_1}[(r_1, r_2, r_3)_\mu] \\
&= \phi_{C_3}[\mathbf{r}_\mu] - \phi_{C_3}[(r_1 - 1, r_2, r_3)_\mu] + n_3\pi r_2 - n_2\pi r_3 \\
&= n_{C_3 T_3} \pi.
\end{aligned} \tag{B.14c}$$

Therefore

$$\phi_{C_3}[\mathbf{r}_\mu] = f_{C_3}(r_1, r_3) - r_2(n_{C_3 T_1} \pi + n_1\pi r_1), \tag{B.15a}$$

$$\phi_{C_3}[\mathbf{r}_\mu] = f_{C_3}(r_1, r_2) - r_3(n_{C_3 T_2} \pi + n_3\pi r_1 - n_2\pi r_2 - n_1\pi r_2), \tag{B.15b}$$

$$\phi_{C_3}[\mathbf{r}_\mu] = f_{C_3}(r_2, r_3) - r_1(n_{C_3 T_3} \pi + n_3\pi r_2 - n_2\pi r_3). \tag{B.15c}$$

Since the function $f_{C_3}(r_1, r_3)$ in (B.15a) can not include any terms that feature r_2 it can not include terms like $r_1 n_3 \pi r_2$ that have to appear in $\phi_{C_3}[\mathbf{r}_\mu]$ due to (B.15c). To fulfill equations (B.15a)-(B.15c) we have to infer a relationship between n_1, n_2, n_3 . With $n_1 = n_2 = n_3$ we get the following solution:

$$\phi_{C_3}[\mathbf{r}_\mu] = \phi_{C_3}[\mathbf{0}_\mu] - (r_1 n_{C_3 T_3} + r_2 n_{C_3 T_1} + r_3 n_{C_3 T_2})\pi - n_3\pi(r_1 r_2 + r_1 r_3). \tag{B.16}$$

Plugging Eq. (B.16) into (B.2c) gives:

$$\begin{aligned}
& \phi_{C_3}[\mathbf{r}_\mu] + \phi_{T_1}[(r_2, r_3, r_1)_{\pi_{321}(\mu)}] + \phi_{T_1}[(r_3, r_1, r_2)_{\pi_{123}(\mu)}] \\
&= \phi_{C_3}[\mathbf{0}_\mu] + \phi_{C_3}[\mathbf{0}_{\pi_{123}(\mu)}] + \phi_{C_3}[\mathbf{0}_{\pi_{321}(\mu)}] + \sum_{i,j} r_i n_{C_3 T_j} \pi \\
&= n_{C_3} \pi,
\end{aligned} \tag{B.17}$$

which constrains $\sum_j n_{C_3 T_j} = 0$. $\pi_{123}(\mu)$ permutes μ in the cycle (123).

Phase for C'_3 Rotation

Writing out Eq. (B.2e) we get:

$$\begin{aligned}
 & \phi_{C'_3}[\mathbf{r}_\mu] - \phi_{C'_3}[(r_1 - 1, r_2 + 1, r_3)_\mu] + \phi_{T_1}[(r_2, -r_1 - r_2 - r_3 - 1, r_3)_{\pi_{021}(\mu)}] \\
 & \quad - \phi_{T_2}[(r_1 - 1, r_2, r_3)_\mu] + \phi_{T_1}[(r_1 + 1, r_2, r_3)_\mu] \\
 = & \phi_{C'_3}[\mathbf{r}_\mu] - \phi_{C'_3}[(r_1 - 1, r_2 + 1, r_3)_\mu] + n_3\pi(r_1 + 1) \\
 = & n_{C'_3 T_1} \pi, \tag{B.18a}
 \end{aligned}$$

$$\begin{aligned}
 & \phi_{C'_3}[\mathbf{r}_\mu] - \phi_{C'_3}[(r_1 + 1, r_2, r_3)_\mu] + \phi_{T_2}[(r_2, -r_1 - r_2 - r_3 - 1, r_3)_{\pi_{021}(\mu)}] \\
 & \quad + \phi_{T_1}[(r_1 + 1, r_2, r_3)_\mu] \\
 = & \phi_{C'_3}[\mathbf{r}_\mu] - \phi_{C'_3}[(r_1 - 1, r_2, r_3)_\mu] + n_3\pi r_2 \\
 = & n_{C'_3 T_2} \pi, \tag{B.18c}
 \end{aligned}$$

$$\begin{aligned}
 & \phi_{C'_3}[\mathbf{r}_\mu] - \phi_{C'_3}[(r_1 - 1, r_2, r_3 + 1)_\mu] + \phi_{T_3}[(r_2, -r_1 - r_2 - r_3 - 1, r_3)_{\pi_{021}(\mu)}] \\
 & \quad - \phi_{T_3}[(r_1 - 1, r_2, r_3)_\mu] + \phi_{T_1}[(r_1 + 1, r_2, r_3)_\mu] \\
 = & \phi_{C'_3}[\mathbf{r}_\mu] - \phi_{C'_3}[(r_1 - 1, r_2, r_3 + 1)_\mu] + n_3\pi(r_2 + r_3) \\
 = & n_{C'_3 T_3} \pi. \tag{B.18d}
 \end{aligned}$$

From Eq. (B.18c) we can infer that

$$\phi_{C'_3}[\mathbf{r}_\mu] = f_{C'_3}(r_2, r_3) + n_3\pi r_1 r_2 + n_{C'_3 T_2} \pi r_1, \tag{B.19}$$

where $f_{C'_3}(r_2, r_3)$ is some function of r_2 and r_3 . Using this and Eq. (B.18d) we get

$$\phi_{C'_3}[\mathbf{r}_\mu] = f_{C'_3}(r_2) + n_3\pi r_1 r_2 + n_{C'_3 T_2} \pi r_1 + r_3\pi \left(\frac{r_3 - 1}{2} n_3 + n_{C'_3 T_2} + n_{C'_3 T_3} \right). \tag{B.20}$$

Plugging this into Eq. (B.18a) finally gives

$$\begin{aligned}
 \phi_{C'_3}[\mathbf{r}_\mu] = & \phi_{C'_3}[\mathbf{0}_\mu] + r_1\pi n_{C'_3 T_2} + r_3\pi \left(\frac{r_3 - 1}{2} n_3 + n_{C'_3 T_2} + n_{C'_3 T_3} \right) + n_3\pi r_1 r_2 \\
 & + r_2\pi \left(\frac{r_2 - 1}{2} n_3 + n_{C'_3 T_2} + n_{C'_3 T_1} \right). \tag{B.21}
 \end{aligned}$$

Inserting Eq. (B.29f) into Eq. (B.2d) gives

$$\begin{aligned}
 & \phi_{C'_3}[\mathbf{r}_\mu] + \phi_{C'_3}[(r_2, -r_1 - r_2 - r_3 - 1, r_3)_{\pi_{021}(\mu)}] \\
 & \quad + \phi_{C'_3}[(-r_1 - r_2 - r_3 - 1, r_1, r_3)_{\pi_{120}(\mu)}] \\
 = & \phi_{C'_3}[\mathbf{0}_\mu] + \phi_{C'_3}[\mathbf{0}_{\pi_{021}(\mu)}] + \phi_{C'_3}[\mathbf{0}_{\pi_{120}(\mu)}] \\
 & \quad + (n_{C'_3 T_1} + n_3)\pi + r_3\pi(n_{C'_3 T_1} + n_{C'_3 T_2} + n_{C'_3 T_3}) \\
 = & n_{C'_3} \pi, \tag{B.22}
 \end{aligned}$$

which gives two constraints

$$n_{C'_3 T_1} + n_{C'_3 T_2} + n_{C'_3 T_3} = 0, \tag{B.23}$$

$$\phi_{C'_3}[\mathbf{0}_\mu] + \phi_{C'_3}[\mathbf{0}_{\pi_{021}(\mu)}] + \phi_{C'_3}[\mathbf{0}_{\pi_{120}(\mu)}] = (n_{C'_3 T_1} + n_3 + n_{C'_3}). \tag{B.24}$$

The last phase equation (B.2b) is then

$$\begin{aligned}
& \phi_{C_3}[\mathbf{r}_\mu] + \phi_{C'_3}[(r_2, r_3, r_1)_{\pi_{132}(\mu)}] + \phi_{C_3}[(r_3, -r_1 - r_2 - r_3 - 1, r_1)_{\pi_{(20)(13)}(\mu)}] \\
& + \phi_{C'_3}[(-r_1 - r_2 - r_3 - 1, r_1, r_3)_{\pi_{120}(\mu)}] \\
& = \phi_{C_3}[\mathbf{0}_\mu] + \phi_{C'_3}[\mathbf{0}_{\pi_{132}(\mu)}] + \phi_{C_3}[\mathbf{0}_{\pi_{(20)(13)}(\mu)}] + \phi_{C'_3}[\mathbf{0}_{\pi_{120}(\mu)}] + (n_{C'_3 T_2} + n_{C_3 T_1})\pi \\
& = n_{C_3 C'_3} \pi, \tag{B.25}
\end{aligned}$$

$\pi_{(20)(13)}(\mu)$ permutes μ in the cycles (20) and (13).

Since equations (B.1b), (B.1c), (B.1e) and (??) have operators that appear an odd number of times, we can use our 5 IGG choices of T_1, T_2, T_3, C_3, C'_3 to set $n_{C'_3 T_1} = n_{C_3 T_2} = n_{C_3 T_3} = n_{C_3} = 0$ and $n_{C'_3} = n_3$. Using $\sum_j n_{C_3 T_j} = 0$ this also implies $n_{C_3 T_1} = 0$.

As a last step we find $\phi_{C_3}[\mathbf{0}_\mu]$ and $\phi_{C'_3}[\mathbf{0}_\mu]$. We have the four constant sublattice gauge choices left (Eq. (B.3d)). By fixing the IGG choices Eqs. (B.17) and (B.24) are reduced to

$$3\phi_{C_3}[\mathbf{0}_0] = 0, \tag{B.26a}$$

$$\phi_{C_3}[\mathbf{0}_1] + \phi_{C_3}[\mathbf{0}_2] + \phi_{C_3}[\mathbf{0}_3] = 0, \tag{B.26b}$$

$$3\phi_{C'_3}[\mathbf{0}_3] = 0, \tag{B.26c}$$

$$\phi_{C'_3}[\mathbf{0}_1] + \phi_{C'_3}[\mathbf{0}_2] + \phi_{C'_3}[\mathbf{0}_0] = 0. \tag{B.26d}$$

The form of equations (B.26) is invariant under gauge transformations. That is why we can fix the constant gauge on sublattices 1,2,3 to set $\phi_{C_3}[\mathbf{0}_2] = \phi_{C_3}[\mathbf{0}_3] = 0$ as well as $\phi_{C'_3}[\mathbf{0}_1] = 0$. Eqs. (B.26) and (B.24) then also imply $\phi_{C_3}[\mathbf{0}_1] = 0$ and $\phi_{C'_3}[\mathbf{0}_2] = -\phi_{C'_3}[\mathbf{0}_0]$. Eq. (B.25) then reduces to

$$\phi_{C_3}[\mathbf{0}_0] - \phi_{C'_3}[\mathbf{0}_2] = (n_{C'_3 T_2} + n_{C_3 C'_3})\pi, \tag{B.27}$$

$$\phi_{C'_3}[\mathbf{0}_2] + \phi_{C'_3}[\mathbf{0}_3] = (n_{C'_3 T_2} + n_{C_3 C'_3})\pi. \tag{B.28}$$

Therefore, $\phi_{C_3}[\mathbf{0}_0] = -\phi_{C'_3}[\mathbf{0}_3] = \frac{2\pi k}{3}$ where $k \in \{-1, 0, 1\}$ and $\phi_{C'_3}[\mathbf{0}_2] = \phi_{C_3}[\mathbf{0}_0] + (n_{C'_3 T_2} + n_{C_3 C'_3})\pi$.

The final solution is then:

$$\phi_{T_1}[\mathbf{r}_\mu] = 0, \tag{B.29a}$$

$$\phi_{T_2}[\mathbf{r}_\mu] = n_3 \pi r_1, \tag{B.29b}$$

$$\phi_{T_3}[\mathbf{r}_\mu] = n_3 \pi (r_1 + r_2), \tag{B.29c}$$

$$\phi_{C_3}[\mathbf{r}_\mu] = \frac{2\pi k}{3} \delta_{\mu 0} + n_3 \pi (r_1 r_2 + r_1 r_3), \tag{B.29d}$$

$$\phi_{C'_3}[\mathbf{r}_\mu] = -\frac{2\pi k}{3} \delta_{\mu 3} + \left(\frac{2\pi k}{3} + n_{C_3 C'_3} + n_{C'_3 T_2}\right)(-\delta_{\mu 0} + \delta_{\mu 2})\pi \tag{B.29e}$$

$$\begin{aligned}
& + r_1 \pi n_{C'_3 T_2} + r_3 \pi \frac{r_3 - 1}{2} n_3 + n_3 \pi r_1 r_2 \\
& + r_2 \pi \left(\frac{r_2 - 1}{2} n_3 + n_{C'_3 T_2}\right). \tag{B.29f}
\end{aligned}$$

There is one gauge choice left to set one field to be real and $n_3, n_{C_3 C'_3}, n_{C'_3 T_2} \in \{0, 1\}$.

Classification of Chiral Ansätze

We will use the short notation $\mathcal{B}_{\mathbf{0}_\mu\mathbf{0}_\mu} = \mathcal{B}_{\mu\nu}$ for bonds on the main tetrahedron and $\mathcal{B}_{I(\mathbf{0}_\mu)I(\mathbf{0}_\mu)} = \mathcal{B}_{I\mu\nu}$ for bonds on the inverse tetrahedron.

As described by Messio et al. [19] we can classify all possible ansätze by looking at the transformation of the minimal set of linearly independent fluxes under elements in χ_o . All elements of χ_o can be written as compositions of S , \overline{C}_6 and elements of χ_e . The elements of χ_e leave the fluxes invariant so we only have to consider the action of S and \overline{C}_6 on the fluxes. For convenience we use the fact that \overline{C}_6 can be written as a composition of $I \in \chi_o$ and $C_3 \in \chi_e$ and ultimately consider the action of S and I on the fluxes. Since $\overline{C}_6 = IC_3$ it follows that $\epsilon_I = \epsilon_{\overline{C}_6}$. Fluxes are independent if they can not be mapped onto each other by symmetry operations in χ_e and can not be created by adding other independent fluxes. The number of independent fluxes depends on the number of present mean field parameters as well.

To find out how many independent fluxes there are we start with how many independent loops of even and odd length there are in the pyrochlore lattice independent of possible bond variables.

1. Triangle (Loop Size = 3): There are 8 triangles in the pyrochlore unit cell. There are two sets of three triangles that can be mapped onto each other by C_3 which leaves us with 2 triangle loops on the inverse and main tetrahedron. These can be mapped onto each other by C'_3 rotation and translation. In total we therefore have two independent triangle loops.
2. Rhombus (Loop size = 4): There are 6 rhombi in the pyrochlore unit cell. Three on each tetrahedron. All rhombi on a tetrahedron can be mapped onto each other by C_3 which leaves us with two independent rhombi.
3. Bow tie (Loop size = 6): There are 12 bow ties and 24 "bent" bow ties in the unit cells (0,0,0), and the three main tetrahedra of the cells (0,0,-1), (0,-1,0), (-1,0,0): 9 per two adjacent tetrahedra. By C_3 mapping we can reduce the number to 12. 3 in the tetrahedra of (0,0,0) and 9 in the tetrahedra of e.g. (0,0,0) and (-1,0,0).

We can further reduce the number by realizing that if we add a rhombus to a bow tie we get a bent bow tie. This reduces the number of loops to $\frac{12}{6} = 2$. These can finally be mapped onto each other by C'_3 rotations which leaves one independent bow tie flux.

4. Hexagon (Loop size = 6) Four unit cells always enclose a hexagon. This can be seen in Fig. 3.1b. There are 4 different hexagons that can not be mapped onto each other by translations. By C_3 symmetry we can reduce this to 2 and by C'_3 symmetry to one independent hexagon.
5. Bigger loops (Loop size > 6): All loops with size larger than 6 can be created by adding loops of smaller size and therefore do not add to the linearly independent loops.

The triangle and rhombus loops on the main tetrahedron can be mapped to the same loops on the inverse tetrahedron by I . From the algebraic relations we can see that $SI = S^2IS$. So screw and inversion symmetries commute modulo $S^2 \in \chi_e$ which leaves fluxes invariant. Therefore, transformation of triangle and rhombus fluxes on the main and inverse tetrahedra give the same constraints. We will therefore only consider them on the inverse tetrahedron.

Transformation of hexagonal loops give the same constraints as the bow ties. We will therefore not consider the hexagonal fluxes here explicitly. Figs. C.1 show how all independent Loops transform under screw and inversion symmetry. When we now specify fluxes by adding bond operators we can transform these loop diagrams into equations. Fluxes can in principle consist of one, two or many different types of bond operators. E.g. $\text{Arg}(\mathcal{B}_{12}\mathcal{B}_{23}\mathcal{B}_{31})$, $\text{Arg}(\mathcal{A}_{12}\mathcal{B}_{23}^{h,z}\mathcal{A}_{31}^*)$, $\text{Arg}(\mathcal{B}_{12}t_{23}^{h,x}t_{31}^{h,z})$. We only have to consider fluxes with one or two fields. Loops with three or more fields can be constructed from these.

Before we can start turning the diagrams into equations we have to define our bond fields. Since there are two independent bonds we will have two independent phases for each field.

We fix these as $\mathcal{B}_{01} = \mathcal{B}e^{-i\phi_{B_1}}$, $\mathcal{A}_{01} = \mathcal{A}e^{-i\phi_{A_1}}$, $\mathcal{A}_{01} = \mathcal{A}e^{-i\phi_{A_1}}$ (on the main tetrahedron) and $\mathcal{B}_{I01} = \mathcal{B}e^{-i\phi_{B_2}}$, $\mathcal{A}_{I01} = \mathcal{A}e^{-i\phi_{A_2}}$, $\mathcal{A}_{I01} = \mathcal{A}e^{-i\phi_{A_2}}$ (on the inverse tetrahedron) and equivalently for $t_{ij}^{h,z}$ and $t_{ij}^{p,z}$.

Transformation of x and y triplet operators is not as trivial because symmetry operations change the direction. For example:

$$C_3(C_3(\hat{t}_{01}^x)) = C_3(-\frac{1}{2}\hat{t}_{02}^x + \frac{\sqrt{3}}{2}\hat{t}_{02}^y) = -\frac{1}{2}\hat{t}_{0,3}^x - \frac{\sqrt{3}}{2}\hat{t}_{03}^y, \quad (\text{C.1a})$$

$$C_3(C_3(\hat{t}_{01}^y)) = C_3(-\frac{\sqrt{3}}{2}\hat{t}_{02}^x - \frac{1}{2}\hat{t}_{02}^y) = \frac{\sqrt{3}}{2}\hat{t}_{03}^x - \frac{1}{2}\hat{t}_{03}^y. \quad (\text{C.1b})$$

We will define new operators with easier transformation properties:

$$\hat{t}_{03}^{h,x'} := C_3(\hat{t}_{0,2}^{h,x'}) := C_3(C_3(\hat{t}_{0,1}^{h,x'})) := C_3(C_3(\hat{t}_{0,1}^{h,x})), \quad (\text{C.2a})$$

$$\hat{t}_{1,2}^{h,x'} := C_3(\hat{t}_{3,1}^{h,x'}) := C_3(C_3(\hat{t}_{2,3}^{h,x'})) := C_3(C_3(\hat{t}_{2,3}^{h,x})) \quad (\text{C.2b})$$

and equivalently for the bonds on the inverse tetrahedron, the pairing triplet operators and the y-triplet fields. The operators $\hat{t}_{ij}^{h,x'}$ and $\hat{t}_{ij}^{h,y'}$ are linearly independent on every bond. We fix their expectation values as $t_{01}^{p,x'} = t^{p,x}e^{-i\phi_{t_1^{p,x}}}$, $t_{I01}^{p,x'} = t^{p,x}e^{-i\phi_{t_2^{p,x}}}$, $t_{01}^{p,y'} = t^{p,x}e^{-i\phi_{t_1^{p,x}}}$, $t_{I01}^{p,y'} = t^{p,x}e^{-i\phi_{t_2^{p,x}}}$ and equivalently for the hopping triplet fields. The operators transform as

$$\hat{B}_{ji} = \hat{B}_{ij}^\dagger, \quad \hat{t}_{ji}^{h,\gamma} = -(\hat{t}_{ij}^{h,\gamma})^\dagger, \quad \hat{A}_{ji} = -\hat{A}_{ij}, \quad \hat{t}_{ji}^{p,\gamma} = \hat{t}_{ij}^{p,\gamma}. \quad (\text{C.3})$$

Table C.1: The signs that fields pick up when being transformed under screw rotation. Note that singlet (s) and y' - triplet fields pick up the same signs.

Bonds	s	x'	y'	z
I01 \rightarrow 31	-	+	-	+
I02 \rightarrow 32	+	-	+	-
I03 \rightarrow 30	+	-	+	-
I12 \rightarrow 12	-	+	-	+
I23 \rightarrow 20	+	-	+	-
I31 \rightarrow 01	-	+	-	+

To keep calculations short we will use the superscript $\gamma \in \{x', y', z\}$ to label the triplet operators. Also note that the triplet x' and z operators pick up an extra π phase when acted upon by the screw operation compared to the singlet and triplet y operators. This is not due to a gauge transformation added to the screw operation but solely due to the spin rotation (see Tab. C.1).

In the following subsections we consider all possible one and two operator fluxes and translate their transformation behavior into constraints for the phases $\phi_{\mathcal{O}_i}$. The solutions to the equations can be found in Tab. 4.2.

Fluxes with \mathcal{B}_{ij} Fields

Hopping operators can be written in gauge invariant loops of odd size. For \mathcal{B}_{ij} fields, the only independent loops we have to consider are the triangles.

Fig. C.1(a) gives the following equations:

$$\text{Arg}(\mathcal{B}_{I01}\mathcal{B}_{I12}\mathcal{B}_{I20}) = \epsilon_I \text{Arg}(\mathcal{B}_{01}\mathcal{B}_{12}\mathcal{B}_{20}), \quad (\text{C.4a})$$

$$\text{Arg}(\mathcal{B}_{I01}\mathcal{B}_{I12}\mathcal{B}_{I20}) = \epsilon_S \text{Arg}(\mathcal{B}_{31}\mathcal{B}_{12}\mathcal{B}_{23}). \quad (\text{C.4b})$$

If we use the transformation property $\mathcal{B}_{ji} = \mathcal{B}_{ij}^*$ (see Eq. (C.3)) we can translate equations (C.4) into equations for the phases

$$\phi_{B_2} + \frac{4k\pi}{3} + n_3\pi = \epsilon_I(\phi_{B_1} + \frac{4k\pi}{3}), \quad (\text{C.5a})$$

$$\phi_{B_2} + \frac{4k\pi}{3} + n_3\pi = 3\epsilon_S\phi_{B_1}. \quad (\text{C.5b})$$

Fluxes with \mathcal{A}_{ij} Fields

Pairing operators can only be written in gauge invariant loops of even length, where \mathcal{A} and \mathcal{A}^* alternate. Therefore, we have to consider the rhombus and bow tie loops of Fig. C.1(b,c).

$$\text{Arg}(\mathcal{A}_{I01}\mathcal{A}_{I12}^*\mathcal{A}_{I23}\mathcal{A}_{I30}^*) = \epsilon_I \text{Arg}(\mathcal{A}_{01}\mathcal{A}_{12}^*\mathcal{A}_{23}\mathcal{A}_{30}^*), \quad (\text{C.6a})$$

$$\text{Arg}(\mathcal{A}_{I01}\mathcal{A}_{I12}^*\mathcal{A}_{I23}\mathcal{A}_{I30}^*) = \epsilon_S \text{Arg}(\mathcal{A}_{31}\mathcal{A}_{12}^*\mathcal{A}_{20}\mathcal{A}_{03}^*), \quad (\text{C.6b})$$

$$\text{Arg}(\mathcal{A}_{I01}\mathcal{A}_{I12}^*\mathcal{A}_{I20}\mathcal{A}_{01}^*\mathcal{A}_{12}\mathcal{A}_{20}^*) = \epsilon_I \text{Arg}(\mathcal{A}_{01}\mathcal{A}_{12}^*\mathcal{A}_{20}\mathcal{A}_{I01}^*\mathcal{A}_{12}\mathcal{A}_{I20}^*), \quad (\text{C.6c})$$

$$\text{Arg}(\mathcal{A}_{I01}\mathcal{A}_{I12}^*\mathcal{A}_{I20}\mathcal{A}_{01}^*\mathcal{A}_{12}\mathcal{A}_{20}^*) = \epsilon_S \text{Arg}(\mathcal{A}_{31}\mathcal{A}_{12}^*\mathcal{A}_{23}\mathcal{A}_{I31}^*\mathcal{A}_{12}\mathcal{A}_{I23}^*). \quad (\text{C.6d})$$

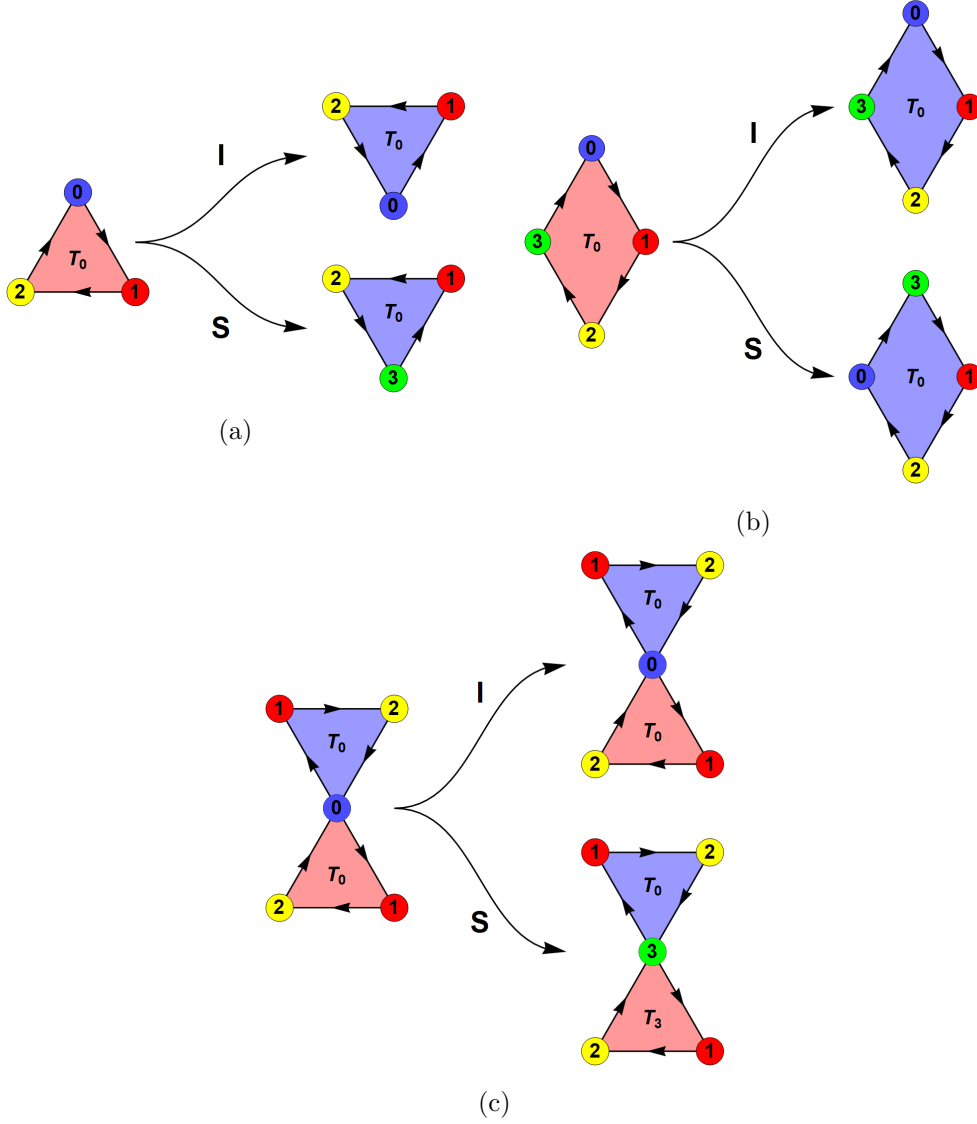


Figure C.1: Transformations of the (a) triangle, (b) rhombus and (c) bow tie loops under inversion (I) and screw (S) symmetry. T_0 labels the tetrahedra of the $(0,0,0)$ unit cell, T_3 labels the tetrahedra of the $(0,0,1)$ unit cell and so on.

The rhombus fluxes give constraints for the PSG parameter k :

$$\frac{4k\pi}{3} = \epsilon_I \frac{4k\pi}{3}, \quad (\text{C.7a})$$

$$\frac{4k\pi}{3} = \epsilon_S \frac{2k\pi}{3}. \quad (\text{C.7b})$$

Therefore, there are only solutions for $k \neq 0$ if $\epsilon_I = -\epsilon_S = 1$. The bow tie loops give constraints for the phases

$$(\phi_{A_1} - \phi_{A_2}) = \epsilon_I (\phi_{A_2} - \phi_{A_1}), \quad (\text{C.8a})$$

$$(\phi_{A_1} - \phi_{A_2}) = \epsilon_S (\phi_{A_2} - \phi_{A_1}). \quad (\text{C.8b})$$

Fluxes with $t_{ij}^{h,\gamma}$ Fields

As for the \mathcal{B}_{ij} fields we only have to consider triangle fluxes:

$$\text{Arg}(t_{I01}^{h,\gamma} t_{I12}^{h,\gamma} t_{I20}^{h,\gamma}) = \epsilon_I \text{Arg}(t_{01}^{h,\gamma} t_{12}^{h,\gamma} t_{20}^{h,\gamma}), \quad (\text{C.9a})$$

$$\text{Arg}(t_{I01}^{h,\gamma} t_{I12}^{h,\gamma} t_{I20}^{h,\gamma}) = \epsilon_S \text{Arg}(t_{31}^{h,\gamma} t_{12}^{h,\gamma} t_{23}^{h,\gamma}) + \pi(1 - \delta_{\gamma,y'}). \quad (\text{C.9b})$$

The terms $\pi(1 - \delta_{\gamma,y'})$ come from the spin rotation part of the screw symmetry. Using $t_{ji}^{h,\gamma} = -t_{ij}^{h,\gamma*}$ we get the phase equations

$$\phi_{t_2^{h,\gamma}} + \frac{4k\pi}{3} + n_3\pi = \epsilon_I(\phi_{t_1^{h,\gamma}} + \frac{4k\pi}{3}), \quad (\text{C.10a})$$

$$\phi_{t_2^{h,\gamma}} + \frac{4k\pi}{3} + n_3\pi = 3\epsilon_S\phi_{t_1^{h,\gamma}} + \delta_{\gamma,y'}\pi. \quad (\text{C.10b})$$

Fluxes with $t_{i,j}^{p,\gamma}$ Fields

Since t^p are pairing fields, we have to consider the even rhombi and bow tie loops.

$$\text{Arg}(t_{I01}^{p,\gamma} t_{I12}^{p,\gamma*} t_{I23}^{p,\gamma} t_{I30}^{p,\gamma*}) = \epsilon_I \text{Arg}(t_{01}^{p,\gamma} t_{12}^{p,\gamma*} t_{23}^{p,\gamma} t_{30}^{p,\gamma*}), \quad (\text{C.11a})$$

$$\text{Arg}(t_{I01}^{p,\gamma} t_{I12}^{p,\gamma*} t_{I23}^{p,\gamma} t_{I30}^{p,\gamma*}) = \epsilon_S \text{Arg}(t_{31}^{p,\gamma} t_{12}^{p,\gamma*} t_{20}^{p,\gamma} t_{03}^{p,\gamma*}), \quad (\text{C.11b})$$

$$\text{Arg}(t_{I01}^{p,\gamma} t_{I12}^{p,\gamma*} t_{I20}^{p,\gamma} t_{01}^{p,\gamma*} t_{12}^{p,\gamma} t_{20}^{p,\gamma*}) = \epsilon_I \text{Arg}(t_{I01}^{p,\gamma} t_{I12}^{p,\gamma*} t_{I20}^{p,\gamma} t_{01}^{p,\gamma*} t_{12}^{p,\gamma} t_{20}^{p,\gamma*}), \quad (\text{C.11c})$$

$$\text{Arg}(t_{I01}^{p,\gamma} t_{I12}^{p,\gamma*} t_{I20}^{p,\gamma} t_{01}^{p,\gamma*} t_{12}^{p,\gamma} t_{20}^{p,\gamma*}) = \epsilon_S \text{Arg}(t_{I31}^{p,\gamma} t_{I12}^{p,\gamma*} t_{I23}^{p,\gamma} t_{31}^{p,\gamma*} t_{12}^{p,\gamma} t_{23}^{p,\gamma*}). \quad (\text{C.11d})$$

The rhombus fluxes give the same constraints ($k \neq 0$ only if $(\epsilon_I, \epsilon_S) = (1, -1)$) as Eq. (C.7). The bow tie fluxes give:

$$(\phi_{t_1^{p,\gamma}} - \phi_{t_2^{p,\gamma}}) = \epsilon_I(\phi_{t_2^{p,\gamma}} - \phi_{t_1^{p,\gamma}}), \quad (\text{C.12a})$$

$$(\phi_{t_1^{p,\gamma}} - \phi_{t_2^{p,\gamma}}) = \epsilon_S(\phi_{t_2^{p,\gamma}} - \phi_{t_1^{p,\gamma}}). \quad (\text{C.12b})$$

Fluxes with \mathcal{A}_{ij} and \mathcal{B}_{ij} Fields

We only have to consider triangle loops with one \mathcal{B}_{ij} field. All bow ties with two or four as well as rhombi with two \mathcal{B}_{ij} fields can be constructed from those together with triangles with three \mathcal{B}_{ij} field.

There are 2 independent choices to place one \mathcal{B}_{ij} field on the triangle loops:

$$\text{Arg}(\mathcal{B}_{I01} \mathcal{A}_{I12}^* \mathcal{A}_{I20}) = \epsilon_I \text{Arg}(\mathcal{B}_{01} \mathcal{A}_{12}^* \mathcal{A}_{20}), \quad (\text{C.13a})$$

$$\text{Arg}(\mathcal{B}_{I01} \mathcal{A}_{I12}^* \mathcal{A}_{I20}) = \epsilon_S \text{Arg}(\mathcal{B}_{31} \mathcal{A}_{12}^* \mathcal{A}_{23}). \quad (\text{C.13b})$$

These give the constraints:

$$\phi_{B_2} + (1 + n_3)\pi = \epsilon_I \phi_{B_1} + \pi, \quad (\text{C.14a})$$

$$\phi_{B_2} + (1 + n_3)\pi = \epsilon_S(\phi_{B_1} + \frac{2k\pi}{3}). \quad (\text{C.14b})$$

Using Eq. (C.5) and (C.7) we can reduce this to:

$$k = 0, \quad (\text{C.15a})$$

$$\epsilon_I \epsilon_S = -1, \quad (\text{C.15b})$$

$$2\phi_{B_1} = \pi, \quad (\text{C.15c})$$

$$\phi_{B_2} = \epsilon_I \phi_{B_1} + \pi n_3. \quad (\text{C.15d})$$

Fluxes with \mathcal{A}_{ij} and $t_{i,j}^{h,\gamma}$ Fields

We only have to consider the triangle loops with one $t_{i,j}^{h,\gamma}$ field:

$$\text{Arg}(t_{I01}^{h,\gamma} \mathcal{A}_{I12}^* \mathcal{A}_{I20}) = \epsilon_I \text{Arg}(t_{01}^{h,\gamma} \mathcal{A}_{12}^* \mathcal{A}_{20}), \quad (\text{C.16a})$$

$$\text{Arg}(t_{I01}^{h,\gamma} \mathcal{A}_{I12}^* \mathcal{A}_{I20}) = \epsilon_S \text{Arg}(t_{31}^{h,\gamma} \mathcal{A}_{12}^* \mathcal{A}_{23}) + \pi(1 - \delta_{\gamma,y'}), \quad (\text{C.16b})$$

They give constraints

$$\phi_{t_2^{h,\gamma}} + (1 + n_3)\pi = \epsilon_I \phi_{t_1^{h,\gamma}} + \pi, \quad (\text{C.17a})$$

$$\phi_{t_2^{h,\gamma}} + (1 + n_3)\pi = \epsilon_S \left(\phi_{t_1^{h,\gamma}} + \frac{2k\pi}{3} \right) + \pi(1 - \delta_{\gamma,y'}). \quad (\text{C.17b})$$

Using Eq. (C.10) we can rewrite this to

$$k = 0, \quad (\text{C.18a})$$

$$\delta_{\gamma,y'} = 0, \quad (\text{C.18b})$$

$$2\phi_{t_1^{h,\gamma}} = 0, \quad (\text{C.18c})$$

$$\phi_{t_2^{h,\gamma}} = \epsilon_I \phi_{t_1^{h,\gamma}} + n_3\pi. \quad (\text{C.18d})$$

Eq. (C.18b) says that there are no valid weakly symmetric ansätze with both \mathcal{A}_{ij} and $t_{ij}^{h,y'}$ fields.

Fluxes with \mathcal{A}_{ij} and $t_{i,j}^{p,\gamma}$ Fields

As established in the main text \mathcal{A}_{ij} and $t_{i,j}^{p,\gamma}$ Fields can not appear simultaneously in an ansatz. Therefore, we do not have to consider loops with both of these fields.

Fluxes with \mathcal{B}_{ij} and $t_{i,j}^{p,\gamma}$ Fields

Here we have to consider similar triangle loops as for \mathcal{A}_{ij} and \mathcal{B}_{ij} fields

$$\text{Arg}(\mathcal{B}_{I01} t_{I12}^{h,p*} t_{I20}^{h,p}) = \epsilon_I \text{Arg}(\mathcal{B}_{01} t_{12}^{h,p*} t_{20}^{h,p}), \quad (\text{C.19a})$$

$$\text{Arg}(\mathcal{B}_{I01} t_{I12}^{h,p*} t_{I20}^{h,p}) = \epsilon_S \text{Arg}(\mathcal{B}_{31} t_{12}^{h,p*} t_{23}^{h,p}). \quad (\text{C.19b})$$

These lead to the constraints:

$$\phi_{B_2} + n_3\pi = \epsilon_I \phi_{B_1}, \quad (\text{C.20a})$$

$$\phi_{B_2} + n_3\pi = \epsilon_S \left(\phi_{B_1} + \frac{2k\pi}{3} \right). \quad (\text{C.20b})$$

With Eq. (C.5) these can be reduced to:

$$k = 0, \quad (\text{C.21a})$$

$$2\phi_{B_1} = 0, \quad (\text{C.21b})$$

$$\phi_{B_1} = \epsilon_I \phi_{B_2} + n_3\pi. \quad (\text{C.21c})$$

Fluxes with \mathcal{B}_{ij} and $t_{i,j}^{h,\gamma}$ Fields

There are 2 independent triangle loops with only \mathcal{B}_{ij} and $t_{i,j}^{h,z}$ fields

$$\text{Arg}(t_{I01}^{h,\gamma} \mathcal{B}_{I12} \mathcal{B}_{I20}) = \epsilon_I \text{Arg}(t_{01}^{h,\gamma} \mathcal{B}_{12} \mathcal{B}_{20}), \quad (\text{C.22a})$$

$$\text{Arg}(t_{I01}^{h,\gamma} \mathcal{B}_{I12} \mathcal{B}_{I20}) = \epsilon_S \text{Arg}(t_{31}^{h,\gamma} \mathcal{B}_{12} \mathcal{B}_{23}) + \pi(1 - \delta_{\gamma,y'}), \quad (\text{C.22b})$$

that give the constraints:

$$\phi_{t_2^{h,\gamma}} + \frac{4k\pi}{3} + n_3\pi = \epsilon_I (\phi_{t_1^{h,\gamma}} + \frac{4k\pi}{3}), \quad (\text{C.23})$$

$$\phi_{t_2^{h,\gamma}} + \frac{4k\pi}{3} + n_3\pi = \epsilon_S (\phi_{t_1^{h,\gamma}} + 2\phi_{B_1}) + \pi(1 - \delta_{\gamma,y'}). \quad (\text{C.24})$$

Which can be reduced with Eq. (C.5) and (C.10) to

$$(1 - \epsilon_I \epsilon_S) (\phi_{t_1^{h,\gamma}} - \phi_{B_1}) = \pi(1 - \delta_{\gamma,y'}), \quad (\text{C.25a})$$

$$\phi_{t_2^{h,\gamma}} + n_3\pi = \epsilon_I \phi_{t_1^{h,\gamma}}. \quad (\text{C.25b})$$

For $\epsilon_I \epsilon_S = -1$ Eq.(C.25a) only has a solution for $\gamma \in \{x', z\}$. For $\epsilon_I \epsilon_S = 1$ it can only be solved for $\gamma = y'$

Fluxes with $t^{p,\gamma}$ and $t^{h,\gamma'}$ Fields

We have to consider the triangle loops

$$\text{Arg}(t_{I12}^{p,\gamma} t_{I20}^{p,\gamma} t_{I01}^{h,\gamma'}) = \epsilon_I \text{Arg}(t_{12}^{p,\gamma} t_{20}^{p,\gamma} t_{01}^{h,\gamma'}), \quad (\text{C.26a})$$

$$\text{Arg}(t_{I12}^{p,\gamma} t_{I20}^{p,\gamma} t_{I01}^{h,\gamma'}) = \epsilon_S \text{Arg}(t_{12}^{p,\gamma} t_{23}^{p,\gamma} t_{31}^{h,\gamma'}) + \pi(1 - \delta_{\gamma',y'}). \quad (\text{C.26b})$$

which give constraints:

$$\phi_{t_2^{h,\gamma'}} + n_3\pi = \epsilon_I \phi_{t_1^{h,\gamma'}}, \quad (\text{C.27a})$$

$$\phi_{t_2^{h,\gamma'}} + n_3\pi = \epsilon_S (\phi_{t_1^{h,\gamma'}} + \frac{2k\pi}{3}) + \pi(1 - \delta_{\gamma',y'}). \quad (\text{C.27b})$$

which can be reduced with Eq. (C.10) to

$$k = 0, \quad (\text{C.28a})$$

$$2\phi_{t_1^{h,\gamma'}} = \pi, \quad (\text{C.28b})$$

$$\phi_{t_1^{h,\gamma'}} = \epsilon_I \phi_{t_4^{h,\gamma'}} + n_3\pi. \quad (\text{C.28c})$$

Fluxes with $t^{p,\gamma}$ and $t^{p,\gamma'}$ Fields

We have to consider the independent rhombus fluxes

$$\text{Arg}(t_{I01}^{p,\gamma} (t_{I12}^{p,\gamma'})^* t_{I23}^{p,\gamma} (t_{I30}^{p,\gamma})^*) = \epsilon_I \text{Arg}(t_{01}^{p,\gamma} (t_{12}^{p,\gamma'})^* t_{23}^{p,\gamma} (t_{30}^{p,\gamma})^*), \quad (\text{C.29})$$

$$\text{Arg}(t_{I01}^{p,\gamma} (t_{I12}^{p,\gamma'})^* t_{I23}^{p,\gamma} (t_{I30}^{p,\gamma})^*) = \epsilon_S \text{Arg}(t_{31}^{p,\gamma} (t_{12}^{p,\gamma'})^* t_{20}^{p,\gamma} (t_{03}^{p,\gamma})^*) + \pi(\delta_{\gamma,y'} + \delta_{\gamma',y'}), \quad (\text{C.30})$$

which give

$$\phi_{t_2^{p,\gamma}} - \phi_{t_2^{p,\gamma'}} + \frac{4k\pi}{3} = \epsilon_I(\phi_{t_1^{p,\gamma}} - \phi_{t_1^{p,\gamma'}} + \frac{4k\pi}{3}), \quad (\text{C.31})$$

$$\phi_{t_2^{p,\gamma}} - \phi_{t_2^{p,\gamma'}} + \frac{4k\pi}{3} = \epsilon_S(\phi_{t_1^{p,\gamma}} - \phi_{t_1^{p,\gamma'}} + \frac{2k\pi}{3}) + \pi(\delta_{\gamma,y'} + \delta_{\gamma',y'}). \quad (\text{C.32})$$

This can be rewritten as

$$\phi_{t_2^{p,\gamma}} - \phi_{t_2^{p,\gamma'}} = \epsilon_I(\phi_{t_1^{p,\gamma}} - \phi_{t_1^{p,\gamma'}}), \quad (\text{C.33a})$$

$$(1 - \epsilon_I \epsilon_S)(\phi_{t_1^{p,\gamma}} - \phi_{t_1^{p,\gamma'}}) = \pi(\delta_{\gamma,y'} + \delta_{\gamma',y'}). \quad (\text{C.33b})$$

When $\epsilon_I \epsilon_S = 1$ there are no solutions for $\gamma \neq \gamma' = y'$.

Fluxes with $t^{h,\gamma}$ and $t^{h,\gamma'}$ Fields

There are two independent triangle fluxes with only $t^{h,\gamma}$ and $t^{h,\gamma'}$ fields where $\gamma \neq \gamma'$:

$$\text{Arg}(t_{I01}^{h,\gamma'} t_{I12}^{h,\gamma} t_{I20}^{h,\gamma}) = \epsilon_I \text{Arg}(t_{01}^{h,\gamma'} t_{12}^{h,\gamma} t_{20}^{h,\gamma}), \quad (\text{C.34})$$

$$\text{Arg}(t_{I01}^{h,\gamma'} t_{I12}^{h,\gamma} t_{I20}^{h,\gamma}) = \epsilon_S \text{Arg}(t_{31}^{h,\gamma'} t_{12}^{h,\gamma} t_{23}^{h,\gamma}) + \pi(1 - \delta_{\gamma',y'}), \quad (\text{C.35})$$

which give the constraints

$$\phi_{t_2^{h,\gamma'}} + \frac{4k\pi}{3} + n_3\pi = \epsilon_I(\phi_{t_1^{h,\gamma'}} + \frac{4k\pi}{3}), \quad (\text{C.36a})$$

$$\phi_{t_2^{h,\gamma'}} + \frac{4k\pi}{3} + n_3\pi = \epsilon_S(\phi_{t_1^{h,\gamma'}} + 2\phi_{t_1^{h,\gamma}}) + \pi\delta_{\gamma',y'}. \quad (\text{C.36b})$$

Using Eq. (C.10) we can rewrite this to

$$(1 - \epsilon_I \epsilon_S)(\phi_{t_1^{h,\gamma}} - \phi_{t_1^{h,\gamma'}}) = \pi(\delta_{\gamma,y'} + \delta_{\gamma',y'}), \quad (\text{C.37a})$$

Solutions of phase equations

We organize the solutions in table 4.2 in the main text.

Fourier Transformation of the Hamiltonian

Our goal is to derive Eq. (5.16) starting from Eq. (4.9). We will use the Fourier transform

$$b_{\mathbf{r}_\mu} = \sqrt{\frac{N_{SL}}{N}} \sum_{\mathbf{k}} b_{\mathbf{k},\mu} e^{-i\mathbf{k}\mathbf{r}_\mu}, \quad b_{\mathbf{k},\mu} = \sqrt{\frac{N_{SL}}{N}} \sum_{\mathbf{r}_\mu} b_{\mathbf{r}_\mu} e^{i\mathbf{k}\mathbf{r}_\mu}, \quad (\text{D.1})$$

where N is the total number of atoms in the lattice and N_{SL} is the number of sublattices in the unit cell and \mathbf{k} is summed over the first Brillouin zone. It appears in the normalization since $\sum_{\mathbf{k}} = \frac{N}{N_{SL}}$. $N_{SL} = 4$ for 0-flux states and $N_{SL} = 16$ for π -flux states. We treat the case $n_3 = 0$ here. The case $n_3 = 1$ can be derived similarly.

The on-site hopping term:

$$\begin{aligned} \sum_{\mathbf{r}_\mu} b_{\mathbf{r}_\mu}^\dagger b_{\mathbf{r}_\mu} &= \sum_{\mathbf{r}_0} \sum_{\mu} \sum_{\mathbf{k}'} \sum_{\mathbf{k}} b_{\mathbf{k},\mu}^\dagger b_{\mathbf{k}',\mu} e^{i(\mathbf{k}-\mathbf{k}')\mathbf{r}_0} = \sum_{\mu} \sum_{\mathbf{k}} b_{\mathbf{k},\mu}^\dagger b_{\mathbf{k},\mu} \\ &= \frac{1}{2} \sum_{\mu} \sum_{\mathbf{k}} (b_{\mathbf{k},\mu}^\dagger b_{\mathbf{k},\mu} + b_{-\mathbf{k},\mu}^\dagger b_{-\mathbf{k},\mu}) \\ &= \frac{1}{2} \sum_{\mu} \sum_{\mathbf{k}} (b_{\mathbf{k},\mu}^\dagger b_{\mathbf{k},\mu} + b_{-\mathbf{k},\mu} b_{-\mathbf{k},\mu}^\dagger) - N. \end{aligned} \quad (\text{D.2})$$

Nearest neighbour hopping term:

$$\begin{aligned}
 & \sum_{\mathbf{r}_\mu \mathbf{r}_\nu} b_{\mathbf{r}_\mu}^\dagger u_{\mathbf{r}_\mu \mathbf{r}_\nu}^h b_{\mathbf{r}_\nu} + \text{h.c.} \\
 &= \sum_{\mathbf{r}_0} \sum_{\mu < \nu} b_{\mathbf{r}_0 + \mathbf{0}_\mu}^\dagger u_{\mathbf{r}_0 + \mathbf{0}_\mu, \mathbf{r}_0 + \mathbf{0}_\nu}^h b_{\mathbf{r}_0 + \mathbf{0}_\nu} + b_{\mathbf{r}_0 + I(\mathbf{0}_\mu)}^\dagger u_{\mathbf{r}_0 + I(\mathbf{0}_\mu), \mathbf{r}_0 + I(\mathbf{0}_\nu)}^h b_{\mathbf{r}_0 + I(\mathbf{0}_\nu)} \\
 &+ \text{h.c.} \\
 &= \sum_{\mathbf{k}} \sum_{\mu < \nu} \left(u_{\mathbf{0}_\mu, \mathbf{0}_\nu}^h e^{\frac{i}{2}(\mathbf{a}_\mu - \mathbf{a}_\nu)\mathbf{k}} + u_{I(\mathbf{0}_\mu), I(\mathbf{0}_\nu)}^h e^{-\frac{i}{2}(\mathbf{a}_\mu - \mathbf{a}_\nu)\mathbf{k}} \right) b_{\mathbf{k}, \mu}^\dagger b_{\mathbf{k}, \nu} + \text{h.c.} \\
 &= \frac{1}{2} \sum_{\mathbf{k}} \sum_{\mu < \nu} \left(u_{\mathbf{0}_\mu, \mathbf{0}_\nu}^h e^{\frac{i}{2}(\mathbf{a}_\mu - \mathbf{a}_\nu)\mathbf{k}} + u_{I(\mathbf{0}_\mu), I(\mathbf{0}_\nu)}^h e^{-\frac{i}{2}(\mathbf{a}_\mu - \mathbf{a}_\nu)\mathbf{k}} \right) b_{\mathbf{k}, \mu}^\dagger b_{\mathbf{k}, \nu} \\
 &+ \text{h.c.} + (\mathbf{k} \rightarrow -\mathbf{k}) \\
 &:= \frac{1}{2} \sum_{\mathbf{k}} \sum_{\mu, \nu} b_{\mathbf{k}, \mu}^\dagger (H^h(\mathbf{k}))_{\mu, \nu} b_{\mathbf{k}, \nu} + b_{-\mathbf{k}, \mu} (H^h(-\mathbf{k}))_{\mu, \nu}^\dagger b_{-\mathbf{k}, \nu}^\dagger. \tag{D.3}
 \end{aligned}$$

The nearest neighbour pairing term:

$$\begin{aligned}
 & \sum_{r_\mu r_\nu} b_{r_\mu}^\dagger u_{r_\mu r_\nu}^p b_{r_\nu}^\dagger + \text{h.c.} \\
 &= \sum_{\mathbf{r}_0} \sum_{\mu < \nu} b_{\mathbf{r}_0 + \mathbf{0}_\mu}^\dagger u_{\mathbf{r}_0 + \mathbf{0}_\mu, \mathbf{r}_0 + \mathbf{0}_\nu}^p b_{\mathbf{r}_0 + \mathbf{0}_\nu}^\dagger + b_{\mathbf{r}_0 + I(\mathbf{0}_\mu)}^\dagger u_{\mathbf{r}_0 + I(\mathbf{0}_\mu), \mathbf{r}_0 + I(\mathbf{0}_\nu)}^p b_{\mathbf{r}_0 + I(\mathbf{0}_\nu)}^\dagger \\
 &+ \text{h.c.} \\
 &= \sum_{\mathbf{k}} \sum_{\mu < \nu} \frac{1}{2} b_{\mathbf{k}, \mu}^\dagger \left(u_{\mathbf{0}_\mu, \mathbf{0}_\nu}^p e^{\frac{i}{2}(\mathbf{a}_\mu - \mathbf{a}_\nu)\mathbf{k}} + u_{I(\mathbf{0}_\mu), I(\mathbf{0}_\nu)}^p e^{-\frac{i}{2}(\mathbf{a}_\mu - \mathbf{a}_\nu)\mathbf{k}} \right) b_{-\mathbf{k}, \nu}^\dagger \\
 &+ \sum_{\mathbf{k}} \sum_{\mu < \nu} \frac{1}{2} b_{-\mathbf{k}, \mu}^\dagger \left(u_{\mathbf{0}_\mu, \mathbf{0}_\nu}^p e^{-\frac{i}{2}(\mathbf{a}_\mu - \mathbf{a}_\nu)\mathbf{k}} + u_{I(\mathbf{0}_\mu), I(\mathbf{0}_\nu)}^p e^{\frac{i}{2}(\mathbf{a}_\mu - \mathbf{a}_\nu)\mathbf{k}} \right) b_{\mathbf{k}, \nu}^\dagger \\
 &+ \text{h.c.} \\
 &= \sum_{\mathbf{k}} \sum_{\mu < \nu} \frac{1}{2} b_{\mathbf{k}, \mu}^\dagger \left(u_{\mathbf{0}_\mu, \mathbf{0}_\nu}^p e^{\frac{i}{2}(\mathbf{a}_\mu - \mathbf{a}_\nu)\mathbf{k}} + u_{I(\mathbf{0}_\mu), I(\mathbf{0}_\nu)}^p e^{-\frac{i}{2}(\mathbf{a}_\mu - \mathbf{a}_\nu)\mathbf{k}} \right) b_{-\mathbf{k}, \nu}^\dagger \\
 &+ \sum_{\mathbf{k}} \sum_{\mu < \nu} \frac{1}{2} b_{\mathbf{k}, \nu}^\dagger \left((u_{\mathbf{0}_\mu, \mathbf{0}_\nu}^p)^T e^{-\frac{i}{2}(\mathbf{a}_\mu - \mathbf{a}_\nu)\mathbf{k}} + (u_{I(\mathbf{0}_\mu), I(\mathbf{0}_\nu)}^p)^T e^{\frac{i}{2}(\mathbf{a}_\mu - \mathbf{a}_\nu)\mathbf{k}} \right) b_{-\mathbf{k}, \mu}^\dagger \\
 &+ \text{h.c.} \\
 &:= \frac{1}{2} \sum_{\mathbf{k}} b_{\mathbf{k}, \mu}^\dagger (H^p(\mathbf{k}))_{\mu, \nu} b_{-\mathbf{k}, \nu}^\dagger + b_{\mathbf{k}, \mu} (H^p(\mathbf{k}))_{\mu, \nu}^\dagger b_{-\mathbf{k}, \nu}. \tag{D.4}
 \end{aligned}$$

After defining the spinor $\psi_{\mathbf{k}}^\dagger = (\hat{b}_{\mathbf{k},0}^\dagger, \hat{b}_{\mathbf{k},1}^\dagger, \hat{b}_{\mathbf{k},2}^\dagger, \hat{b}_{\mathbf{k},3}^\dagger, \hat{b}_{-\mathbf{k},0}, \hat{b}_{-\mathbf{k},1}, \hat{b}_{-\mathbf{k},2}, \hat{b}_{-\mathbf{k},3})^T$ we arrive at Eq. (5.16).

Explicit Hamiltonians

We give the explicit form of the submatrices of Eq. (5.16) for the 0 and π -flux case. To keep things short we introduce the notation $t \in \{h, p\}$:

$$u_{\mu\nu} = u_{\mu\nu}^t e^{\frac{i}{2}(\mathbf{a}_\mu - \mathbf{a}_\nu)\mathbf{k}} = u_{\mathbf{0}_\mu \mathbf{0}_\nu}^t e^{\frac{i}{2}(\mathbf{a}_\mu - \mathbf{a}_\nu)\mathbf{k}} \quad u_{I\mu\nu} = u_{I\mu\nu}^t e^{-\frac{i}{2}(\mathbf{a}_\mu - \mathbf{a}_\nu)\mathbf{k}} = u_{I(\mathbf{0}_\mu)I(\mathbf{0}_\nu)}^t e^{-\frac{i}{2}(\mathbf{a}_\mu - \mathbf{a}_\nu)\mathbf{k}} \quad (\text{E.1})$$

The submatrices fulfil $H^h(\mathbf{k}) = (H^h(\mathbf{k}))^\dagger$ and $H^t(\mathbf{k}) = (H^t(-\mathbf{k}))^T$ so we only need to give the upper triangular part to fully determines the whole matrices. For the 0-flux case $H^t(k)$ are 8×8 matrices given by

$$H^t(\mathbf{k}) = \begin{pmatrix} 0 & u_{01} + u_{I01} & u_{02} + u_{I02} & u_{03} + u_{I03} \\ & 0 & u_{12} + u_{I23} & u_{13} + u_{I23} \\ & & 0 & u_{23} + u_{I23} \\ & & & 0 \end{pmatrix}.$$

For the π -flux case the $H^t(k)$ are 32×32 matrices:

$$H^t(\mathbf{k}) = \begin{pmatrix} H_{11}^t(\mathbf{k}) & H_{12}^t(\mathbf{k}) & H_{13}^t(\mathbf{k}) & H_{14}^t(\mathbf{k}) \\ H_{21}^t(\mathbf{k}) & H_{22}^t(\mathbf{k}) & H_{23}^t(\mathbf{k}) & H_{24}^t(\mathbf{k}) \\ H_{31}^t(\mathbf{k}) & H_{32}^t(\mathbf{k}) & H_{33}^t(\mathbf{k}) & H_{34}^t(\mathbf{k}) \\ H_{41}^t(\mathbf{k}) & H_{42}^t(\mathbf{k}) & H_{43}^t(\mathbf{k}) & H_{44}^t(\mathbf{k}) \end{pmatrix}. \quad (\text{E.2})$$

The unit cell consists out of four tetrahedra $q \in \{1, 2, 3, 4\}$ and the submatrices H_{q_1, q_2}^t include all bonds between tetrahedron q_1 and q_2 . They are given by:

$$H_{ii}^t(\mathbf{k}) = \begin{pmatrix} 0 & u_{01} + u_{I01} e^{in_3 \pi (\delta_{i,2} + \delta_{i,3})} & u_{02} & u_{03} \\ & 0 & u_{12} & u_{13} \\ & & 0 & u_{23} \\ & & & 0 \end{pmatrix},$$

E. Explicit Hamiltonians

$$\begin{aligned}
H_{12}^t(\mathbf{k}) &= \begin{pmatrix} 0 & 0 & u_{I02} & 0 \\ 0 & 0 & u_{I12} & 0 \\ u_{I20} & u_{I21}e^{in_3\pi} & 0 & 0 \\ 0 & 0 & 0 & 0 \end{pmatrix}, & H_{13}^t(\mathbf{k}) &= \begin{pmatrix} 0 & 0 & 0 & u_{I03} \\ 0 & 0 & 0 & u_{I13} \\ 0 & 0 & 0 & 0 \\ u_{I30} & u_{I31}e^{in_3\pi} & 0 & 0 \end{pmatrix}, \\
H_{14}^t(\mathbf{k}) &= \begin{pmatrix} 0 & 0 & 0 & 0 \\ 0 & 0 & 0 & 0 \\ 0 & 0 & 0 & u_{I23} \\ 0 & 0 & u_{I32}e^{in_3\pi} & 0 \end{pmatrix}, & H_{23}^t(\mathbf{k}) &= \begin{pmatrix} 0 & 0 & 0 & 0 \\ 0 & 0 & 0 & 0 \\ 0 & 0 & 0 & u_{I23} \\ 0 & 0 & u_{I32}e^{in_3\pi} & 0 \end{pmatrix}, \\
H_{24}^t(\mathbf{k}) &= \begin{pmatrix} 0 & 0 & 0 & u_{I03} \\ 0 & 0 & 0 & u_{I13}e^{in_3\pi} \\ 0 & 0 & 0 & 0 \\ u_{I30} & u_{I31} & 0 & 0 \end{pmatrix}, & H_{34}^t(\mathbf{k}) &= \begin{pmatrix} 0 & 0 & u_{I02}e^{in_3\pi} & 0 \\ 0 & 0 & u_{I12} & 0 \\ u_{I20}e^{in_3\pi} & u_{I21}e^{in_3\pi} & 0 & 0 \\ 0 & 0 & 0 & 0 \end{pmatrix}.
\end{aligned} \tag{E.3}$$

For the fully symmetric PSG the u matrices are given by

$$u_{01}^t = (a^t, b^t, c^t, d^t), \tag{E.4a}$$

$$u_{02}^t = (a^t, -\frac{1}{2}(b^t + \sqrt{3}c^t), \frac{1}{2}(\sqrt{3}b^t - c^t), d^t), \tag{E.4b}$$

$$u_{03}^t = (a^t, -\frac{1}{2}(b^t - \sqrt{3}c^t), -\frac{1}{2}(\sqrt{3}b^t + c^t), d^t), \tag{E.4c}$$

$$u_{12}^t = (-a^t, -\frac{1}{2}(b^t + \sqrt{3}c^t), -\frac{1}{2}(\sqrt{3}b^t - c^t), d^t)e^{in_{\bar{C}_6}\delta_{t,p}\pi}e^{i(n_3+n_{ST_1})\delta_{t,h}\pi}, \tag{E.4d}$$

$$u_{13}^t = (-a^t, \frac{1}{2}(b^t + \sqrt{3}c^t), -\frac{1}{2}(\sqrt{3}b^t - c^t), -d^t)e^{i(n_3+n_{ST_1})\pi} \tag{E.4e}$$

$$u_{23}^t = (-a^t, b^t, -c^t, d^t)e^{in_{\bar{C}_6}\delta_{t,p}\pi}e^{i(n_3+n_{ST_1})\delta_{t,h}\pi}, \tag{E.4f}$$

$$u_{I01}^t = u_{01}^t e^{i(n_3+n_{\bar{C}_6}\delta_{t,p}+n_{ST_1})\pi}, \tag{E.4g}$$

$$u_{I02}^t = u_{02}^t e^{i(n_3+n_{\bar{C}_6}\delta_{t,p}+n_{ST_1})\pi}, \tag{E.4h}$$

$$u_{I03}^t = u_{03}^t e^{i(n_3+n_{\bar{C}_6}\delta_{t,p}+n_{ST_1})\pi}, \tag{E.4i}$$

$$u_{I12}^t = u_{12}^t e^{in_{\bar{C}_6}\delta_{t,p}\pi}, \tag{E.4j}$$

$$u_{I13}^t = u_{13}^t e^{in_{\bar{C}_6}\delta_{t,p}\pi}, \tag{E.4k}$$

$$u_{I23}^t = u_{23}^t e^{in_{\bar{C}_6}\delta_{t,p}\pi}. \tag{E.4l}$$

For the weakly symmetric PSG:

$$u_{01}^t = (a_1^t, b_1^t, c_1^t, d_1^t)^t \quad (\text{E.5})$$

$$u_{02}^t = (a_1^t, -\frac{1}{2}(b_1^t + \sqrt{3}c_1^t), \frac{1}{2}(\sqrt{3}b_1^t - c_1^t), d_1^t)^t e^{-i\frac{2k}{3}\pi}, \quad (\text{E.6})$$

$$u_{03}^t = (a_2^t, -\frac{1}{2}(b_2^t - \sqrt{3}c_2^t), -\frac{1}{2}(\sqrt{3}b_2^t + c_2^t), d_2^t)^t e^{-i\frac{4k}{3}\pi}, \quad (\text{E.7})$$

$$u_{12}^t = (a_1^t, -\frac{1}{2}(b_1^t - \sqrt{3}c_1^t), -\frac{1}{2}(\sqrt{3}b_1^t + c_1^t), d_1^t)^t e^{-i\frac{2k}{3}\pi} e^{in_{C_3}c_3'\pi}, \quad (\text{E.8})$$

$$u_{31}^t = (a_1^t, -\frac{1}{2}(b_1^t + \sqrt{3}c_1^t), \frac{1}{2}(\sqrt{3}b_1^t - c_1^t), d_1^t)^t e^{-i\frac{2k}{3}\pi} e^{in_{C_3}c_3'\pi}, \quad (\text{E.9})$$

$$u_{23}^t = (a_1^t, b_1^t, c_1^t, d_1^t)^t e^{-i\frac{2k}{3}\pi} e^{in_{C_3}c_3'\pi}, \quad (\text{E.10})$$

$$u_{I01}^t = (a_2^t, b_2^t, c_2^t, d_2^t)^t, \quad (\text{E.11})$$

$$u_{I02}^t = (a_2^t, -\frac{1}{2}(b_2^t + \sqrt{3}c_2^t), \frac{1}{2}(\sqrt{3}b_2^t - c_2^t), d_2^t)^t e^{-i\frac{2k}{3}\pi}, \quad (\text{E.12})$$

$$u_{I03}^t = (a_2^t, -\frac{1}{2}(b_2^t - \sqrt{3}c_2^t), -\frac{1}{2}(\sqrt{3}b_2^t + c_2^t), d_2^t)^t e^{-i\frac{4k}{3}\pi}, \quad (\text{E.13})$$

$$u_{I12}^t = (a_2^t, -\frac{1}{2}(b_2^t - \sqrt{3}c_2^t), -\frac{1}{2}(\sqrt{3}b_2^t + c_2^t), d_2^t)^t e^{-i\frac{2k}{3}\pi} e^{i(n_3+n_{C_3}c_3')\pi}, \quad (\text{E.14})$$

$$u_{I31}^t = (a_2^t, -\frac{1}{2}(b_2^t + \sqrt{3}c_2^t), \frac{1}{2}(\sqrt{3}b_2^t - c_2^t), d_2^t)^t e^{-i\frac{2k}{3}\pi} e^{i(n_3+n_{C_3}c_3')\pi}, \quad (\text{E.15})$$

$$u_{I23}^t = (a_2^t, b_2^t, c_2^t, d_2^t)^t e^{-i\frac{2k}{3}\pi} e^{i(n_3+n_{C_3}c_3')\pi}. \quad (\text{E.16})$$

Analytic Results for Energy Bands

The spinon dispersions $\omega_i(\mathbf{k})$ are eigenvalues of the matrix $\tau^3 \mathcal{H}(\mathbf{k})$. For symmetric ansätze with U(1) symmetric parametrization there are nice analytical formulas available. For all 0-flux PSGs with $n_{ST_1} = 1$ we have shifted $\vec{k} \rightarrow \vec{k} - \pi(1, 1, 1)$ and for all π -flux PSGs we shifted $\vec{k} \rightarrow \vec{k} - \frac{\pi}{2}(1, 1, 1)$. This makes the spinon dispersion symmetric around the Brillouin zone origin. Such a shift can be seen as a gauge transformation and does not change any physical quantities [18]. For better readability we introduce the functions

$$f_1(k) = \cos\left(\frac{k_1}{2}\right) \cos\left(\frac{k_2}{2}\right) + \cos\left(\frac{k_2}{2}\right) \cos\left(\frac{k_3}{2}\right) + \cos\left(\frac{k_1}{2}\right) \cos\left(\frac{k_3}{2}\right) \quad (\text{F.1})$$

$$f_2(k) = \cos\left(\frac{k_1}{2}\right) + \cos\left(\frac{k_2}{2}\right) + \cos\left(\frac{k_3}{2}\right) \quad (\text{F.2})$$

and we denote degeneracy μ as a superscript $\omega^\mu(\mathbf{k})$

- PSG 0-(101)

$$\omega^4(\mathbf{k}) = \lambda + 2a^h \quad (\text{F.3a})$$

$$\omega^2(\mathbf{k}) = \left| 2a^h \sqrt{(1 + f_1(k))} \pm \sqrt{(2a^h - \lambda)^2 - (2d^p)^2(3 - f_1(k))} \right| \quad (\text{F.3b})$$

- PSG 0-(110)

$$\omega^4(\mathbf{k}) = \sqrt{(\lambda - 2a^h)^2 - (2d^p)^2} \quad (\text{F.4a})$$

$$\omega^2(\mathbf{k}) = \sqrt{\left(\lambda + 2a^h(1 + \sqrt{f_1(k) + 1})\right)^2 - (2d^p)^2 \left(1 + \sqrt{f_1(k) + 1}\right)^2} \quad (\text{F.4b})$$

- PSG 0-(010)

$$\omega^2(\mathbf{k}) = \sqrt{\left(\lambda \pm_2 2d^h \sqrt{f_{\pm_1}(k)}\right)^2 - (2a^p)^2 f_{\pm_1}(k)} \quad (\text{F.5a})$$

$$f_{\pm_1}(k) = \frac{1}{2} \left(3 + f_1(k) \pm_1 \sqrt{(3 + f_1(k))^2 - 4f_2(k)^2} \right) \quad (\text{F.5b})$$

- PSG 0-(001)

$$\omega^2(\mathbf{k}) = \sqrt{\lambda^2 - (2a^p)^2(3 - f_{\pm 1}(k))} \pm_2 d^h \sqrt{f_{\pm 1}(k)} \quad (\text{F.6a})$$

$$f_{\pm 1}(k) = \frac{1}{2} \left(3 + f_1(k) \pm_1 \sqrt{(3 + f_1(k))^2 - 4f_2(k)^2} \right) \quad (\text{F.6b})$$

- PSG π -(111)

$$\omega^{16}(\mathbf{k}) = \lambda + 2a^h \quad (\text{F.7a})$$

$$\omega^8(\mathbf{k}) = \left| \sqrt{(2a^h - \lambda)^2 - (2d^p)^2(3 \pm_1 f(k))} \pm_2 2a^h \sqrt{1 \mp_1 f(k)} \right| \quad (\text{F.7b})$$

$$f(k) = \frac{1}{2} \sqrt{3 - f_1(2k)} \quad (\text{F.7c})$$

- PSG π -(100)

$$\omega^{16}(\mathbf{k}) = \sqrt{(\lambda - 2a^h)^2 - (2d^p)^2} \quad (\text{F.9})$$

$$\omega^8(\mathbf{k}) = \sqrt{(\lambda + 2a^h f_{\pm 1, \pm 2}(k))^2 - (2d^p)^2 f_{\pm 1, \pm 2}(k)^2} \quad (\text{F.9a})$$

$$f_{\pm 1, \pm 2}(k) = 1 \pm_1 \sqrt{1 \pm_2 \frac{1}{2} \sqrt{3 - f_1(2k)}} \quad (\text{F.9b})$$

- PSG π -(011)

$$\omega^8(\mathbf{k}) = \left| \sqrt{\lambda - (2a^p)^2 \frac{1}{2}(3 - r_i) \pm 2d^h \sqrt{\frac{1}{2}(3 + r_i)}} \right| \quad (\text{F.10a})$$

$$r_i := i^{\text{th}} \text{ Root of :} \quad (\text{F.10b})$$

$$6 - 15f_1(2k) + 4f_2(2k)^2 - 2(1 + f_1(2k))x + (f_1(2k) - 9)x^2 + x^4$$

- PSG π -(000)

$$\omega^8(\mathbf{k}) = \sqrt{\left(\lambda \pm 2d^h \sqrt{\frac{1}{2}(3 + r_i)} \right)^2 - (2a^p)^2 \frac{1}{2}(3 + r_i)} \quad (\text{F.11a})$$

$$r_i := i^{\text{th}} \text{ Root of :} \quad (\text{F.11b})$$

$$6 - 15f_1(2k) + 4f_2(2k)^2 - 2(1 + f_1(2k))x + (f_1(2k) - 9)x^2 + x^4$$

For all π -flux states we observe the higher spectral periodicity described in [29]

Sublattice Boson Density in the AF_{\perp} Phase

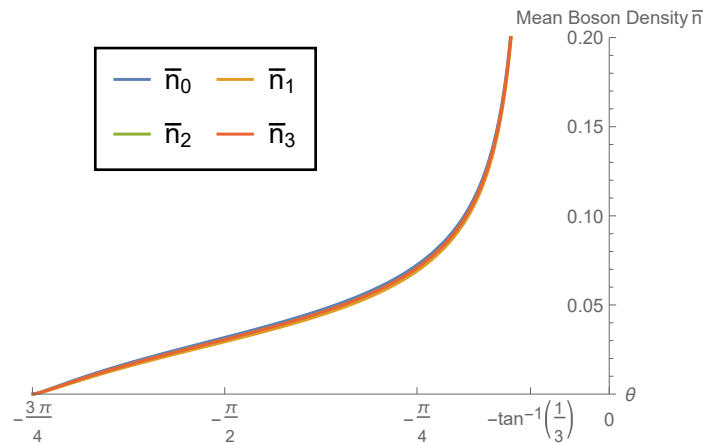


Figure G.1: Mean boson density for each sublattice $i \in \{0, 1, 2, 3\}$. The graphs of n_2 and n_3 lie on top of each other.

Altering the derivation in section 6.2 a bit we can not only calculate the mean boson density over all lattice sites but also the mean boson density per sublattice (see figure G.1). The formula is given by

$$\bar{n}_i = \frac{1}{2\text{Vol}_{BZ}} \int_{BZ} ((U \cosh(2D)U^\dagger)_{ii} - 1) \quad (\text{G.1})$$

where $U = (u_1, u_2, u_+, u_-)$ is defined by the unit vectors u_i

$$u_1(4\mathbf{k}) = \frac{1}{\mathcal{N}(\mathbf{k})} (f_1(\mathbf{k}) \sin((k_x - k_z)), f_2(\mathbf{k}) \sin(k_y - k_z), \quad (\text{G.2a})$$

$$- f_1(\mathbf{k}) \sin(k_x + k_y) - f_2(\mathbf{k}) \sin(k_x - k_z), \\ f_2(\mathbf{k}) \sin(k_x - k_y) + f_1(\mathbf{k}) \sin(k_x + k_z))^T$$

$$u_2(4\mathbf{k}) = \frac{1}{\mathcal{N}(\mathbf{k})} (f_1(\mathbf{k}) \sin(k_x - k_z), -f_2(\mathbf{k}) \sin(k_y - k_z), \quad (\text{G.2b})$$

$$- f_1(\mathbf{k}) \sin(k_x + k_y) + f_2(\mathbf{k}) \sin(k_x - k_z), \\ - f_2(\mathbf{k}) \sin(k_x - k_y) + f_1(\mathbf{k}) \sin(k_x + k_z))^T$$

$$u_{\pm}(2\mathbf{k}) = \frac{1}{\mathcal{N}(\mathbf{k})} \left(\frac{1}{2} (\sin(k_x + k_y) + \sin(k_x + k_z) + \sin(k_y + k_z)), \quad (\text{G.2c})$$

$$\cos((k_y - k_z)/2) \sin(k_z) \pm f_3(\mathbf{k}) \sin((k_y + k_z)/2), \\ \cos((k_x - k_z)/2) \sin(k_y) \pm f_3(\mathbf{k}) \sin((k_x + k_z)/2), \\ \cos((k_x - k_y)/2) \sin(k_x) \pm f_3(\mathbf{k}) \sin((k_x + k_y)/2))^T$$

with normalization factor $\mathcal{N}(\mathbf{k})$ and functions

$$f_1(\mathbf{k}) = \sqrt{\sin(k_x - k_y)^2 + \sin(k_x - k_z)^2 + \sin(k_y - k_z)^2} \quad (\text{G.3a})$$

$$f_2(\mathbf{k}) = \sqrt{\sin(k_x + k_y)^2 + \sin(k_x + k_z)^2 + \sin(k_y - k_z)^2} \quad (\text{G.3b})$$

$$f_3(\mathbf{k}) = \sqrt{1 + \cos(k_x) \cos(k_y) + \cos(k_x) \cos(k_z) + \cos(k_y) \cos(k_z)} \quad (\text{G.3c})$$

Supplementary Observables

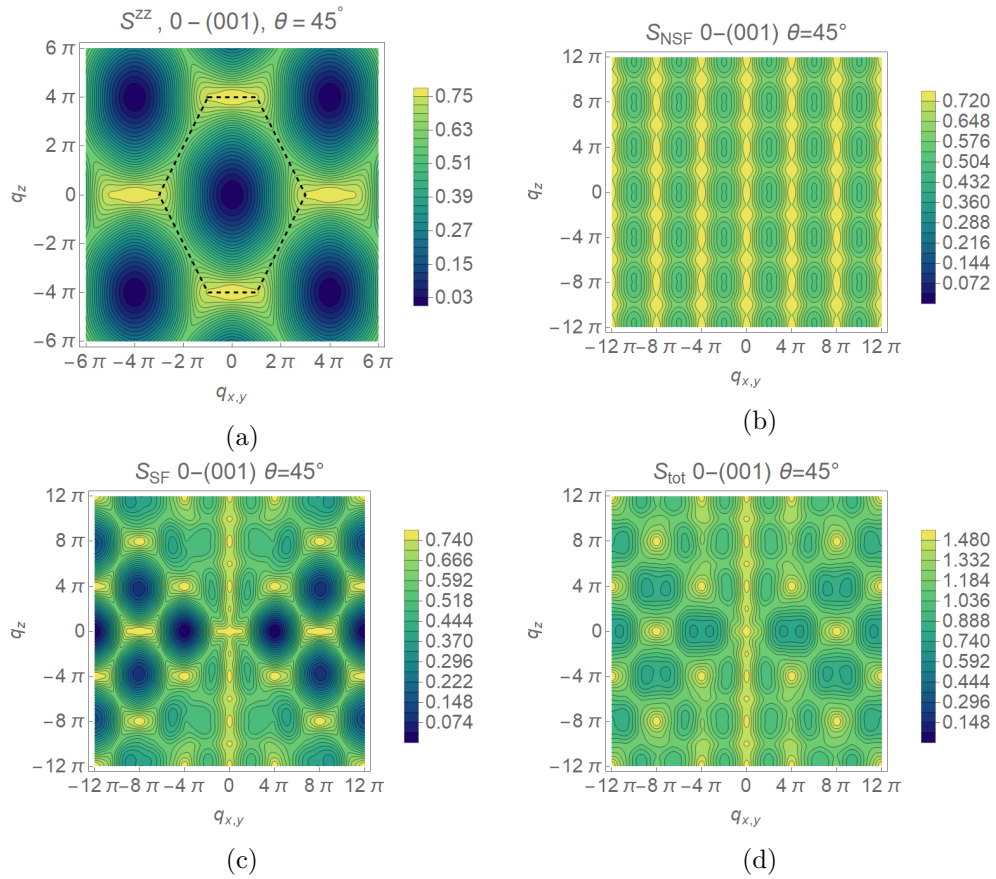


Figure H.1: (a) Local spin structure factor, (b) neutron scattering amplitude in NSF channel, (c) NSA in SF channel, (d) total neutron scattering amplitude of 0-(001) plotted in the $[q_x, q_y, q_z]$ plane for $\theta = 45^\circ$. The black dashed line shows the boundary of the extended Brillouin zone.

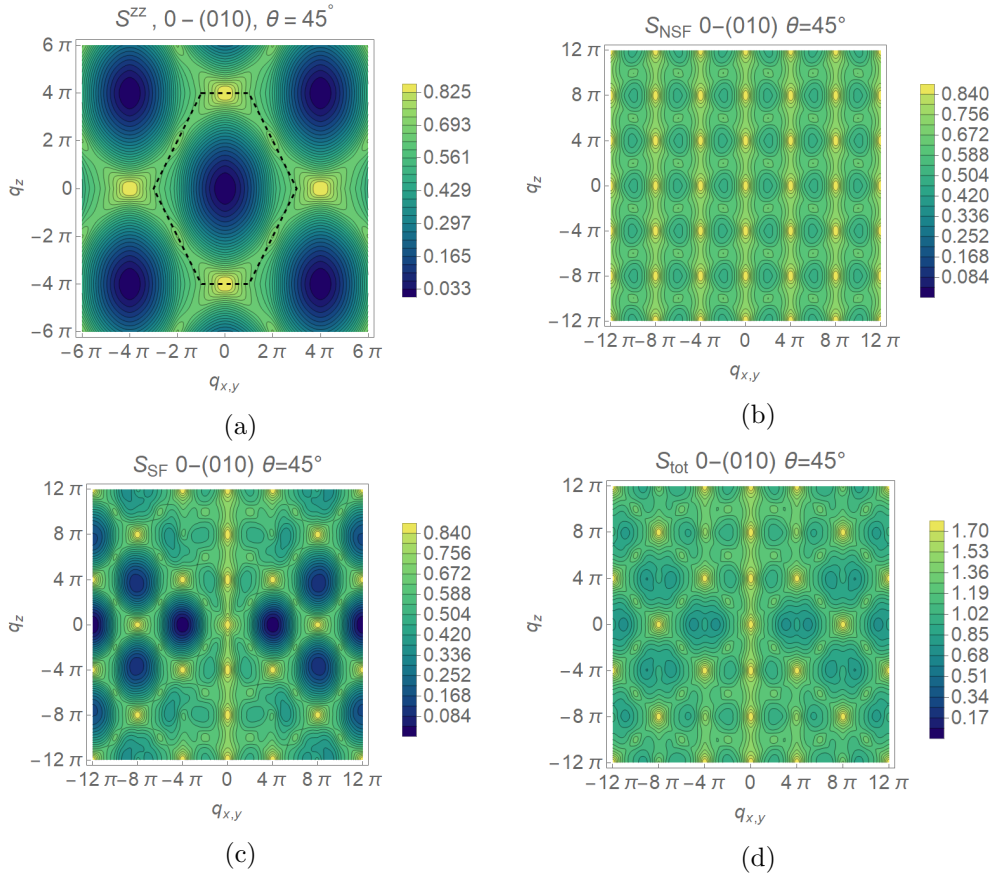


Figure H.2: (a) Local spin structure factor, (b) neutron scattering amplitude in NSF channel, (c) NSA in SF channel, (d) total neutron scattering amplitude of 0-(010) plotted in the $[q_{x,y}, q_{x,y}, q_z]$ plane for $\theta = 45^\circ$. The black dashed line shows the boundary of the extended Brillouin zone.

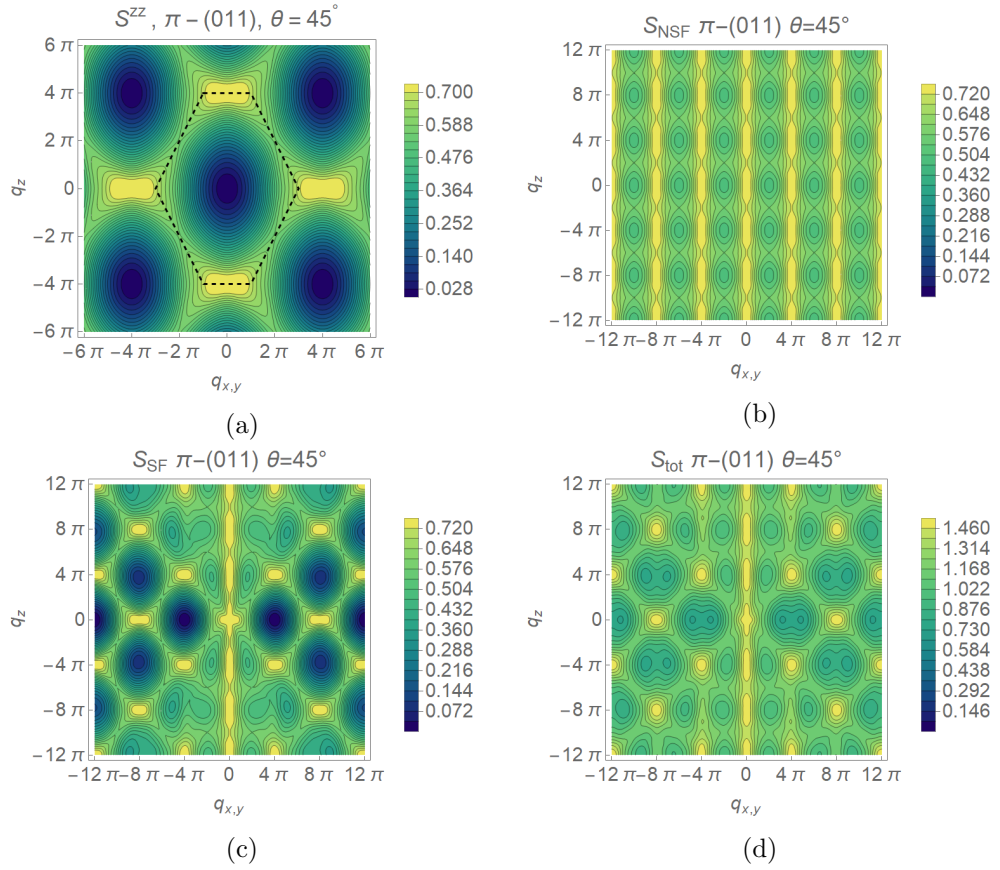


Figure H.3: (a) Local spin structure factor, (b) neutron scattering amplitude in NSF channel, (c) NSA in SF channel, (d) total neutron scattering amplitude of π -(011) plotted in the $[q_x, q_y, q_z]$ plane for $\theta = 45^\circ$. The black dashed line shows the boundary of the extended Brillouin zone.

Bibliography

- [1] B. Schneider, J. C. Halimeh, and M. Punk, “Projective symmetry group classification of chiral \mathbb{Z}_2 spin liquids on the pyrochlore lattice: Application to the spin- $\frac{1}{2}$ XXZ Heisenberg model”, [Physical Review B](#) **105**, 125122 (2022).
- [2] X.-G. Wen, *Quantum Field Theory of Many-Body Systems: From the Origin of Sound to an Origin of Light and Electrons* (OUP Oxford, June 2004).
- [3] A. Y. Kitaev, “Fault-tolerant quantum computation by anyons”, en, [Annals of Physics](#) **303**, 2 (2003).
- [4] P. W. Anderson, “The Resonating Valence Bond State in La₂CuO₄ and Superconductivity”, en, [Science](#) **235**, Publisher: American Association for the Advancement of Science Section: Reports, 1196 (1987).
- [5] J. G. Rau and M. J. P. Gingras, “Frustrated quantum rare-earth pyrochlores”, [Annual Review of Condensed Matter Physics](#) **10**, arXiv: 1806.09638, 357 (2019).
- [6] A. Kitaev, “Anyons in an exactly solved model and beyond”, en, [Annals of Physics](#), January Special Issue **321**, 2 (2006).
- [7] O. Benton, L. D. C. Jaubert, R. Singh, J. Oitmaa, and N. Shannon, “Quantum spin ice with frustrated transverse exchange: from pi-flux phase to nematic quantum spin liquid”, [Physical Review Letters](#) **121**, arXiv: 1802.09198, 067201 (2018).
- [8] M. TAILLEFUMIER, O. Benton, H. Yan, L. D. C. Jaubert, and N. Shannon, “Competing Spin Liquids and Hidden Spin-Nematic Order in Spin Ice with Frustrated Transverse Exchange”, [Physical Review X](#) **7**, Publisher: American Physical Society, 041057 (2017).
- [9] M. J. P. Gingras and P. A. McClarty, “Quantum Spin Ice: A Search for Gapless Quantum Spin Liquids in Pyrochlore Magnets”, [Reports on Progress in Physics](#) **77**, arXiv: 1311.1817, 056501 (2014).
- [10] E. Berg, E. Altman, and A. Auerbach, “Singlet Excitations in Pyrochlore: A Study of Quantum Frustration”, [Physical Review Letters](#) **90**, Publisher: American Physical Society, 147204 (2003).

- [11] B. Canals and C. Lacroix, “Quantum spin liquid: The Heisenberg antiferromagnet on the three-dimensional pyrochlore lattice”, [Physical Review B **61**](#), Publisher: American Physical Society, 1149 (2000).
- [12] A. B. Harris, A. J. Berlinsky, and C. Bruder, “Ordering by quantum fluctuations in a strongly frustrated Heisenberg antiferromagnet”, [Journal of Applied Physics **69**](#), Publisher: American Institute of Physics, 5200 (1991).
- [13] H. Tsunetsugu, “Antiferromagnetic Quantum Spins on the Pyrochlore Lattice”, [Journal of the Physical Society of Japan **70**](#), Publisher: The Physical Society of Japan, 640 (2001).
- [14] H. Tsunetsugu, “Spin-singlet order in a pyrochlore antiferromagnet”, [Physical Review B **65**](#), Publisher: American Physical Society, 024415 (2001).
- [15] F. J. Burnell, S. Chakravarty, and S. L. Sondhi, “Monopole flux state on the pyrochlore lattice”, [Physical Review B **79**](#), Publisher: American Physical Society, 144432 (2009).
- [16] B. Canals and C. Lacroix, “Pyrochlore Antiferromagnet: A Three-Dimensional Quantum Spin Liquid”, [Physical Review Letters **80**](#), Publisher: American Physical Society, 2933 (1998).
- [17] J. H. Kim and J. H. Han, “Chiral spin states in the pyrochlore Heisenberg magnet: Fermionic mean-field theory and variational Monte Carlo calculations”, [Physical Review B **78**](#), arXiv: 0807.2036, 180410 (2008).
- [18] C. Liu, G. B. Halász, and L. Balents, “Competing orders in pyrochlore magnets from a Z 2 spin liquid perspective”, en, [Physical Review B **100**](#), 075125 (2019).
- [19] L. Messio, C. Lhuillier, and G. Misguich, “Time reversal symmetry breaking chiral spin liquids: Projective symmetry group approach of bosonic mean-field theories”, en, [Physical Review B **87**](#), 125127 (2013).
- [20] M. Ritter, *Multiloop Pseudofermion Functional Renormalization Group Study of the Pyrochlore XXZ Model*, Master’s thesis, Mar. 2021.
- [21] K. A. Ross, L. Savary, B. D. Gaulin, and L. Balents, “Quantum Excitations in Quantum Spin Ice”, [Physical Review X **1**](#), Publisher: American Physical Society, 021002 (2011).
- [22] H. Yan, O. Benton, L. Jaubert, and N. Shannon, “Theory of multiple-phase competition in pyrochlore magnets with anisotropic exchange with application to $\text{Yb}_2\text{Ti}_2\text{O}_7$, $\text{Er}_2\text{Ti}_2\text{O}_7$, and $\text{Er}_2\text{Sn}_2\text{O}_7$ ”, [Physical Review B **95**](#), Publisher: American Physical Society, 094422 (2017).
- [23] J. G. Rau and M. J. P. Gingras, “Frustration and anisotropic exchange in ytterbium magnets with edge-shared octahedra”, [Physical Review B **98**](#), arXiv: 1802.03024, 054408 (2018).
- [24] O. Benton, O. Sikora, and N. Shannon, “Seeing the light: Experimental signatures of emergent electromagnetism in a quantum spin ice”, en, [PHYSICAL REVIEW B](#), 25 (2012).
- [25] C. Castelnovo, R. Moessner, and S. L. Sondhi, “Magnetic Monopoles in Spin Ice”, [Nature **451**](#), arXiv: 0710.5515, 42 (2008).

-
- [26] L. Savary and L. Balents, “Coulombic Quantum Liquids in Spin-1/2 Pyrochlores”, en, [Physical Review Letters](#) **108**, 037202 (2012).
- [27] S. Sanyal, K. Dhochak, and S. Bhattacharjee, “Interplay of uniform $U(1)$ quantum spin liquid and magnetic phases in rare earth pyrochlore magnets : a fermionic parton approach”, [Physical Review B](#) **99**, arXiv: 1808.04861, 134425 (2019).
- [28] M. Hermele, M. P. A. Fisher, and L. Balents, “Pyrochlore photons: the $U(1)$ spin liquid in a $S = \frac{1}{2}$ three-dimensional frustrated magnet”, [Phys. Rev. B](#) **69**, 064404 (2004).
- [29] G. Chen, “Spectral periodicity of the spinon continuum in quantum spin ice”, [Physical Review B](#) **96**, Publisher: American Physical Society, 085136 (2017).
- [30] S. Onoda and Y. Tanaka, “Quantum fluctuations in the effective pseudospin- $\frac{1}{2}$ model for magnetic pyrochlore oxides”, [Physical Review B](#) **83**, Publisher: American Physical Society, 094411 (2011).
- [31] R. Moessner, S. L. Sondhi, and M. O. Goerbig, “Quantum dimer models and effective Hamiltonians on the pyrochlore lattice”, [Physical Review B](#) **73**, Publisher: American Physical Society, 094430 (2006).
- [32] F. Wang and A. Vishwanath, “Spin Liquid States on the Triangular and Kagome Lattices: A Projective Symmetry Group Analysis of Schwinger Boson States”, [Physical Review B](#) **74**, arXiv: cond-mat/0608129, 174423 (2006).
- [33] D.-V. Bauer and J. O. Fjærestad, “Schwinger boson mean field study of the $J_1 - J_2$ Heisenberg quantum antiferromagnet on the triangular lattice”, arXiv:1710.08720 [cond-mat], arXiv: 1710.08720, 10.1103/PhysRevB.96.165141 (2017).
- [34] D. P. Arovas and A. Auerbach, “Functional integral theories of low-dimensional quantum Heisenberg models”, en, [Physical Review B](#) **38**, 316 (1988).
- [35] S. Bieri, C. Lhuillier, and L. Messio, “Projective symmetry group classification of chiral spin liquids”, [Physical Review B](#) **93**, Publisher: American Physical Society, 094437 (2016).
- [36] M.-w. Xiao, “Theory of transformation for the diagonalization of quadratic Hamiltonians”, arXiv:0908.0787 [math-ph], arXiv: 0908.0787 (2009).
- [37] T. Fennell, P. P. Deen, A. R. Wildes, K. Schmalzl, D. Prabhakaran, A. T. Boothroyd, R. J. Aldus, D. F. McMorrow, and S. T. Bramwell, “Magnetic Coulomb Phase in the Spin Ice $\text{Ho}_2\text{Ti}_2\text{O}_7$ ”, en, [Science](#) **326**, Publisher: American Association for the Advancement of Science Section: Report, 415 (2009).
- [38] T. Holstein and H. Primakoff, “Field Dependence of the Intrinsic Domain Magnetization of a Ferromagnet”, [Physical Review](#) **58**, Publisher: American Physical Society, 1098 (1940).
- [39] M. Vogl, P. Laurell, H. Zhang, S. Okamoto, and G. A. Fiete, “Exact resummation of the Holstein-Primakoff expansion and differential equation approach to operator square-roots”, arXiv:2006.06871 [cond-mat], arXiv: 2006.06871 (2020).

- [40] D. Kiese, T. Mueller, Y. Iqbal, R. Thomale, and S. Trebst, “Multiloop functional renormalization group approach to quantum spin systems”, [arXiv:2011.01269 \[cond-mat\]](#), [arXiv: 2011.01269 \(2020\)](#).
- [41] Y. Huang, K. Chen, Y. Deng, N. Prokof’ev, and B. Svistunov, “Spin-Ice State of the Quantum Heisenberg Antiferromagnet on the Pyrochlore Lattice”, [Physical Review Letters](#) **116**, [Publisher: American Physical Society](#), 177203 (2016).
- [42] Y. Iqbal, T. Müller, P. Ghosh, M. J. P. Gingras, H. O. Jeschke, S. Rachel, J. Reuther, and R. Thomale, “Quantum and Classical Phases of the Pyrochlore Heisenberg Model with Competing Interactions”, [Physical Review X](#) **9**, [Publisher: American Physical Society](#), 011005 (2019).
- [43] P. Müller, A. Lohmann, J. Richter, and O. Derzhko, “Thermodynamics of the pyrochlore-lattice quantum Heisenberg antiferromagnet”, [Physical Review B](#) **100**, [Publisher: American Physical Society](#), 024424 (2019).

Selbständigkeitserklärung

Hiermit erkläre ich, die vorliegende Arbeit selbständig verfasst und keine anderen als die angegebenen Quellen und Hilfsmittel benutzt zu haben.

München, 07. Juni 2021

Benedikt Schneider